



DGK Deutsche Geodätische Kommission
bei der Bayerischen Akademie der Wissenschaften

Reihe C

Dissertationen

Heft Nr. 671

Jens Göpfert

**Snakes for Adapting GIS Road and River Objects
to Airborne Laser Scanning Data**

München 2012

**Verlag der Bayerischen Akademie der Wissenschaften
in Kommission beim Verlag C. H. Beck**

ISSN 0065-5325

ISBN 978-3-7696-5083-9

**Diese Arbeit ist gleichzeitig veröffentlicht in:
Wissenschaftliche Arbeiten der Fachrichtung Geodäsie und Geoinformatik der Leibniz Universität Hannover
ISSN 0174-1454, Nr. 296, Hannover 2011**



Snakes for Adapting GIS Road and River Objects to Airborne Laser Scanning Data

Von der Fakultät für Bauingenieurwesen und Geodäsie
der Gottfried Wilhelm Leibniz Universität Hannover
zur Erlangung des Grades
Doktor-Ingenieur (Dr.-Ing.)
genehmigte Dissertation

von

Dipl.-Ing. Jens Göpfert

München 2012

Verlag der Bayerischen Akademie der Wissenschaften
in Kommission bei der C. H. Beck'schen Verlagsbuchhandlung München

ISSN 0065-5325

ISBN 978-3-7696-5083-9

Diese Arbeit ist gleichzeitig veröffentlicht in:
Wissenschaftliche Arbeiten der Fachrichtung Geodäsie und Geoinformatik der Leibniz Universität Hannover
ISSN 0174-1454, Nr. 296, Hannover 2011

Adresse der Deutschen Geodätischen Kommission:



Deutsche Geodätische Kommission

Alfons-Goppel-Straße 11 • D – 80 539 München

Telefon +49 – 89 – 23 031 1113 • Telefax +49 – 89 – 23 031 -1283 / - 1100

e-mail hornik@dgfi.badw.de • <http://www.dgk.badw.de>

Prüfungskommission

Vorsitzender: Prof. Dr.-Ing. Steffen Schön

Referent: Prof. Dr.-Ing. Christian Heipke

Korreferenten: Prof. Dr.-Ing. Monika Sester

Prof. Dr.-Ing. George Vosselman

PD Dr.techn. Franz Rottensteiner

Tag der mündlichen Prüfung: 11.10.2011

© 2012 Deutsche Geodätische Kommission, München

Alle Rechte vorbehalten. Ohne Genehmigung der Herausgeber ist es auch nicht gestattet,
die Veröffentlichung oder Teile daraus auf photomechanischem Wege (Photokopie, Mikrokopie) zu vervielfältigen

ISSN 0065-5325

ISBN 978-3-7696-5083-9

Abstract:

For historical reasons many national mapping agencies store their topographic data in a dual system consisting of a Digital Landscape Model (DLM) and a Digital Terrain Model (DTM). The DLM contains 2D vector data representing objects on the Earth's surface, such as roads and rivers, whereas the DTM is a 2.5D representation of the related terrain heights, often acquired by Airborne Laser Scanning (ALS). Today, many applications require reliable 3D topographic data. Therefore, it is advantageous to convert the dual system into a 3D DLM. However, as a result of different methods of acquisition, processing, and modelling, the registration of the two data sets often presents difficulties. Thus, a simple overlay of the DTM and the DLM might lead to inaccurate and semantically incorrect 3D objects.

In this thesis a new approach for the adaptation of the two data sets is proposed that exploits parametric active contours (also called snakes). The method is focused on networks of roads and small rivers, which are represented by their centrelines in the GIS data base, as well as on broader rivers having a region-based description. These road and river objects can be extracted from the DLM. Afterwards, they are used to initialise snakes, defining their topology and their internal energy, whereas ALS features, such as gradients of the DTM, exert external forces to the snake via the image energy. After the optimisation process the shape and position of the snakes coincide with the ALS features.

The centrelines of linear GIS objects are adapted by applying the concept of network snakes. However, these centrelines are usually not well represented by the ALS features. Therefore, a new concept is proposed that allows to model networks having ribbon-like characteristics. This approach considers the topology as well as cross section information and is able to increase the accuracy of the matched centrelines significantly. An additional problem arises from the fact that the significance of the ALS features strongly varies for larger networks. For instance, these features are affected by the general slope of the terrain in the neighbourhood of the objects or by the reflection properties of different surface materials. Thus, a balanced weighting between the internal energy and the image energy of the basic snake model is hard to find even for small networks. Therefore, the new method combines the network snake approach with another concept that redefines the internal energy and thus the geometrical model of the snake in order to prevent changes in shape or position not caused by significant features in the sensor data. For that purpose the initial shape is utilized creating template-like snakes with the ability of local adaptation. The proposed unified snake model benefits from the topology as well as from the initial shape of the GIS data. This aspect improves the ability of the approach to deal with systematic errors. In addition to ALS features of the considered objects, context information, such as the outlines of bridges and buildings detected in the ALS data, is introduced as a new component of the image energy to support the optimisation process.

In contrast to the linear objects, larger rivers having a region-based description in GIS data bases are adapted to ALS features by means of a twin snake approach. Different constraint energies that exploit the semantics of rivers are introduced in this approach in order to increase the robustness of the optimisation process. In this context, information about the flow direction and the cross section of the rivers are integrated.

Active contour models suffer from the lack of a suitable internal evaluation. In this thesis a new approach is suggested that analyses the different energy terms after the optimisation process in order to automatically detect contour parts that did not reach a suitable position in the ALS data. This concept is able to guide the user in the post processing.

Experiments are presented that emphasize and evaluate the applicability and robustness of the proposed method. For that purpose four different data sets are used that have different specifications with respect to the ALS and GIS data. In all tests the accuracy of the original GIS data sets is significantly improved by the proposed approach.

Keywords: network snakes, roads, rivers, ALS, GIS vector data

Zusammenfassung:

Aufgrund historischer Gegebenheiten speichern die Landesvermessungen ihre topographischen Daten in einem dualen System. Dieses besteht aus dem Digitalen Landschaftsmodell (DLM) und dem Digitalen Geländemodell (DGM). Das DLM modelliert die Objekte der Erdoberfläche mit Hilfe von 2D Vektordaten, während das DGM eine 2.5D Repräsentation der zugehörigen Geländehöhen darstellt. Dabei wird das Airborne Laserscanning (ALS) oft eingesetzt, um diese Höhendaten zu erfassen. Heutzutage benötigen jedoch viele Anwendungsbereiche zuverlässige 3D Objekte. Deshalb ist es von Vorteil dieses duale System in ein 3D DLM zu überführen. Infolge unterschiedlicher Methoden für die Erfassung, Verarbeitung und Modellierung weisen die beiden Datensätze Inkonsistenzen auf. Deshalb führt eine einfache Integration des DLM und des DGM zu ungenauen und semantisch fehlerhaften Ergebnissen.

In dieser Arbeit wird deshalb eine neue Methode für die Anpassung der beiden Datensätze vorgestellt, die parametrisch aktive Konturen (auch Snakes genannt) verwendet. Der Ansatz konzentriert sich auf Netzwerke von Straßen und kleineren Flüssen, die in GIS Datenbanken üblicherweise durch ihre Mittelachsen repräsentiert werden, sowie auf breitere Flüsse mit einer flächenhaften Modellierung. Diese Straßen- und Flussobjekte können aus dem DLM einer GIS Datenbank entnommen werden. Danach werden sie genutzt, um die Snake zu initialisieren. Sie definieren somit die Topologie sowie die interne Energie der aktiven Kontur. ALS Merkmale hingegen üben über die Bildenergie externe Kräfte auf die Snake aus. Nach dem Optimierungsprozess sollten sich die Position und Form der Snake den ALS Merkmalen angepasst haben.

In dieser Arbeit werden lineare GIS Objekte mit Hilfe des Konzeptes der Network Snakes angepasst. Ihre Mittelachsen sind jedoch in den ALS Merkmalen schlecht repräsentiert. Deshalb wird ein neues Konzept vorgeschlagen, das es ermöglicht, Netzwerke mit bandartigen Eigenschaften zu modellieren. Dieser Ansatz berücksichtigt die Topologie sowie Informationen über das Profil der Objekte, was die Genauigkeit der angepassten Mittelachsen signifikant steigert. Ein weiteres Problem erwächst aus der Tatsache, dass die Signifikanz der ALS Merkmale für größere Netzwerke stark variiert. So beeinflussen zum Beispiel die Neigung des Geländes in der Nähe der Objekte oder die Reflexionseigenschaften des Oberflächenmaterials diese Merkmale. Aus diesem Grunde ist eine geeignete Gewichtung zwischen der internen Energie des ursprünglichen Snake Modells und der Bildenergie sogar für kleine Netzwerke schwierig. Deswegen kombiniert der neue Algorithmus das Network Snake Konzept mit einem weiteren Ansatz, der die interne Energie und somit das geometrische Modell der Snake so abwandelt, dass Veränderungen der Snake ohne Merkmale in den Sensordaten nicht zugelassen werden. Für diesen Zweck wird die anfängliche Form in eine starre Snake Geometrie überführt, die trotzdem zur lokalen Anpassung an die ALS Daten fähig ist. Das vorgeschlagene vereinigte Snake Modell profitiert somit sowohl von der Topologie als auch von der ursprünglichen Geometrie der GIS Daten. Dieser Aspekt verbessert die Fähigkeit der Methode mit systematischen Fehlern in den Daten umzugehen. Zusätzlich zu den Merkmalen der behandelten Objekte werden Kontextinformationen, wie die Begrenzungen von Brücken und Gebäuden in den ALS Daten, als neue Bestandteile in die Bildenergie integriert, um den Optimierungsprozess zu unterstützen.

Im Gegensatz zu den linearen GIS Objekten werden größere Flüsse, welche in den GIS Daten flächenhaft modelliert sind, mit Hilfe von Twin Snakes angepasst. Zusätzliche Bedingungen werden eingeführt, welche die Semantik von Flüssen nutzen, um die Robustheit des Verfahrens zu erhöhen. In diesem Zusammenhang werden die Fließrichtung und der Querschnitt typischer Flüsse berücksichtigt.

Ein großer Nachteil der meisten Snake Algorithmen besteht in dem Fehlen einer internen Evaluierung der Ergebnisse. Hierfür wird ein Ansatz vorgeschlagen, der die verschiedenen Energieterme nach der Optimierung analysiert, um automatisch Konturabschnitte zu detektieren, die nicht zu einer zufriedenstellenden Position konvergieren.

Experimente werden präsentiert, welche die Anwendbarkeit und Robustheit des vorgeschlagenen Ansatzes zeigen. Dafür werden vier verschiedene Testdatensätze verwendet, die sowohl für die ALS als auch die GIS Daten unterschiedliche Spezifikationen aufweisen. In allen durchgeführten Tests wird die Genauigkeit der GIS Daten durch die vorgestellte Methode signifikant verbessert.

Schlagerworte: Network Snakes, Straßen, Flüsse, ALS, GIS Vektordaten

Table of contents:

1	Introduction	9
1.1	Motivation	9
1.2	Objectives	10
1.3	Structure of the thesis	12
2	Background and related research	13
2.1	Basics	13
2.1.1	Airborne laser scanning	13
2.1.1.1	Basic principle.....	13
2.1.1.2	Interaction of the laser pulse with the target	15
2.1.2	Parametric active contours (snakes)	17
2.1.2.1	Contours	17
2.1.2.2	Energy functional	18
2.1.2.3	Optimisation	20
2.2	Related research.....	21
2.2.1	Methods for the adaptation of spatial data sets.....	21
2.2.1.1	General comments.....	21
2.2.1.2	Images and DTM.....	23
2.2.1.3	Different 2D vector data sets.....	24
2.2.1.4	Vector data and DTM.....	27
2.2.2	ALS based extraction of topographic features and objects.....	31
2.2.2.1	Filtering of point clouds	31
2.2.2.2	Break lines.....	32
2.2.2.3	Roads and bridges	33
2.2.2.4	Rivers and water areas.....	36
2.2.2.5	Buildings	37
2.2.3	Snakes for the extraction of topographic objects.....	38
2.3	Summary and conclusions of the literature review.....	41
3	A new method for the adaptation of GIS objects to ALS data by means of active contours.....	43
3.1	Basic concept and outline	43
3.2	Contour initialisation from GIS data base	47
3.2.1	Description of the vector data provided by the NMA using the example of ATKIS.....	47
3.2.2	Selected objects for the adaptation process	47
3.3	Pre-processing of the ALS data	48
3.4	Network snake strategy	51
3.4.1	Internal energy	51
3.4.1.1	Rigid snake model.....	52
3.4.1.2	Network snakes	53
3.4.1.3	Ribbon network snakes	54
3.4.2	Image energy	56

3.4.2.1	General image energy for network objects.....	56
3.4.2.2	ALS energy for road networks	57
3.4.2.3	Building energy	57
3.4.2.4	Bridge energy	58
3.4.2.5	Image energy for ribbons	59
3.4.2.6	Modification of the image energy for river networks.....	60
3.5	Twin snake strategy	61
3.5.1	Image energy for the twin snake model of broader rivers	61
3.5.2	Constraints for the twin snake model of broader rivers	62
3.5.2.1	Twin snakes.....	63
3.5.2.2	Flow direction	63
3.5.2.3	Gradient direction.....	64
3.6	On the relationship of ribbon and twin snakes	66
3.7	Interpretation of the energy terms with respect to an internal evaluation.....	68
3.8	Parameters and setup	71
3.9	Discussion	74
4	Experiments.....	76
4.1	Overview	76
4.1.1	Description of the test methodology	76
4.1.2	Test data.....	77
4.2	Test of the adaptation of roads	80
4.2.1	Sensitivity analysis	80
4.2.1.1	Quality of reference data	81
4.2.1.2	Quality of the original GIS data	82
4.2.1.3	Node distance	82
4.2.1.4	Shifted initialisation	83
4.2.1.5	Rotated initialisation	86
4.2.1.6	Variation of initial ribbon width.....	87
4.2.1.7	Convergence behaviour.....	88
4.2.1.8	Weighting between E_{int} and E_{image}	89
4.2.1.9	Summary of the sensitivity analysis	91
4.2.2	Tests of the rigid snake model	92
4.2.3	Bridges.....	95
4.2.4	Evaluation of larger road networks.....	98
4.2.5	Internal evaluation	106
4.3	Test of the adaptation of rivers	108
4.3.1	Evaluation of river networks	108
4.3.2	Evaluation of the twin snake strategy for broader rivers	110
4.3.2.1	Effects of the constraint energy terms	110
4.3.2.2	Evaluation of larger river segments.....	112
5	Conclusion and outlook.....	115
	References.....	118

Table of contents	7
-------------------	---

Curriculum Vitae - Lebenslauf	126
Acknowledgement - Danksagung	127

1 Introduction

1.1 Motivation

During the last thirty years Geographic Information System (GIS) have been introduced to many sectors of modern societies, such as science, economy, and public administration. Applications range from spatial analysis in scientific research or industry to resource management and urban planning. Like any other information system a computer-assisted GIS consists of a data base and application software. However, entities of GIS data bases are always related to some kind of spatial coordinates as a main property. The set of tools embedded in a GIS enables the user to collect, edit, store, reorganise, model, analyse, and visualise and distribute the spatial information (Kraus, 2000).

The presented work is focused on GIS data provided by national mapping agencies (NMA). NMA supply the basic topographical data that contain the natural and artificial objects on the Earth's surface, such as roads, rivers, urban areas or forests. For further analysis these data can be combined with specialist knowledge in various fields, such as geology or transportation. In many respects the applicability of the topographical information for a certain use is closely related to the quality of the data. Zhang and Goodchild (2002) differentiate several quality criteria for geo-spatial data, namely completeness, positional accuracy, attribute correctness, and temporal correctness, all of them defined for each object. For instance, a few years ago the NMA generated Digital Terrain Models (DTMs) with a ground resolution of 20 m and a height accuracy of 0.5 m. This data set was not suitable for modelling flood risk scenarios. However, with new technologies, such as Airborne Laser Scanning (ALS) or automatic stereo matching, both capable of providing high densities of 3D points ($>2 \text{ pts/m}^2$) and a better height accuracy ($<0.15 \text{ m}$), DTMs can be derived that have opened such fields of application. Thus, the different quality criteria of geospatial data strongly depend on the application. If the quality of the data can be improved without considerable expenditure, data providers should take this opportunity in order to increase the applicability of their data and thus the number and size of their user groups.

For historical reasons national topographic data bases are available in a dual system in many countries, e.g. in Germany and Switzerland. Such a dual system usually consists of a digital landscape model (DLM) and a DTM. The DLM describes the objects on the Earth's surface using 2D vector data and additional attributes, whereas the DTM is a continuous 2.5D representation of the Earth's surface modelled by terrain points in a regular grid or in a triangulated irregular network (TIN). Today, 3D modelling of the topographic objects is required in many applications in administration, research, and industry, e.g. for planning infrastructure or for flood risk modelling. For this purpose an integration of the 2D vector data and the height information is necessary. In this context, an important quality criterion is the *consistency* of two or more data sets that cover similar areas or model identical objects in a different way. Of course, the consistency is closely related to the four quality criteria of the individual data sets mentioned above. If the quality of both data sets is high, the consistency should be high as well. However, there are discrepancies between the DLM and the DTM due to different methods of acquisition, processing, and modelling (Fig. 1 left). This inconsistency may result in bodies of standing waters having physically impossible height variations or streets with invalid gradients. As a consequence, integration without matching and adapting the data sets to each other leads to semantically incorrect results, i.e. the object geometry will not be consistent with the rules and laws that arise from the meaning and function of the objects. For example, a river transports water from its spring to its mouth. In this process the potential energy is transformed into kinetic energy. Thus, the flow direction of the river in a 3D DLM has to point from higher to lower

terrain. In addition to physical constraints, man-made objects also have to follow anthropogenic rules and laws. For instance, the slopes of roads in as well as across the driving direction should be adapted to the capabilities of cars. Following these considerations the semantic correctness may suffer from the inconsistency between the data sets. Therefore, the semantics of the 3D objects has to be considered by the data integration process. This is the reason why the DLM and the related height information have to be adapted as a basis for accurate combined visualization and processing (Fig. 1 right).

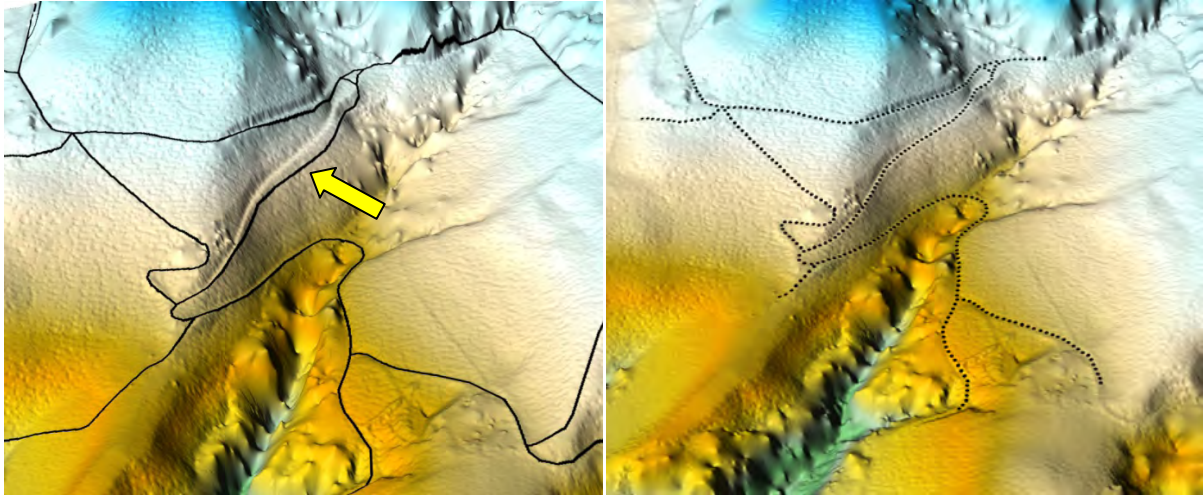


Figure 1. Left: large differences between GIS roads and ALS data (yellow arrow); right: roads adapted using the proposed method.

Furthermore, the restored consistency also facilitates the simultaneous updating of the two data sets. For instance, the incorporation of new 3D objects or object parts into the GIS data base will suffer from discrepancies between DLM objects and the DTM in their vicinity. Additionally, consistent and accurate data sets can also be used for GIS-supported object extraction without extensive pre-processing, for instance by using prior knowledge from GIS data bases for the determination of accurate probability density functions for a supervised classification.

Today, consistent height and position information of topographic objects are not available in many countries. In order to overcome this problem, some NMA discard the old data and capture consistent and accurate 3D topographic information from scratch. Nevertheless, this strategy is very time and cost consuming. The alternative is an automatic adaptation of the DLM and the DTM, but there are no ready-to-use solutions for that task. The following objectives of this thesis are derived from these considerations.

1.2 Objectives

The general goal of this thesis is to develop an algorithm for the adaptation¹ of 2D Digital Landscape Models (DLM) and the related DTM. In this context the thesis is mainly focused on linear DLM objects relevant for traffic, namely roads and rivers. The NMA are strongly interested in the improvement of the quality of their road and river networks. The importance of these objects within the DLM is expressed by short updating cycles and the highest acquisition accuracy standard defined by the NMA. The generalisation priorities for the derivation of topographic maps give also hints for the

¹ The term *adaptation* in this thesis refers to the process of establishing data sets congruent with respect to their coordinates. Similar concepts with a slightly different meaning are *matching*, *alignment*, *conflation* or *registration*.

relevance of these objects. The main reason is that due to their importance as transportation links, roads and rivers in topographic data bases are of special interest for the economy, for instance in navigation systems. However, the reliability, accuracy, consistency, and short updating cycles are crucial aspects for the applicability of this data. Beside the relevance for the users the chosen objects fulfil some requirements emerging from the goal of this work. Significant features have to reveal the position of these objects in the DTM. These features enable the adaptation and the improvement of the vector data. Because roads and rivers often provide only weak and fragmented features in the DTM, the use of these objects for the adaptation is challenging and not extensively analysed in the literature. However, as will be seen the network property of roads and rivers is able to bridge gaps between significant features and thus support the adaptation process. Furthermore, for the determination of area-wide transformation parameters a dense net of shift vectors provided by the algorithm is crucial. Therefore, an appropriate spatial distribution of the adapted objects is necessary. In contrast to buildings, which have indeed stronger features in ALS data, roads and rivers provide a more homogeneous spatial coverage.

ALS is assumed to be the primary data source for the derivation of the DTM. Besides digital stereo matching, this technique is frequently used by the NMA for the acquisition of area-wide height information. Thus, not only the DTM heights but also various other features can be exploited for the adaptation process. ALS basically delivers a 3D point cloud, from which a digital surface model (DSM) can be derived. Many filtering methods have been developed in order to separate the bare ground information from the point cloud that can be used for the interpolation of the DTM. The DSM also contains information about objects situated on the terrain that can be integrated in the algorithm. In addition, some ALS data sets include first and last echoes or even the digitised full waveform of the entire reflected signal. Furthermore, radiometric features can be determined from the backscattered signal, such as amplitude and width of the echoes, describing the reflectance properties of the illuminated objects. In general, the new adaptation method should work only with height information, but also has to enable the uncomplicated integration of other available ALS features.

The considered GIS objects, such as road or river networks, typically have an accuracy of 3-5 m in topographic data bases of the NMA, with local deviations that may reach 15 m (for Germany cf.: ADV, 2011). Other less important object classes, such as borderlines of land use, are even of considerably lower quality. Based on the fact that the horizontal accuracy of the ALS data (<0.5 m) is much better than the DLM accuracy, it is the objective of the thesis to present a new algorithm for the adaptation of the 2D GIS data to the position of the related ALS features. GIS objects adapted to the ALS data should also match the DTM.

An integral part of the objectives is the restoration of the semantic correctness of the considered objects in an integrated 3D data set. Based on the assumption that objects with consistent 3D coordinates are also semantically correct within the modelling accuracy, a geometric adaptation of the DLM data to the ALS features will consider this objective. 3D modelling of the precisely adapted data sets generates an image of the reality within the modelling accuracy and thus automatically establishes the semantic correctness. For instance, if the 2D borderline of a lake matches the ALS features, the requirement of a horizontal lake surface will be fulfilled considering the accuracy of the ALS heights. Obviously, the semantics of the objects provide valuable information for the adaptation process. Therefore, the new method should be able to exploit the semantic properties within the algorithm. For example, constraints can be derived from the semantics in order to support the choice of suitable features for the adaptation guiding the vector objects to the correct position in the ALS data.

A search through the relevant literature offers different approaches in order to tackle the adaptation problem. The most obvious strategy extracts suitable features, object parts, or entire objects from the height data at first and matches the extraction results to the entities of the DLM vector data. However, the extraction step contains some difficulties. The DTM, which is to be considered as the minimum input for the adaptation method to be developed, often provides only weak, fragmented, or in flat terrain almost no features concerning especially road objects. Because of this fact, to the knowledge of the author an efficient road extraction algorithm that relies only on the DSM or DTM does not exist. Even the detection of suitable DTM features, such as break lines, that could be used as input for the vector-to-vector matching is sophisticated. Furthermore, the transition from implicit to explicit object description is always associated with a loss of information inherent in the grid cells. Another challenge of this strategy is the assignment of the unclassified features to the correct objects or object parts.

Parametric active contours, also called snakes, present an alternative strategy for the adaptation of the two data sets avoiding an explicit feature extraction in the height data and the subsequent assignment of these features to the DLM objects. The network snake approach (Butenuth, 2008) seems to provide a suitable basis for the adaptation of the roads and smaller rivers that are modelled as linear features using their centre lines in the DLM. However, the weak features of the considered objects in the height data hamper a well-balanced global parameter setup even for small networks. The image energy derived from these features is often not able to compensate the straightening and shortening effects of the internal energy in curved snake parts or at dead ends of the contour network. As could be shown experimentally this fact may result in undesired changes of the DLM objects that are not caused by features in the height data. Another drawback of network snakes arises from the aspect that the image energy is sampled only at one point for each contour node corresponding to the centre lines of the road and river objects, where the position of these objects is not well defined by the features. It is therefore one goal of this thesis to considerably extend the basic network snake approach in order to present a unified snake model that overcomes these drawbacks and is additionally tailored to the objectives mentioned above. In this context the work is focused on the design of an appropriate internal energy determining the main object model and on the derivation of a suitable image energy based on the ALS data. The proposed method should also be able to integrate context objects, which can support the adaptation process. Furthermore, a second strategy based on twin snakes (Kerschner, 2003) is suggested for the adaptation of larger rivers that have a region-based description in the DLM. For this strategy knowledge about the semantics of the objects, such as the flow direction of rivers, is integrated via several constraint energies.

1.3 Structure of the thesis

This introduction containing the motivation and the objectives of the thesis is followed by the theoretical background of the proposed method and the status of research in the second chapter. In chapter 3, the new method for the adaptation of DLM objects to ALS data is explained in detail. Afterwards, experiments considering different strategies and data sets are presented and evaluated in chapter 4. Finally, the conclusion in chapter 5 summarises the advantages and disadvantages of the proposed approach and deduces suggestions for further research.

2 Background and related research

The main goal of this thesis is the adaptation of 2D DLM vector objects to ALS data using active contours in order to support the semantically and geometrically correct integration of the two given data sets. The first part of this chapter presents the theoretical background for the new adaptation approach. Initially, the basic principles of ALS as the main data source and the theory of parametric active contours are given. In the second part of this chapter several research areas with connections to the objectives of this thesis are briefly reviewed. A classification of methods for the adaptation of spatial data sets is given in order to provide the background for a subsequent analysis of strategies which deal with the adaptation of 2D topographic data and height information or can be applied for this task. Subsequently, literature about feature and object extraction from ALS or other height-related data is summarised. In this context the focus lies on roads and rivers, but also other objects, such as bridges and buildings, are briefly discussed due to their relevance for the adaptation process in this thesis. Subsequently, applications of active contour models in photogrammetry and remote sensing are reviewed. This chapter is closed with an assessment of possible strategies based on existing approaches highlighting their pros and cons as well as drawing conclusions for the design of a new method.

2.1 Basics

2.1.1 Airborne laser scanning

In the first part of this section the principles of airborne laser scanning (ALS) are briefly described. In this context the measurement process and the related error sources are mentioned. This analysis contributes to an improved understanding of the data generated by this measurement method and specifies the achievable accuracy, which is important for the adaptation process. ALS provides area-wide 3D points, which can be used to generate a DSM or, in combination with filtering algorithms, a DTM. Additionally, some ALS devices are able to record intensity values of each echo or even the full backscattered waveform of the emitted laser beams. For a useful integration of such features in the adaptation process the complex interaction of the laser beam and the objects of the Earth's surface is explained in the second part of this section. Afterwards, relationships between these features and the reflectance properties of the illuminated objects can be derived and exploited for the new adaptation algorithm.

2.1.1.1 Basic principle

Good overviews about some of the basic principle of ALS, also called Lidar (light detection and ranging) or laser radar, can be found in Baltsavias (1999), Wagner et al. (2006), and Mallet & Bretar (2009), the latter focusing on modern full waveform systems. ALS is an active remote sensing technique, which provides area-wide height information in the form of irregularly distributed 3D points. Most ALS systems are based on pulsed lasers, which emit short laser pulses into the direction of the target. During the interaction of the laser beam with the target surface, a part of the emitted energy may be absorbed by the surface material, whereas the rest is backscattered into different directions. In the receiver, a photo diode records the portion of the signal reflected into the direction of the sensor and the round-trip time of flight t of the signal is measured. The distance R from the sensor to the target is then calculated by:

$$R = c \cdot \frac{t}{2} \quad (1)$$

using the group velocity of light c . For flat target surfaces Schenk (2001) specifies the error contribution of the ranging systems including systematic and random errors with ± 5 cm.

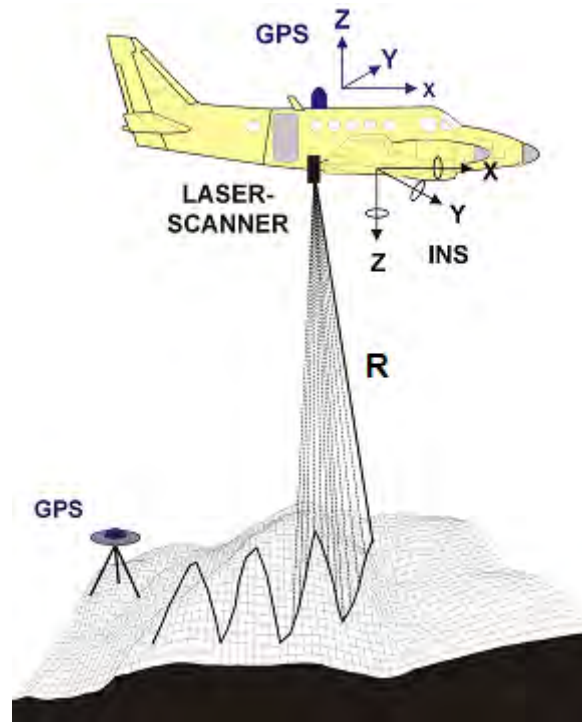


Figure 2: ALS principle (Pfeifer, 2007, adapted)

In order to calculate the 3D coordinates of the backscattering target, the position and orientation of the scanner and the direction of emission have to be known. For that purpose the airborne platform is equipped with a global positioning system (GPS) antenna and an inertial measurement unit (IMU). From the observations of these onboard systems the parameters of the exterior orientation can be determined, which enables the reconstruction of the flight path and thus a direct georeferencing (see Fig. 2). Under good conditions the flight path can be determined in post-processing with an accuracy of ± 5 -10 cm (Pfeifer & Briese, 2007). This value includes different systematic errors, such as mounting errors of the different measurement devices, errors in GPS and IMU observations, and synchronisation as well as interpolation errors. Calibration flights are conducted in order to determine the IMU misalignment and to improve the GPS offset vector (Pfeifer & Briese, 2007). A detailed overview about the different systematic errors of the ALS measurement systems can be found in Schenk (2001).

In order to provide a 2D horizontal distribution of the gathered points a scanning device is required. Various deflection methods for the laser beam, such as oscillating and rotating mirrors, are used, which result in different scan patterns as the platform moves over the ground. In this process the velocity of the airborne platform ensures the spatial distribution of the scanned 3D points in flight direction. Depending on the speed of the platform, the pulse repetition rate, the flying altitude, and the scanning method, modern systems can generate point clouds with more than 100 points/m² for specific applications (Mallet & Bretar, 2009). 3D points gathered by modern ALS systems usually have a planimetric accuracy better than 0.4 m and a vertical accuracy better than 0.1 m in flat terrain (Ahokas, 2003). In order to achieve ALS points of high accuracy, post processing has to be applied to the raw data. An additional quality improvement can be obtained by the adjustment of neighbouring flight strips, which are frequently somewhat tilted and shifted with respect to each other due to the systematic errors already mentioned. Two mathematical models have been used for strip adjustment. One

is based on discrepancies within the point cloud in combination with correction functions, whereas the other uses the original observations and models of the sensor orbit similar to the error model of the system calibration. However, the original observations, such as laser range, deflection angle, GPS and INS measurements, are not always delivered by the companies. Due to the lack of homologous points, linear features (Vosselman, 2002), planar features, such as roof planes (Kager, 2004), or gradient correspondences in TIN structures (Maas, 2000) are used in order to determine the discrepancies between the different strips. The parameters of the correction model can then be derived from the discrepancies.

ALS systems are able to gather not only one discrete echo per emitted pulse, but also several echoes with related intensity values characterising the power incident at the receiver. Modern full waveform scanners even record a discretized form of the entire signal that is backscattered to the receiver. Although full waveform data is not used in this work, an improved understanding of the physical principles that govern the interaction between the laser beam and different illuminated targets facilitates the interpretation of the ALS height and intensity data and the derivation of suitable features for the adaptation process. Therefore, in the next section this aspect is analysed in more detail.

2.1.1.2 Interaction of the laser pulse with the target

Based on the radar equation, Jelalian (1992) describes the fundamental relations between the transmitted power P_t , the reflecting object and the received power P_r of the backscattered laser signal (Fig. 3). Sensor and target dependent parameters are separated and an object dependent cross section σ is defined (see also Ulaby et al., 1982):

$$P_r = \frac{P_t \cdot D_r^2}{4 \cdot \pi \cdot R^4 \beta_t^2} \cdot \eta_{sys} \cdot \eta_{atm} \cdot \sigma \quad \text{with} \quad \sigma = \frac{4 \cdot \pi}{\Omega} \cdot \rho \cdot dA \quad (2)$$

D_r	aperture diameter
R	distance between sensor and target
β_t	laser beam divergence
Ω	solid angle of a cone containing the backscattered power (assuming a uniform distribution)
η_{sys}	system transmission factor
η_{atm}	atmospheric transmission factor
dA	effective illuminated area of the scatterer
ρ	reflectivity of the backscattering surface material

The backscattering model behind this cross section term postulates a uniform reflection into a cone of the solid angle Ω . Outside the cone no reflection occurs, yielding a cross section of zero. Surfaces that are rough compared to the wavelength of the incoming radiation result in a large Ω value, which corresponds to diffuse reflection, whereas a small Ω indicates a specular behaviour of the illuminated surface. For a complete Lambertian scatterer the solid angle becomes π , and the cross section results in (Wagner et al., 2006):

$$\sigma = 4 \cdot \rho \cdot dA \quad (3)$$

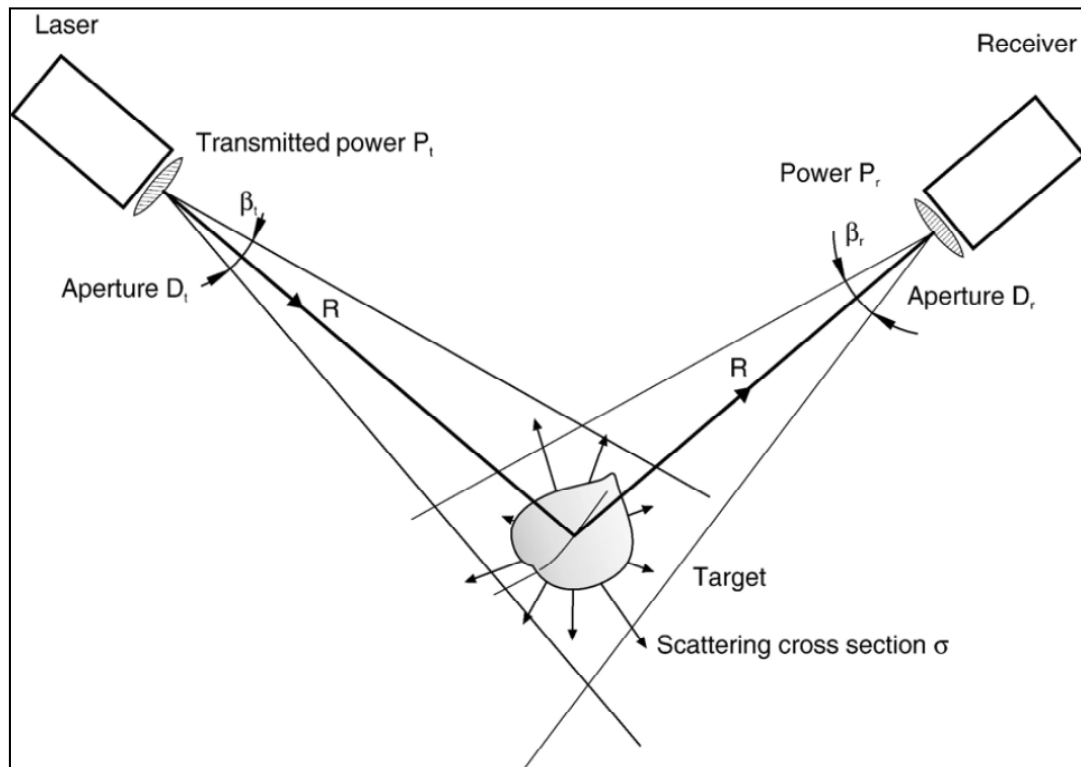


Figure 3: Radar equation: geometry and important parameters (Wagner et al., 2006)

The ALS intensity value might be derived from the reflected signal (the received power) in different manners by the providers. However, in any case it is a function of the signal energy, which is responsible for the major part of the spatial variation of the cross section (Wagner et al., 2006). Therefore, the ALS intensity contains information about reflectivity, directivity, and the effective area of the reflecting surface of an object and is thus an important feature for the adaptation process. Most ALS devices operate in the near infrared domain ($\lambda = 1000\text{-}1500\text{nm}$). The objects of interest in this thesis (roads and rivers) have a low reflectivity and thus a small cross section in this domain (asphalt 0.2, water except for illumination in nadir direction < 0.3 (Jelalian, 1992)). Therefore, these objects usually appear dark in ALS intensity images and suitable features for the adaptation process can be derived from this fact. However, for the illumination in nadir direction the specular reflection of smooth waveless water surfaces sometimes disturbs this assumption (high reflectivity and thus high ALS intensity). Some authors (e.g., Höfle & Pfeifer, 2007) propose a radiometric correction of the intensity values based on the laser range equation. For that purpose the parameters of the reflection model for the actual surface have to be known (e.g., solid angle of the reflection cone Ω in Eq. 2). However, this implies that also the object class of the illuminated surface is available, which is not the case for classification tasks. Another possible strategy for the pre-processing of the ALS intensity is suggested by Brzank et al. (2008), who use training areas in order to evaluate the significance of the intensity values for the separation of water and land areas by statistical tests under consideration of the incidence angles of the laser beams (cf. section 2.2.2.4). However, the definition of suitable training areas is difficult for the small river networks and even for broader rivers. Therefore, in this thesis the uncorrected intensity values are used to define the image energy of active contours. The applicability of these values is visually checked.

2.1.2 Parametric active contours (*snakes*)

First introduced by Kass et al. (1988), active contour models combine feature extraction and geometric object representation in image analysis in a sophisticated way. Two realisations of this model are distinguished in the literature. Whereas a *parametric active contour* (Kass et al., 1988; Blake & Isard, 1998), also called *snake*, is an explicit representation of the contour in its parametric form, the *geometric active contour* (Malladi et al., 1995; Caselles et al. 1997) describes the contour as a zero level line of a level set function. The main advantage of the level set approach arises from its flexible topology. In contrast, the parametric method has to be extended in order to enable splitting and merging of entities, e.g. (McInerney & Terzopoulos, 1995). For the goals in this thesis the given topology of the road network has to be preserved and even exploited to stabilise the adaptation process. Furthermore, even the geometry of the initialisation from the GIS database should not change too much. Thus, parametric active contours are better suited for this particular application than level sets. Additionally, the front of level sets propagates into the direction of the curve normal according to the curve evolution theory and should be stopped by the image edges. This process is controlled by the related weights and the contour tends to leak out at weak edges. Considering the often fragmented features of road and river objects in height data, this aspect heavily influences the applicability of level sets to our task. For these reasons parametric active contours are preferred over geometric active contours, and the description of theory will be focused on that method.

2.1.2.1 Contours

In analogy to contour lines in topographic maps (i.e., lines of constant elevation), the term *image contours* is originally applied to lines of constant brightness or gradient in the context of image processing (Russ, 1995). Such image contours often represent continuous outlines of objects. If there is a pair of neighbouring pixels in a discrete representation of an image with one value brighter than and one value darker than the contour level, then the contour line must pass somewhere between them. This aspect requires the possibility of a sub-pixel representation of the contour in Euclidean space \mathbb{R}^2 . One representation of contours or objects in general in this space is the *vector model*, where the point v_i defined as coordinate pair (x,y) carries the geometric information (Bartelme, 2005). The vector model represents one-dimensional objects as lines that connect two points. Curvilinear objects and the boundaries of area objects, which both can be described as contours, are modelled as polynomials or concatenated line segments. For area objects the first and the last point of the sequence of line segments are identical, resulting in a closed object boundary as well as in a closed contour. Analogous to contours as well as active contours, objects in GIS data bases, such as the German Authoritative Topographic Cartographic Information System (ATKIS), are normally represented by the vector model. Therefore, the data representations can be easily transferred to active contour models. The vector model is closely related to the graph theory (Bartelme, 2005), which can be used to model the concept of topology for objects with network characteristics. In this theory points are called *nodes* or vertices of the graph, which are linked by line segments also named *edges*. The number of edges terminating at a node determines the *degree* of this node. The degree of a node and the connected edges give cues about the contribution of this node to the topology as well as to the network property of the entire object. The objects of interest of this thesis, roads and rivers, form network structures on the Earth's surface. Thus, the topology carries valuable information for the adaptation of these objects. An interesting extension of the graph theory assigns directions to the edges resulting in a directed graph. For example, this concept is suitable in order to model the flow direction in a river network.

2.1.2.2 Energy functional

In the general model of snakes the optimal shape and position of a contour in an image are determined in an iterative energy minimisation process starting from an initialisation. In the taxonomy of image analysis, snakes represent a top down strategy for the extraction of linear features or objects. Knowledge about the geometric and topological model of the desired object contour is integrated in the initialisation, in the form of smoothness terms, as well as in additional constraints. After defining the related parameters, snakes are able to find the locally optimal position and shape of this object model in an image. In this process the current status of the contour model with respect to the image features is assessed by an energy functional. Three energy terms (Eq. 4) were introduced by Kass et al. (1988). The internal energy E_{int} defines the elasticity and rigidity of the curve. The image energy E_{image} should represent the features of the object of interest in an optimal manner in order to attract the contour step by step to the desired position. Additional terms (constraint energy E_{con}) can be integrated in the energy functional forcing the contour to fulfil predefined external constraints. The total energy E_{snake}^* along the contour is minimised:

$$\begin{aligned} E_{snake}^* &= \int_0^1 E_{Snake} [\mathbf{v}(s)] ds = \\ &= \int_0^1 \left\{ E_{int} [\mathbf{v}(s)] + E_{image} [\mathbf{v}(s)] + E_{con} [\mathbf{v}(s)] \right\} ds \rightarrow \min \end{aligned} \quad (4)$$

In Eq. 4, $\mathbf{v}(s) = [x(s), y(s)]$ is the curve parameterised by its arc length $s \in [0, 1]$. Kass et al. (1988) proposed a model for the internal energy motivated by the definition of splines:

$$E_{int} [\mathbf{v}(s)] = 0.5 \cdot \left[\alpha(s) \cdot |\mathbf{v}_s(s)|^2 + \beta(s) \cdot |\mathbf{v}_{ss}(s)|^2 \right] \quad (5)$$

In Eq. 5, \mathbf{v}_s and \mathbf{v}_{ss} are the derivatives of \mathbf{v} with respect to s . The first order term, weighted by α , is responsible for the elasticity of the curve. Minimising this term minimises the arc length of the curve, so that high values of α result in very straight and short curves. The second order term, weighted by β , forces the snake to act like “a stiff but flexible rod” (Blake & Isard, 1998) and determines the rigidity of the curve. High values of β cause a smooth curve while contour parts with a small β are able to model the behaviour of corners. Both weights α and β can be varied depending on the parameter s , in order to consider prior knowledge about the change of the smoothness model along the curve. However, for the sake of simplicity many approaches try to find a suitable setting of the weights for the entire curve. The internal energy and especially its first order term generate a shrinking effect, which is desired for closed contours (first node is equal to the last node) with initialisations outside the desired object border. Therefore, the distance between neighbouring nodes continuously decreases if no compensation force, such as image energy, exists. In order to reduce this shrinking effect, several approaches suggest an alternative term for the internal energy. Williams & Shah (1992) propose a first order smoothness term whose energy increases if the deviation of the distance of two neighbouring nodes from the average distance of two nodes is large. This formulation preserves an equal node distance and thus avoids the accumulation of nodes at strong image features. However, the mean distance of the nodes has to be updated for each iteration. In a similar manner Radeva et al. (1995) uses the difference between the original internal energy of the initialisation and the current internal energy as prior shape model. Due to the geometry-preserving property, this

approach is especially interesting for the adaptation of spatial data sets. An adaptation of this approach is used in this thesis and will be explained in section 3.4.1.1. Other algorithms tackle the shrinking problem by fixing the end nodes (e.g., Butenuth 2008) or by introducing hard constraints, such as a minimum distance of consecutive nodes (Amini et al. 1988). Kerschner (2003) suggests that the first order term be completely removed and the second order term be replaced by the square of the finite differences of two normalised first order differences.

Additionally, the internal energy has been modified in order to model networks of connected snakes (Butenuth 2008). His extension enables the integration of nodes of higher degree having more than two related edges into the contour model. These particular nodes take part in the calculation of the smoothness terms of each adjacent edge, but smoothing across these nodes is avoided. This modification allows the preservation and exploitation of the network topology, thus stabilising the simultaneous optimisation of connected contour parts.

Fua (1996) introduces the width $w(s)$ of ribbon-like structures as additional parameter, resulting in an extended contour model of the form $\mathbf{v}(s) = [x(s), y(s), w(s)]$. Like x and y , the width is also affected by the smoothing of the internal energy avoiding rapid changes between neighbouring nodes. Instead of a single line this concept allows the simultaneous extraction of the two borderlines of ribbon objects by using the related image features. The network and ribbon snake concepts are especially interesting for the goal of this thesis. The basic models and the combination of the concepts proposed in this thesis will be explained in detail in chapter 3.

The image energy can be simply defined using the image intensity itself, in order to attract the contour to dark or (with a negative sign) to bright lines. If the desired objects are represented by image edges, functions of the magnitudes of the gradient image are able to describe the image energy in a sufficient manner. Other authors use terms derived from a distance map related to the closest edge pixel (Cohen & Cohen, 1993) or the gradient vector flow (GVF) (Xu & Prince, 1997) for an improved representation of the image energy. In the original formulation of the image energy the edges provide a small attraction range for the contour, which can be extended by smoothing. The GVF principle alleviates this drawback by extending the influence of image edges into homogeneous regions. Thus, contours can be also attracted towards concave object border lines. However, in the presence of many fragmented edges this vector field can be affected by disturbances, which may prevent the convergence of the snake optimisation process. Generally, the design of the image energy is strongly related to the actual application and has to be based on knowledge about the appearance of the objects of interest in the image data. In our particular case the image energy is derived from ALS data. Thus, the overview about feature and object extraction from ALS in section 2.2.2 gives valuable information for the modelling of the image energy in this thesis.

Constraints can be considered by additional energy terms (E_{con}), which apply external forces on the snake. For example, the contour could be connected to fixed points using spring forces (Kass et al., 1988). Two points v_1 and v_2 can be coupled with a suspension rate k by the following equation:

$$E_{con} = -k \cdot (v_1 - v_2)^2 \quad (6)$$

One point in Eq. 6 (e.g., v_1) represents a certain snake node, whose position has to be linked to the second point v_2 according to prior knowledge or by user interaction. This connection of the snake to predefined points, such as precisely

measured landmarks, can be also interpreted as the setting of a geodetic datum in order to fix the position and orientation in a coordinate system to some extent. Kerschner (2003) uses a similar term in order to optimise two approximately parallel contours of known distance simultaneously. In order to establish network characteristics between different snakes, Fua (1995) and Jasiobedski (1993) install angular constraints and also spring forces. Another idea of Kass et al. (1988) is the implementation of repulsive forces by integrating so-called volcanoes. This prevents the snake from entering undesired areas.

2.1.2.3 Optimisation

In order to obtain the optimal position and shape of the snake in the image, the energy functional in Eq. 4 has to be minimised. This task is carried out by Kass et al. (1988) by applying variational calculus. This method is also used in this thesis, so that it is briefly explained. For the sake of simplicity the sum of the image and constraint energies is combined to the *external energy* E_{ext} and the weight parameters α and β are kept constant along the entire contour. In that case the minimisation of the functional results in the two independent Euler equations (for x and y):

$$\frac{\delta E_{ext}[\mathbf{v}(s)]}{\delta \mathbf{v}(s)} + \alpha \cdot \mathbf{v}_{ss}(s) + \beta \cdot \mathbf{v}_{ssss}(s) = 0 \quad (7)$$

The derivatives of \mathbf{v} can not be calculated analytically. Thus, they are approximated by means of finite differences. With the substitution $f_v(\mathbf{v}_i) = \delta E_{ext} / \delta \mathbf{v}_i$ (where the node index i replaces the arc length s), the Euler equations can be rewritten:

$$\begin{aligned} & \alpha \cdot (\mathbf{v}_i - \mathbf{v}_{i-1}) - \alpha \cdot (\mathbf{v}_{i+1} - \mathbf{v}_i) \\ & + \beta \cdot (\mathbf{v}_{i-2} - 2\mathbf{v}_{i-1} + \mathbf{v}_i) - 2\beta \cdot (\mathbf{v}_{i-1} - 2\mathbf{v}_i + \mathbf{v}_{i+1}) \\ & + \beta \cdot (\mathbf{v}_i - 2\mathbf{v}_{i+1} + \mathbf{v}_{i+2}) + (f_v(\mathbf{v}_i)) = 0 \end{aligned} \quad (8)$$

In the basic formulation all necessary finite differences can be calculated if $\mathbf{v}(s)$ represents a closed contour with $\mathbf{v}(0) = \mathbf{v}(n)$, where n is the number of nodes in the snake. In matrix form, Eq. 8 reads:

$$\mathbf{A} \cdot \mathbf{v} + f_v(\mathbf{v}) = 0 \quad (9)$$

\mathbf{A} is a pentadiagonal banded matrix, except for the entries concerning the connection of the first and the last point of a closed contour; the extension to contours that are not closed is explained in the context of the network snakes model in section 3.4.1.2. In order to solve Eq. 9 in an iterative way, the right hand side is set equal to the product of a defined step size γ and the negative time derivatives of the left side. By assuming that the derivatives of the external energy $f_v(\mathbf{v}_i)$ are constant during a time step, an explicit Euler step regarding the image energy is obtained. The internal energy, completely determined by the banded matrix \mathbf{A} , results in an implicit Euler step if the time derivative is calculated at time t rather than $t-1$. Following these considerations the problem is now specified by:

$$\mathbf{A} \cdot \mathbf{v}_t + f_v(\mathbf{v}_{t-1}) = -\gamma \cdot (\mathbf{v}_t - \mathbf{v}_{t-1}) \quad (10)$$

The time derivative vanishes at equilibrium and Eq. 10 corresponds to Eq. 9. By means of matrix inversion the final solution results from:

$$\mathbf{v}_t = (\mathbf{A} + \gamma \cdot \mathbf{I})^{-1} \cdot [\gamma \cdot \mathbf{v}_{t-1} - f_v(\mathbf{v}_{t-1})] \quad (11)$$

In Eq. 11, \mathbf{I} is an identity matrix. Analysing Eq. 11, the position and the shape of the current contour \mathbf{v}_t can be determined if the connections and weights between the nodes, which define the internal energy in matrix \mathbf{A} , the previous state of the contour \mathbf{v}_{t-1} , and the derivatives of all external energies for the iteration $t-1$ are available. Thus, the image energy as well as the constraint energy have to be differentiable with respect to the image coordinates.

There are also other methods for the optimisation of parametric active contours. Amini et al. (1988) suggest dynamic programming. Trinder et al. (2000) combine the snake model with a simulated annealing approach in order to tackle problems with local minima. Gruen & Li (1997) suggests a least squares adjustment for optimisation and defines the image energy based on template matching of simple edge patterns.

2.2 Related research

2.2.1 Methods for the adaptation of spatial data sets

2.2.1.1 General comments

The combination of two spatial data sets towards a consistent entity contains on the one hand an adaptation step in order to remove the inconsistencies between the data sets and on the other hand an integration step, which is responsible for a unified data model. This section classifies, reviews, and assesses approaches that either deal with the adaptation, the integration, or tackle both tasks simultaneously. In this context not only methods combining GIS vector data and height data are analysed but also algorithms dealing with other spatial data sets that could be adapted to the objectives of this thesis.

In the literature various terms are used for the first step, such as matching, registration, alignment, conflation or adaptation. Although the precise meaning varies, the methods either only deal with finding the correspondences between the data sets or additionally with determining transformation parameters for the mapping of one data set to the other. Although Vosselman (1992) is focused on stereo matching, his taxonomy for matching algorithms is also suitable for the adaptation problem to be dealt with in this thesis. Active contour models are not necessarily considered as a matching approach, but we will see that these methods perfectly fit into this taxonomy. Vosselman (1992) characterizes matching methods based on three key points:

1. *the level of abstraction of the data which have to be matched*

Concerning the data, Vosselman (1992) differentiates three levels of descriptions that may be used for the matching process. The first level simply contains pixels or small patches of pixels (*pixel-based matching*). The next level consists of features such as points, lines, and regions. These features can be extracted using image processing methods in order to represent object information explicitly and to reduce the search space for correspondences

(*feature based matching*). The third level considers relations between objects or features. These geometric and topological relations can further limit the search space, increase the robustness of the matching, and thus decrease the number of false matches (*relational matching*).

2. *the evaluation function which has to be optimised for the determination of the best match*

The selection of a suitable evaluation function that defines a similarity measure for the correspondences and enables the determination of the optimal match represents the second key point in this taxonomy. One very common similarity measure is the cross-correlation coefficient, for instance of the grey values of two image patches, which has to be maximised in order to find the best match. Alternatively, the similarity measure between two data descriptions is also often formulated as a cost, distance, or energy function that has to be minimised. This function is usually composed of the sum of all primitive costs, which contain the sum of all attribute costs for single primitives. For numerical attribute values, such as position or size, the absolute difference (L1-norm) or the squared difference (L2-norm) can be chosen as a suitable distance measure. Another definition of the cost function that can also consider non-numerical attributes is derived from the probability theory. In this context, conditional probability density functions describing how likely the attribute A of an object is under the premise that an attribute B belongs to the corresponding object are used. In any case, the relevance of a certain attribute for the matching can be controlled by weights. Furthermore, the evaluation function can be extended by soft and hard constraints in order to integrate prior knowledge such as limitations for attributes of corresponding objects. Hard constraints can be considered as infinitely high costs in the evaluation function.

3. *the searching or optimisation method*

Finally, an optimisation method has to be chosen in order to find the best configuration among the possible matches with respect to the evaluation function. Vosselman (1992) describes several methods, such as tree search or simulated annealing, in order to demonstrate their applicability for relational matching.

The data source of stereo matching algorithms always consists of two or more images, i.e. data sets having the same representation. Therefore, there is no need for the taxonomy of these algorithms to consider the similarity of the data representation that should be matched. However, this is an important aspect for the classification and evaluation of methods that can be applied to the objectives of this thesis, because the two original data sets used here differ strongly from each other with respect to their representation. On the one hand the *GIS vector data* from the topographical data base can be seen as *explicit information* with direct access to the objects. These data are modelled as point, line and polygon features with attributes, but include also geometrical and topological relations. Therefore, they correspond to the third level of the data representation mentioned above (relational data description). On the other hand *ALS data*, though acquired in an irregular scanning pattern, are often modelled as regular height and intensity grids generated by interpolation. These data contain only *implicit information* about the objects on the Earth's surface and without further processing correspond to the first level of data representation (pixel based data description). In order to adapt these two different data sets, two general strategies exist:

1. One data set is transferred to the representation of the other, for instance by feature extraction in the ALS data, and an adaptation method for similar data sets can be used.
2. Algorithms have to be applied that are able to adapt data sets having these different representations.

For the evaluation of suitable adaptation methods we have to consider that algorithms following to the first strategy require a transfer of at least one data representation to another. However, a change of the data representation is often a source of errors and can also be associated with a loss of valuable information. In the context of this thesis, feature based matching approaches need an explicit feature and attribute extraction step from ALS data. Additionally, geometric and topological relations between the extracted features or objects have to be established in order to continue to a relational description of the ALS data and to exploit the relational information inherent in the GIS vector data during the matching process.

The following sections review methods for the adaptation of spatial data sets starting from three different data descriptions:

1. Images and DTM

The two data sets are represented by a pixel-based description and the methods of this section can be classified as belonging to the first strategy. In the context of this thesis, the way back to pixel-based matching can be done by considering aerial photos or digitised maps as basic source for the vector data. However, this strategy is more a theoretical aspect and not very applicable because of the dissimilarity of the original GIS data sources. Therefore, in this section matching approaches starting from a pixel-based data description are just briefly analysed and only if they are related to a DTM. The latter provides also the historical background and a nice access for the adaptation of 2D spatial information and the related terrain heights. Despite their relation to the height in case of aerial imagery or more general to disparities, especially the large group of pixel- and patch-based stereo matching algorithms is beyond the scope of the thesis.

2. Different 2D vector data sets

The methods reviewed in this section deal with the adaptation of data sets that are modelled by feature-based and relational descriptions. In order to apply these algorithms to the objectives of this thesis, a feature extraction step in the ALS data is required. They thus can be assigned also to the first strategy mentioned above.

3. Vector data and DTM

The methods of this section are focused on the integration of DLM objects into the DTM, which is often carried out based on TIN structures. They can be applied without an extensive pre-processing of the input data (second strategy). However, only a few algorithms consider the inconsistencies between the two data sets and the semantic correctness of the combined TIN structure or incorporate components for an adaptation of the data sets into the process.

2.2.1.2 Images and DTM

Already in 1979 Horn & Bachman stated the importance of a precise registration of 2D spatial information in the form of satellite images and DTM for combined applications. In the context of pixel-based matching methods they proposed an approach for the DTM-to-image registration motivated by the analysis of the image intensities. Based on known positions of the light source in real images they calculated synthetic images from the DTM using a reflectance map which describes the surface reflectance as a function of the surface gradient. The related reflection model of the Earth's surface in every pixel was assumed to be a Lambertian scatterer. This concept can be seen as an inverse of shape from shading idea (Horn 1975), also called photoclinometry, which exploits the reflectance map in order to obtain shape information from single images. The obtained synthetic image from DTM and the real image are matched on the basis of correlation

of the intensities as similarity measure. The best match with respect to the four transformation parameters is determined using a standard hill-climbing search. The proposed method works well for the analysed LANDSAT images with small sun elevation and hilly landscape, because the predominant part of the image intensity is caused by surface topography. For flat terrain and high sun elevation more sophisticated reflectance models have to be applied considering the influence of the surface cover. This approach does not fit to our initial data situation.

Another method, also based on directional illumination, segues into the group of feature based and relational matching. Papanikolaou & Derenyi (1988) cover the entire procedure from feature extraction in the DTM as well as in the image to the alignment of groups of linear structures and their geometric relations. The paper describes the challenges to be faced in the combination of imagery and height information. Initially, features have to be detected which can be identified in both data sets. For that reason, ridges are extracted in the DTM by local methods and in images using magnitude and direction of the grey value gradients. Edges in the image are considered to be ridges if the gradient direction points into the direction of the illumination source. After finding the ridges in form of line segments in the DTM and the related image, triplets of the lines are created in certain neighbourhoods and intersecting angles and distance ratios are calculated forming geometrical relations for the matching of single triplets. A general assessment of the method is difficult, because the tests are conducted on synthetic images only. In any case distinctive ridges in hilly terrain are crucial for a successful application. The choice of suitable features in height data, which have equivalents for matching in 2D spatial information, is also an important issue in the context of this thesis.

2.2.1.3 Different 2D vector data sets

Methods for the matching of vector data sets can be found in photogrammetric applications, such as feature based or relational stereo matching, or in cartography, such as map conflation. This section is focused on the latter due to the close relationship to the topic of this thesis. The term *conflation* is used for the adaptation of spatial data sets especially in the cartographic community. Conflation consists of the detection of correspondences as well as the subsequent alignment of the found matches. Furthermore, this section is mainly focused on network objects, particularly on roads.

The first approaches for the matching of vector data sets in GIS applications were focused on the merging of similar simple geometrical elements, whereas subsequent algorithms search for identical object structures in order to exchange attributes or homogenize their geometry. However, these methods are not able to deal with different geometric or topological data models, which is an important task in cartographic applications. In this context fundamental work has been conducted by Rosen and Saalfeld (1985) and Saalfeld (1988), who merge digital spatial data sets, such as road networks, provided by the Bureau of the Census in Washington and the United States Geological Survey. In an iterative algorithm corresponding nodes in a graph structure are interactively identified on the screen or by automatically analysing topological and geometric criteria, such as the position and degree of nodes. In a second stage the approved matched nodes are exactly aligned by rubber sheeting (Gillman, 1985). After rubber sheeting new likely matches may occur among the other nodes, which can be additionally used in the next iteration. The process terminates when no new matches are suggested. Under the assumption of isomorphic data sets only 1:1 matches are tackled. More sophisticated algorithms require the treatment of topology differences and thus n:m relations. Such differences may arise during the matching of two road networks modelled by different levels of detail. A classification of various potential conflicts between spatial databases can be found in Parent et al. (1996). Mustière & Devogele (2008) define three groups of criteria for the matching of network structures, in particular for road networks:

1. *Geometric internal properties:* Without common identifiers in the spatial database the geometrical position often represents the main criterion for the detection of homologous objects in two data sets. A distance measure, for instance the Euclidean, the Hausdorff (Deng et al., 2005), or Fréchet distance (Alt & Godau, 1995), is required for the evaluation of the position criterion. In contrast to simple point features, the shape and orientation of linear or polygon objects can additionally be compared.
2. *Spatial organisation among objects:* A matching process further benefits from the analysis of the spatial organisation of the entities. Especially topological relations between the nodes and arcs (connections between pairs of nodes) of a network structure facilitate the recognition of correspondences, an aspect that is also considered in the idea of network snakes (section 3.4.1.2).
3. *Non-spatial internal properties* The final group consists of non-spatial properties, such as certain attributes from GIS objects. In this context qualitative (e.g., traffic restrictions for roads) and quantitative attributes (e.g., number of road lanes) can be distinguished. These properties should be similar for homologous objects and thus provide useful information for the matching.

This taxonomy has obviously many connections to the data part of the classification made by Vosselman (1992, see page 20) and emphasizes the strong relationship between cartographic and photogrammetric matching tasks.

Walter & Fritsch (1999) propose a statistical approach for the matching of two road networks motivated by the ideas of Vosselman (1992) about relational matching. In a pre-processing step the method applies an affine transformation based on control points to correct large systematic errors. These points are either selected manually or extracted automatically. This aspect is important for the second step that determines matching candidates. A buffer growing approach is applied to the data sets searching for potential n:m line matches. The width of the buffer depends on the relative accuracy of the two data sets. In order to reduce the number of matching pairs for computational reasons the third step uses geometric constraints, such as length difference, angle, shape, and distance of the line pairs (centre line of roads in this particular approach). Frequency distributions of these features from manually matched elements are calculated to determine suitable thresholds for unlikely matches. Subsequently, the selected line pairs are assessed by a cost function based on the mutual information of the line features. In addition to the geometric features the mutual information of the topological relation “connected” represents the relational part of the algorithm. This relation contains the information which line features are connected by common nodes in the particular data set. The conditional probabilities determining the mutual information are derived by training based on manually generated matches. The overall mutual information of the two data sets is defined by the sum of the mutual information of all matching primitives considering all features. The best match, i.e. the best unique combination of potential matching pairs with respect to the entire data sets, is detected by maximising the overall mutual information with a tree search concept.

An interesting additional aspect deals with quality measures of the matching result. In this context Vosselman (1992) uses the relationship between self information, conditional information, and mutual information based on the information theory. Considering this framework the average conditional information of all matching pairs describes the amount of information loss during the matching process. A higher average loss indicates a larger number of potentially wrong matching pairs and can also be a measure for the overall similarity of the two data sets.

Another interesting approach (Mustière & Devogele, 2008) is especially designed for networks with different levels of detail. The strength of the algorithm is based on the interaction of node and arc matching, thus considering the topology

of the networks. After transforming the networks into generic graph structures, the method pre-matches arcs and nodes separately by applying local geometric criteria. The results of the pre-matching of arcs and nodes are considered in the final matching of the nodes by analysing their emanating arcs. For *complete* node candidates, correspondences for all connected arcs of the less detailed network and for some of the arcs of the detailed network have to be detected in the pre-matches. Similar other rules exploiting the topology of both networks guide the further node matching process. The final arc matching is based on nodes already matched and thus linked by potential correspondences, on pre-matched arcs, and on the minimisation of the area between the potential matches. Finally, a global evaluation of the consistency of the matches is carried out considering the levels of detail of the two networks. Haunert (2005) proposes another approach that is able to handle data sets with different levels of detail. Starting from some given links between the data sets, which at least partly represents the same object, the method analyses these links and the topology of the network in order to obtain coordinate differences in points with well-defined correspondences. To overcome the differences with respect to the level of detail, additional points are inserted on arcs between previously matched points in both datasets in a second step. Finally, the shift vectors for points that have not yet been matched are interpolated from the matching pairs in the neighbourhood.

Several other methods propose interesting approaches for certain parts of the vector-to-vector matching problem. For example, Olteanu (2007) applies the Dempster-Shafer theory to evaluate the similarity of the different attributes. Similar to the information theory this concept allows also the integration of non-numerical attribute values in the evaluation function. Von Goesseln & Sester (2004) tackle the problem of different data representations in two vector data sets that should be matched. After identifying corresponding semantic objects in the respective object catalogues, they harmonise for instance rivers modelled as linear features in one data set with an area based description of another data set by using GIS attributes and buffers. Based on geometric criteria object correspondences are detected. Finally, transformation parameters are determined based on the iterative closest point (ICP) algorithm (Besl & McKay, 1992).

This brief review of existing methods emphasizes the complexity of these approaches even if similar objects, such as centre lines of road networks from different data bases, have to be matched. Considering the data available in this thesis the second set of vector primitives would have to be generated by feature extraction in the ALS data. Therefore, the features of the corresponding object class, such as roads, have to be identified in the first place. Subsequently, the matching of homologous objects of this class can be carried out. This two-tier process consisting of the matching on schema (object class) level and on data (object) level is also stated in Devogele et al. (1998). This aspect increases the complexity and decreases the applicability of this strategy for the goal of this thesis. For instance, Fig. 4 illustrates the difficult task of detecting suitable features for the adaptation of a road network if only the DTM is available (minimum configuration for the desired algorithm). Many pixels that have large edge amplitudes in the DTM belong to other object classes and crucially disturb the selection of correct edges for the desired object class. Another problem arises from the fact that even if the extracted DTM edges can be assigned to the desired objects of the correct class, such as edges belonging to a certain road, the identification of the exact object part for these features is not guaranteed. Such a situation can be observed if roads from GIS data bases are modelled as centre lines and the extracted terrain edges belong to the left and right border or even to roadside ditches.

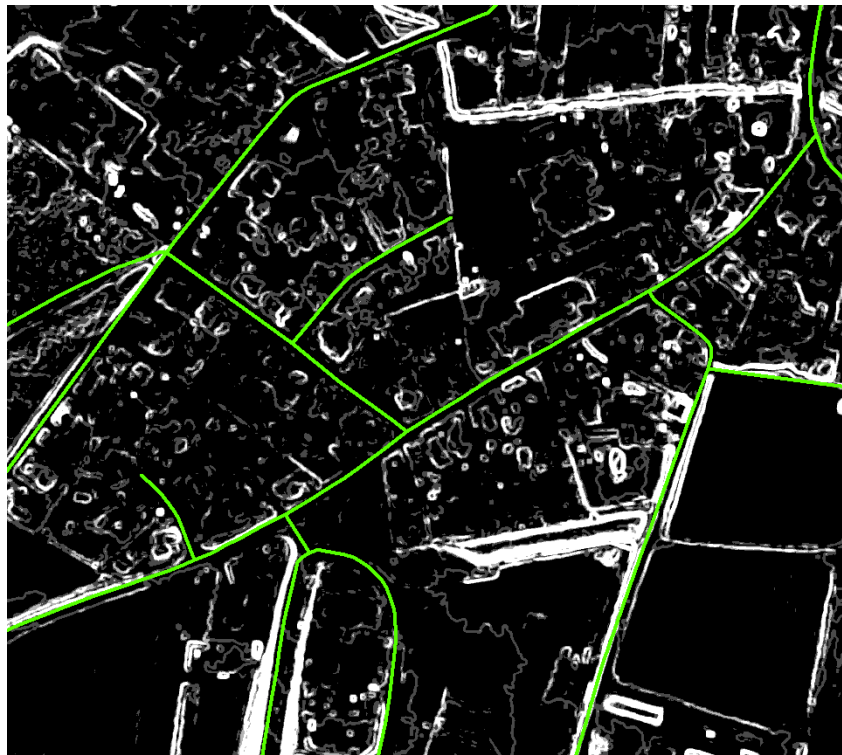


Figure 4. Example of road centre lines (green) overlaid on an edge amplitude image derived from the DTM

2.2.1.4 Vector data and DTM

In this section methods that

- (1) enrich 2D GIS object geometry by height information or
- (2) integrate the geometry of vector objects into a DTM

are reviewed. In principle they are more or less able to deal with the different data representations of this thesis. However, we will see that the methods often change the initial representation, which may be an undesired side effect. The integration of a DTM with 2D GIS data has been analysed for several years. Initially, methods of the first group, such as height attributing of object points or adding interactive DTM interfaces to GIS software, were developed (Weibel, 1993; Fritsch & Pfannenstien, 1992). These methods do not realize a real integration process of the two data sets and result only in a semantically correct solution if the data sets are already geometrically consistent. Consistency is not a prerequisite of this thesis; on the contrary, it is the goal of this work to eliminate the discrepancies between the two data sets in order to enable a semantic correct integration.

Some recent approaches of the first group model smaller discrepancies within the integration process. Oude Elberink & Vosselman (2006) reconstruct 3D topographic objects such as complex road crossings by combining medium scale maps and the national height model of the Netherlands, which is derived from ALS. Initially, a densification of the 2D map polygons is carried out. Afterwards, the ALS points are segmented into smooth planar surface patches by region growing. The seed regions are determined by means of a 3D Hough transform of k nearest neighbours of randomly chosen ALS points. In the first step of the 3D reconstruction, heights are assigned to the boundary points of the map objects considering the segmentation result. For each map point the heights of all adjacent objects are determined from the ALS data. For that purpose the k nearest ALS points of the current map vertex inside one object are selected. Then, among

these ALS points the most frequent segment number is determined. A plane is fitted through those ALS points that belong to this segment number and the height of the current map point is interpolated from this plane. The use of the most frequent segment number enables the method to deal with a slight misregistration between the map and the ALS data. Some rules are defined for combining the heights of the adjacent objects at the current map point. New 3D boundaries with the same horizontal coordinates are integrated between the map objects if significant height discontinuities occur. Otherwise the objects share a common 3D boundary and the related heights are determined following some semantic properties, such as horizontal lake surfaces. Also the accuracy of the estimated heights is considered in this process. Assuming a higher accuracy of the ALS data of road surfaces, these heights are assigned to the road boundaries if the height difference is below a certain threshold. With the generated 3D boundaries a constrained triangulation is performed and a subsequent morphological filtering eliminates spikes due to the misregistration. Generally, the method contains some features to deal with small discrepancies between the two data sets. However, larger horizontal differences cause problems during the determination of the heights of the map objects. Therefore, an adaptation of the data sets in a pre-processing step might be useful.

Similar to Oude Elberink & Vosselman (2006), Hatger & Brenner (2003) propose a method that combines road databases and ALS data in order to enrich the road geometry by several features. For that purpose, the DTM is segmented by two different algorithms. The first algorithm uses a region growing, realised as a scan line grouping, in order to detect planar surfaces, but does not include the road data base information. It is assumed that the planar regions can be assigned to the road centre lines in post-processing. If there are large inconsistencies between the two data sets, this assumption may fail. A second segmentation algorithm is proposed that requires a road centre line from the data base that is located within the road borders. For each sampled road cross section a horizontal line is estimated by applying the random sample consensus principle (RANSAC). Subsequently, the road borderlines are determined using a median filter for the ends of the extracted line segments. Because both algorithms suffer from poor road centre lines in the data base, Hatger (2005) extended his applied segmentation algorithm based on a line simplification method by a decision process. This process maps the segmentation results to a road model created from prior information. The model contains the position of the centre lines and the road width from the data base, as well as admissible slopes from construction guidelines. The decision process detects those segments that best fit to the model using hypotheses and test methods based on support functions. In general, this method is closely related to the objectives of this thesis. If the road segments that are extracted for the corresponding centre lines are reliable, the adaptation of the road object to the DTM is possible. However, the misregistration of the two data sets is modelled in the decision process by thresholds. These thresholds have to be adapted for different inconsistencies between the data sets. This aspect strongly hampers the transferability of the method. Furthermore, information about the maximal geometric inconsistencies between the data sets that the algorithm can handle is not available and the results are only visually analysed. Especially in urban areas many horizontal profiles belonging to other objects are located in the neighbourhood of roads, which disturb the robustness of the algorithm. Thus, it seems that the algorithm can only deal with a slight misregistration and an adaptation algorithm is a suitable pre-processing step as well. Another drawback of the algorithm arises from the fact that only small individual road segments are extracted and the network topology is not considered in the object model.

In summary, the recent algorithms that enrich the road geometry by features extracted from the DTM supported by a road data base are able to deal with a slight misregistration between the vector data and the DTM. However, the robustness of these methods with respect to larger inconsistencies is not well analysed. Due to simple object models that do not exploit the network topology and geometry as well as only a few semantic properties of the GIS data, we assume that the

assignment of DTM features to the corresponding GIS objects strongly suffer from larger discrepancies, which are subject of the objectives of this thesis (up to 10-12 m). An adaptation process seems to be a suitable pre-processing step for these algorithms.

Many algorithms of the second group model the terrain by various kinds of TIN structures and insert points at the positions of the vector objects (Klötzer 1997; Lenk 2001). In this process only a few approaches consider the semantics of the objects during the integration process, but even less attention is placed on the geometric inconsistencies between the two data sets and thus on the required adaptation task that enables a consistent 2.5D modelling of the earth surface. In most cases the authors assume that the horizontal accuracy of the vector objects outperforms the quality of the DTM, which is typically modelled with low resolution in their applications (grid size of 20 m). Therefore, the vector objects are often “dug” into the DTM without considering terrain features. Among these methods the one of Klötzer (1997) starts with the incremental integration of the object points into the DTM represented by a TIN. The heights of all object points are interpolated using the related DTM triangle and the points are added to the triangulation considering the Delaunay-criterion. Subsequently, the borderlines of the objects, i.e. the edges connecting the integrated object points, are inserted and new points resulting from the intersection of object and TIN edges are introduced in the triangulation. However, the Delaunay-criterion is not considered during the local triangulation of these points. The shape of the resulting triangles depends on the order of object edge integration and the results of the algorithm are thus ambiguous.

Lenk (2001, see also Lenk & Heipke, 2006) proposes an extended radial-topological algorithm for the purpose of integration of vector data into a DTM represented by a TIN. Initially, one object point, whose height is interpolated using the related triangle, is added to the triangulation. Starting from this point, angular sectors with respect to the surrounding TIN edges are created in order to calculate the direction of the integration progress considering the topology of the TIN. In the direction thus determined, the object boundary and the closest TIN edge are intersected and a new point is integrated into the TIN without considering the Delaunay-criterion. The algorithm proceeds with the construction of new angular sectors based on this intersection point. In the course of data integration intersection points between object boundaries and edges generated earlier in this process are established, leading to redundant triangles. Finally, the redundant points, which do not contribute to the reconstruction of the surface, are removed and a re-triangulation is conducted. Similar to Klötzer (1997) this approach deals only with the geometric integration and does not consider possible inconsistencies between the data sets and their influence on the semantic correctness of the integrated data set.

A semantically correct integration of a road network into a triangulated DTM is presented by Polis et al. (1995). For this purpose they create a buffer around the centre line of the road and assign the interpolated heights of this centre line to the buffer borderline, thus establishing horizontal profiles. T-junctions and crossings are modelled using horizontal planes. The TIN is reconstructed in the vicinity of the road surface, but the road itself is represented by a separate polygon. Abdelguerfi (1997) proposes a similar modelling strategy, but at the end the object surface is integrated into the triangulation using the objects borders as constrained edges. Whereas these algorithms do consider semantic correctness to a certain degree, they do not take into account the different accuracies and possible inconsistencies between the vector data and the DTM.

In contrast, Rousseaux & Bonin (2003) do consider at least the different height accuracy. In their method 2D linear objects are modelled by a 2.5D Delaunay triangulation using height information from GIS attributes and the DTM triangulated from contour lines. In case of conflicts the z-attributes of the vector data are preferred over the contour lines

because the latter are considered to be less accurate. Additionally, the nature and semantics of the vector objects, such as roads, rivers or break lines, are considered in the process. For this purpose, slopes and regularization constraints are used to check the semantic correctness of the integrated objects. However, no information is given about the restoration of the semantic correctness if this verification fails. Finally, a new DTM is computed using the original DTM heights and the 2.5D objects of the GIS data. The enriched DTM has an improved applicability, e.g. for instance for flood risk modelling.

Whereas all previous TIN-based algorithms enforce the semantic correctness by simple changes of the DTM heights and interpolation, Koch (2006, see also Koch & Heipke, 2006) extends these integration methods by a least squares adjustment. This approach was motivated by algorithms for the homogenization of 2D cartographic data (Scholz, 1992; Hettwer, 2003). He uses equality and inequality constraints in order to incorporate the semantic properties of the objects, such as horizontal road profiles or the downhill flow direction of rivers. Two alternatives of the approach can be distinguished. The first variant only modifies the DTM heights and neglects systematic as well as random errors of the 2D positions of the vector objects. The shapes of the objects are integrated into the DTM so that constraints resulting from the semantics are fulfilled. The second variant additionally introduces the x and y coordinates of the vertices at the boundaries of natural objects (lakes and rivers) as observations and allows a planar 4-parameter transformation of rigid road sectors. The weights of these observations in the adjustment can be derived from the standard deviations of both data sets and a realistic data integration can be achieved. However, the simultaneous correction of position and height is very sensitive to the definition of the weights. Furthermore, some configurations do not guarantee the convergence of the algorithm. Experiments have shown that even small changes of the weights can cause larger variations in the positions of the vector objects. In addition, the implicit information about the vector objects contained in DTM, such as abrupt slope changes at road embankments, is not considered in either of the two variants in Koch (2006). This is a consequence of the quality of the DTM. Koch (2006) used a DTM with 12.5 m resolution and a vertical accuracy better than 0.5 m. Thus, detailed terrain structures, which can be exploited for adaptation purposes, are not available in the DTM. For that reason the method is focused on the joint data representation, taking into consideration the semantics of the objects rather than a geometric adaptation of the two data sets.

Generally, many methods of the second group analysed in this section aimed at integrating vector data into a DTM based on a TIN. Although the extensions of Koch (2006) introduce a simultaneous optimisation of height and position in order to enforce semantic properties of the objects, this group of algorithms has several drawbacks. One major problem arises from the fact that the methods ignore the implicit semantic information of the structure elements in the DTM during the integration process. Indeed some surfaces with large slopes or also terrain edges may cause some changes in the position of the object outlines in favour of a small height variation of the TIN during the simultaneous optimisation due to lower costs in the least squares evaluation function (Koch, 2006). Nevertheless, an explicit integration of the terrain structures as features in the adaptation process is desirable and has not yet been achieved. This aspect becomes even more important if we consider the accuracy and richness in detail of the height information provided by ALS or dense stereo matching techniques. Most of the methods in this section follow the strategy to “cut” the topographic objects into the DTM under simultaneous considerations of geometrical constraints (e.g., horizontal road profiles). In contrast, height information of high quality often has a better horizontal accuracy than GIS objects of the highest importance, such as traffic routes. Thus, these objects have to be adapted to the DTM features. After this adaptation the geometrical constraints from the semantics should be automatically satisfied in the combined data set up to a limit given by the modelling accuracy. Another drawback of the TIN-based integration methods results from the change of the given representation of the two data sets.

2.2.2 *ALS based extraction of topographic features and objects*

In this section literature about feature and object extraction from ALS data or more general from height information is evaluated. Firstly, algorithms for the filtering of 3D point clouds, i.e. a classification into ground and non ground points, are briefly analysed, because a suitable DTM is one prerequisite of the suggested adaptation process. Subsequently, a few methods that deal with the determination of structure lines in DTM or in 3D point clouds are reviewed. These algorithms potentially represent a requirement for the application of the vector-to-vector matching approaches discussed in section 2.2.1.3 to our task and emphasize the difficulties of this required pre-processing step. In the subsequent section, object extraction methods focused on roads and rivers, which are the object classes most relevant to this thesis, are investigated. These methods can provide valuable information for the choice of suitable features for the adaptation process. Finally, the extraction of context objects from ALS data, such as bridges and buildings, is briefly reviewed due to their relevance for the proposed approach.

2.2.2.1 **Filtering of point clouds**

In the proposed new method the design of the image energy for active contours relies on a good quality of the DTM for two reasons. First, DTM features, such as parameters of estimated planes, are directly integrated in the algorithm. Second, the extraction of context objects used in this thesis, such as buildings and bridges, also suffers from a low accuracy of the DTM. However, ALS as well as stereo image matching essentially provides a DSM that includes objects, such as buildings, vegetation, or cars. Thus, the filtering of ALS data is an important topic for DTM generation as well as for this thesis.

The filtering of ALS data is actually a classification task for every 3D point. Various filter algorithms for eliminating non-ground points in ALS data sets were developed considering different landscape types. Sithole (2005) provides a comprehensive overview about the existing methods and a thorough investigation of those algorithms in the context of an international test of the International Society of Photogrammetry and Remote Sensing (ISPRS) (Sithole & Vosselman, 2004). Sithole (2005) classifies the filter algorithms according to the data structure, the considered neighbourhood, measure of discontinuity, single step vs. iterative, basic filter concepts, and external information. The basic filter concepts of the methods contain the main assumption of the structure of the bare ground in a local neighbourhood. All approaches rely on some measure of discontinuity. Such useful discontinuities occur in the terrain itself (e.g., height jumps caused by escarpments) or in the first derivatives of the surface (e.g., rapid slope changes at break lines). For instance, slope based algorithms (Vosselmann, 2000; Roggero, 2001) use thresholds for slopes or height differences between two points as decision criteria for removing non-terrain points. Other authors (e.g., Kraus & Pfeifer, 1998) model the ground by parametric surfaces and exploit the distance of the current point to this surface for classification. Methods based on a progressive TIN densification (Axelsson, 1999) follow a similar strategy. Another interesting approach (Brovelli, 2002) does not classify single points, but connected components of a previous segmentation. In contrast to the classification of single points, the parameters of the segments provide additional information that can be used in the filtering process. An important quality measure of the filtering concepts is the preservation of the terrain features, such as break lines. Since all filtering approaches are based on some discontinuity measures, this aspect is one of the major problems. For example, the adaptation of roads or rivers to ALS data, the main objective of this thesis, will suffer from a loss of terrain features, too. In the ISPRS test, surface based approaches outperform slope based algorithms with respect to this criterion.

The use of multiple echoes and reflectance information is another decisive factor. Among all contributors of the ISPRS test only the algorithm of Brovelli (2002) considered the difference between the first and last echoes in the filtering

process. The stored intensity values given for every ALS point were not yet integrated in any of the filtering methods analysed by Sithole (2005). In this context, Goepfert et al. (2008) propose the transformation of the intensity values into additional weights for robust filtering (Kraus & Pfeifer, 1998). If each point can be assigned to a certain object class, bare ground and raised points can be easily separated. Tóvári and Vögtle (2004) use the intensity values among other features in order to discriminate buildings, vegetation, and terrain. Mallet et al. (2008) exploit features from full waveform data for the classification of urban areas. During filtering or classification, valuable information is generated also for the adaptation of topographic objects from a GIS data base to ALS data. For example, information about context objects, such as buildings, trees and bridges, can be used later on.

2.2.2.2 Break lines

Break lines are defined as discontinuities of the bare ground (height jumps - step edges) or discontinuities in the first derivative of the bare ground (slope jumps - ramp edges). They stand for distinctive terrain features, which are relevant for the objects of interest in this thesis, such as edges at road or river embankments. Therefore, this information is used in several bottom-up strategies for object extraction and can also be exploited for the adaptation task. Furthermore, the extraction of break lines in the ALS data represents also a requirement in order to apply vector-to-vector matching approaches to the objectives of this thesis. Additionally, DTM are mainly modelled in a regular grid by interpolation methods from irregularly distributed point clouds. The largest approximation errors in these grids usually occur at the break lines. Thus, the accuracy of the DTM can be significantly increased if break lines are considered in the modelling process. Furthermore, the use of available break lines allows modelling the terrain with larger grid size but equal accuracy. This is a crucial contribution to the reduction of quantity of raw data acquired for instance by ALS systems.

Some approaches detect break lines in DTM grids using image processing methods, whereas other algorithms reconstruct the terrain in the vicinity of the features based on 3D point clouds, extracting the break lines by intersecting approximating surfaces. The method in Gomes-Pereira & Wicherson (1999) belongs to the first group and is designed for edges along dikes and rivers. Based on the Prewitt gradient operator, the approach separates “horizontal” from “tilted” pixels using a threshold. If at least one pixel is “tilted” and one pixel is “horizontal” in an eight pixel neighbourhood of a tilted pixel, the latter is classified as potential break line point. Subsequently, these candidates are thinned out and transformed to polylines. Brügelmann (2000) calculates the second derivatives of the terrain model as homogeneity measure and determines candidates for break line points based on a statistical test assuming a χ^2 -distribution. The regions passing the test are thinned out by non-maxima-suppression and 3D vector polygons are created. Other algorithms use different edge detectors, such as the Canny detector (Sui, 2002), but the general strategy does not vary from the approaches already mentioned.

In general, grid based methods strongly suffer from the previous interpolation of the acquired height data due to the loss of information especially in the vicinity of the break lines. Therefore, approaches based on the original point cloud usually perform better. The results of grid based methods are often used as an approximation for the second group of methods. In this context, Brzank (2001) uses a 2D approximation of the break line to separate the 3D points into a left and a right side. Afterwards, the terrain surface in the neighbourhood of the break line is approximated by planar patches at each side. The solution for the break line of the first iteration results from the intersection of these two groups of planes. This procedure is repeated using the results of the previous iteration as approximation in the subsequent iteration. The iteration process stops if the classification of the 3D points does not change or if the maximum number of iterations is achieved. In order to apply the method to vegetated areas, Briese (2004) extends the approach by robust filtering,

modulating the weight of each observation according to its residual in the previous iteration (Kraus & Pfeifer, 1998). Furthermore, he integrates a strategy that propagates the direction of the break line from the current to the next patch. Thus, the method only requires a starting point and the starting direction rather than a 2D approximation of the entire break line. Various structures, such as embankments, roadside ditches, or tidal trenches, are characterized by a group of break lines that belong together. Applying the previous methods, every surface between two break lines has to be approximated by a plane. Additionally, using airborne acquisition techniques the point density on strongly inclined terrain is sometimes too small for a robust approximation of these planes. Thus, Brzank et al. (2008) propose the simultaneous extraction of two related break lines on the upper and lower edge of such structures, e.g. dikes. For this purpose they approximate the terrain locally by a hyperbolic tangent function (\tanh). The iterative estimation of the parameters of the hyperbolic tangent function is carried out in small patches. However, a 2D approximation of the centre line between the two terrain edges is also required in order to select the 3D points that take part in the adjustment and to determine the initial values of the surface parameters. For every patch two break line points (upper and lower edge) are derived from the approximated surface. Finally, the points from consecutive patches are connected by splines. Borkowski (2004) pursues a slightly different approach. He also detects break lines by intersecting two surfaces, but uses a thin plate spline (Duchon, 1976) as interpolation method for terrain approximation. The intersection line of the two interpolated surfaces is determined by a tracing algorithm. He also proposes an interesting alternative using the original snake approach in order to detect the break lines between the interpolated surfaces. The external energy (cf. section 2.1.2.2) is designed based on the vertical differences of the two surfaces, whereas the initialisation of the contour is derived from the 2D approximation of the break line.

In general the methods based on 3D point clouds approximate the surface in the vicinity of the break line in small patches. Algorithms using simple surfaces (e.g., planes) are often not able to sufficiently model the terrain resulting in less accurate break lines, whereas the approximation based on more complex surface functions (e.g., \tanh) does not converge for every patch. In the latter case large gaps between the break line segments may occur, which can not be bridged by post-processing. Furthermore, the extracted break lines are not assigned to certain object classes. These aspects hamper the applicability of the break lines as input data for vector-to-vector matching approaches.

2.2.2.3 Roads and bridges

In contrast to break line detection, the extraction of roads from ALS data exclusively is not performed and analysed very frequently in the literature, because especially in flat terrain there are not many features in height data that give indications for roads. Structure lines in the vicinity of roads are often fragmented and not characteristic enough. Thus, some authors tackle this sophisticated task by using additional data sources, such as ALS intensities, optical images, or GIS data, whereas others apply special strategies, such as twin snakes (Kerschner, 2003) to overcome these problems.

After filtering and interpolating the ALS data by linear prediction with robust estimation (Kraus & Pfeifer, 1998) Rieger et al. (1999) calculate a grid of the second derivatives of the DTM, which represents the local curvature. Subsequently, different features are extracted based on the grid by Polymorphic Feature Extraction (Fuchs & Förstner, 1995), but only the linear structures are kept. These linear fragments are used to initialise the twin snakes (Kerschner, 2003), though this process of combination and classification of line pieces is not clearly described. However, the integration of model based knowledge via twin snakes stabilises the extraction process and enables the algorithm to bridge gaps in the structure lines with respect to one road edge.

Road extraction can also be improved by fusing ALS and image data. Zhu et al. (2004) propose a method especially designed for urban areas. Firstly, they extract edges in ALS as well as in image data using the Canny operator and some morphological post-processing steps. The extracted ALS edges belong to elevated objects, namely trees and buildings. These ALS edges are selected if they are parallel to the main road directions, which are previously determined. A buffer is created for the chosen edges and the fragments are linked by a Cardinal spline algorithm in order to generate a connected graph. This so called *complete* road graph from ALS data is mapped to the *incomplete* image based graph by applying a homeomorphism-matching operation (topologically invariant). This strategy is able to fill the gaps in the road network from optical images, which result from blurred edges in shadow areas, by ALS edge information.

With the increasing reliability of the intensity values recorded for ALS points, assumed to be a by-product until a few years ago, more information can be included in the extraction process. ALS points on asphalt roads usually have small intensity values and are thus often well distinguishable from their neighbourhood along with the fact that they are usually situated on the terrain. These aspects are used to extract roads by Alharthy & Bethel (2003) and Clode et al. (2007). The algorithm of Alharthy & Bethel (2003) starts with a supervised classification of ALS intensity values in road and non-road areas. The training samples are generated from prior knowledge and cover the range of different road materials in the scene. Various misclassifications exist due to similar intensity values for building roofs or vegetated areas. Thus, two refinement steps are implemented. At first the difference between the first and last echo is exploited in order to eliminate penetrable objects probably belonging to vegetation. In a second refinement step, morphological filtering is applied for the separation of terrain and non-terrain pixels. Following the assumption that roads are located on the terrain, the non-terrain areas are discarded, too. Finally, a connected component analysis removes small isolated regions. Clode et al. (2007) also apply a binary classification of the ALS points. The method starts with hierarchical morphological filtering in combination with building detection in order to generate the DTM from raw ALS data. The final DTM is interpolated by inverse distance weighting without considering the off-terrain points. The vertical distance of the ALS points from the DTM represents the first criterion for road classification, assuming again that roads lie on or near the ground. Secondly, the intensity values of points belonging to the road class have to be within a certain interval whose borders are derived by training. Following the assumption of continuous road surfaces, the classification results within a circular neighbourhood of every ALS point is analysed. An ALS point is classified as a road point if more than 50% of the neighbouring points also belong to the road class according to the initial classification based on DTM and intensity values. The final classification result is stored in a binary image, which is further processed in order to build up 2D vector data. For this purpose the binary image is convolved by a phase coded disk (PCD). The convolution results in a magnitude and phase image, which can be used to determine the centre line, orientation and width of the road.

There are quite a few papers about road extraction from optical imagery supported by height information (e.g., Grote et al., 2011). The authors of these papers emphasise the importance of the additional height data for the quality of the extraction result. However, just a few methods rely exclusively on ALS data and none of them uses only height information. These algorithms achieve both completeness and correctness rates of 80% (Clode et al., 2007). Problems result from roads occluded by vegetation, bridges, and parking lots, which do not belong to the public road network. The centre lines in Clode et al. (2007) attain a R.M.S. error of 1.7 m. The authors also compare the detected intersections with manually acquired reference data and calculate a topological completeness and correctness of 80%. In the context of this thesis, road extraction from ALS data could represent the potential preparation step for a vector-to-vector matching strategy. One major problem is the loss of information due to incomplete extraction results. Incorrect classification results may further disturb the mapping of the GIS vector data to the extracted objects. Matching approaches strongly

relying on topological similarities by comparing for instance the degree of the nodes suffer from missing connections or from wrong links. If ALS intensity values or optical images are not available, the extraction is limited to break lines or other significant terrain details, because the DTM features are not sufficient for the classification of complete roads. This aspect additionally causes problems for the matching task due to more fragmented features possibly belonging to other object classes.

ALS data have also been used to detect bridges. Bridges are strong features and reveal the position of roads or other traffic routes in the ALS data reliably. Thus, bridges are valuable context objects for the adaptation of road and river networks. Clode et al. (2005) use the fact that bridges frequently appear as false positives (FP) in building detection from height data. They compare the results of road extraction (Clode et al., 2007) to the results of building detection. As Clode et al. (2007) includes a method for bridging small gaps between road segments, bridges are usually part of the final road network. Thus, the overlapping areas of roads and buildings are classified as bridges if their size exceeds a threshold. Sithole & Vosselman (2006) propose an algorithm for bridge extraction that relies on three properties of bridges:

1. Bridges are connected to bare ground at least on two sides.
2. Points raised above the bare ground are located along the length of the bridge at its borders.
3. The bridge is usually longer than it is wide.

The method is designed for the bridge detection in a pre-classified point cloud. The method used for filtering of the ALS points is based on a segmentation approach (Sithole & Vosselman, 2003) in order to preserve the bridges as bare ground. Contiguous profiles of ground points are created in different directions and partitioned into line segments with the labels “raised” or “not raised” using a slope threshold. If the majority of the line segments passing through an ALS point is labelled as “raised”, then this point is treated as a seed point for bridges. The seed points are segmented by a triangulation in their neighbourhood. The outlines of these segments are determined using the convex hull and a refinement step. A smoothness parameter (standard deviation from plane estimation in every point) is calculated and used in combination with the outlines in order to check the three bridge criteria mentioned above. The outline of the segments passing the test is refined and the points inside are labelled as bridge points. One advantage of this method results from the fact that it does not rely on a certain shape of the bridge, such as a fixed width or straight parallel borders. Thus, the algorithm is very flexible and able to detect also bridges with curvature or holes.

A sound evaluation of the described methods is difficult due to the small number of analysed bridges in the experiments of the papers (<10). In Clode et al. (2005) eight bridges in two data sets are correctly detected, but also three false positives are observed. A poor filtering strategy and the resulting low quality of the DTM are assumed to be responsible for two false positives. In contrast the method of Sithole & Vosselman (2006) detects all bridges in the analysed data sets even if they have a very complex geometry. However, this sophisticated algorithm, which uses various processing steps based on the ALS point cloud, seems to be quite expensive with respect to the computational time. In order to detect bridges, whose majority has a more simple geometry, as context objects for the algorithm of this thesis, a more straightforward algorithm may be sufficient. However, the classification of bridge points as ground during the filtering process and their detection in the resulting DTM seems to be a promising strategy.

2.2.2.4 Rivers and water areas

The new method of this thesis is also focused on the adaptation of river objects to ALS features. Thus, algorithms that extract rivers in height data can give valuable hints for suitable features with respect to the adaptation process. Furthermore, the performance of these algorithms has to be analysed in order to evaluate their ability to provide significant features for vector-to vector matching.

Due to the frequent occurrence of flooding events, the extraction of water areas in ALS data and also the monitoring of the waterbed and the surrounding terrain are a relevant research area. However, sensors that are able to acquire height information for both the water surface and the river bed are not available. Standard ALS systems use lasers that operate in the near-infrared domain (cf. section 2.1.1) and thus are usually not able to penetrate water surfaces¹. Therefore, ALS measurements are often combined with sonar data for the determination of a consistent DTM of the water bed and its vicinity. For that purpose all ALS points reflected by the water surface have to be detected and removed from the data set before DTM interpolation. Brockmann & Mandlbürger (2001) suggest an iterative algorithm in order to determine the water-land borderline from ALS and sonar data. Based on the a priori known centre line of the river the mean heights of ALS points in a buffer are used to approximate a digital model of the water surface (DMWS). Subsequently, an ALS-DTM is calculated using all ALS points that belong to the ground after filtering. Afterwards, the 20 cm contour line of the difference model between the ALS-DTM and the DMWS is determined as the preliminary borderline of the river (PBR). The ALS points inside the PBR are replaced by the points acquired by sonar and a preliminary DTM (PDTM) including the water bed is interpolated. The zero level line of the difference model between the PDTM and the DMWS represents the final river border. The main drawback of the method is the requirement for sonar data. Mandlbürger (2006) tries to overcome this disadvantage. He determines the DMWS similar to the previous method and uses a height threshold with respect to this model in order to classify the ALS points into land and water. The water bed is divided into segments of equal length along the course of the river. For every segment an adjusted straight line profile is calculated using the ALS points of the river embankment separately for each side. The intersection of these profile lines with the DMWS represents the river border for the particular segment. The extracted intersection points of the consecutive segments can be connected to the river borderline.

In addition to geometric criteria, Brzank & Lohmann (2004) and Brzank et al. (2008) exploit the reflectance properties of water surfaces of tidal flats represented by the intensity values of the ALS points in order to classify the ALS points into water and land. Assuming that low intensities indicate water areas, the first algorithm uses water shed transformation applied to an interpolated grid of the intensity values in order to determine possible water seed regions. Starting from seed areas with an intensity value below a predefined threshold, region growing based on two homogeneity criteria is carried out. A border pixel is added to a region if its height difference to an adjusted plane of the current water region and its intensity value fulfil predefined thresholds. The algorithm stops as soon as all border pixels of the region are classified as land area. However, several problems occur during the application of this method. On the one hand the specular reflection on water surfaces may disturb the general assumption of low intensity values in water areas. Some ALS data sets show very high intensity values for water areas that are located directly beneath the sensor (where the incidence angle is zero). On the other hand, the processing of larger data sets with several time delayed flight strips hampers the assumption of an equal height of contiguous water surface. These problems are considered in the second approach (Brzank et al., 2008), which separates the ALS points into land and water using a supervised fuzzy logic classification.

¹ Some ALS systems operate in more than one wavelength, with green light being used to reach up to 12 m water depth depending on the water composition.

The decision process is based on the following three criteria: height, intensity and point density of the ALS points. In order to avoid height jumps due to differences in time and strongly varying physical conditions, every ALS strip is classified individually. The membership functions of each feature for the class “water” and class “land” are determined by analysing training areas which are digitised manually. Simultaneously, a statistical test is conducted which determines the significance of the features for the classification process. Based on this test, weights are assigned to the features. Additionally, the dependency of the ALS intensity values and the point density on the angle of incidence is determined for both classes based on the training data in order to model the reflectance behaviour. The applicability of these features and thus their weights in the classification can vary depending on the angle of incidence. Since the ALS intensity as well as the point density both depend on the model of reflection, they are strongly correlated. Due to the test of the feature significance this approach overcomes some of the drawbacks of previous methods. However, the intensity values and the point density are often not suitable to separate land from water. In this case the classification is only based on the height information.

Brockmann & Mandlbürger (2001) use sonar data, which are not available for the task of this thesis. Thus, this strategy is not suitable. The second approach (Mandlbürger, 2006) relies only on ALS height data. In this case the accuracy of the extracted river border lines may suffer from a small slope of the river embankment. Nevertheless, the slope change between water and land represents one valuable feature in order to reveal the course of the river. The methods of Brzank & Lohmann (2004) and Brzank et al. (2008) are tailored for large water areas in the wadden sea, where the height differences are not significant enough in order to differentiate between land and water. Therefore, features based on reflectance properties are additionally exploited. Because these features are often not significant, statistical tests are carried out using training data. For the small rivers and ditches of this thesis, representative training samples are difficult to define. Furthermore, the modelling of the dependency of the features on the angle of incidence requires training data that cover half the width of the flight strip.

2.2.2.5 Buildings

The general purpose of roads is to connect locations of human interests, such as settlements. Thus, buildings are linked by roads and can provide valuable context information for the adaptation of roads. Therefore, a short review of methods for building extraction in height data is presented. Brenner (2000) distinguishes between the classification/detection and the 3D reconstruction problem, whereby the detection of buildings often is a prerequisite for the more complex 3D reconstruction decreasing the search space. For roads in ALS data, building outlines already provide sufficient context information. Thus, this brief review will be focused on the detection task. The set of features in ALS data that is mainly used for the discrimination of buildings from other topographical objects consists of the height above the ground, different measures of surface roughness, such as derivatives or local curvature and variance of the DSM, first and last echo differences, as well as reflectance information from intensity values. The height above the ground is able to separate elevated objects such as buildings from objects situated on the ground, whereas roughness parameters and different echoes can distinguish between vegetated areas and smooth building roofs. The early approach of Weidner & Förstner (1995) extracts buildings from a DSM. Initially, they use morphological operations in order to generate the DTM. The difference model between the DSM and the DTM (NDSM) is segmented by a threshold that is determined from prior knowledge about the building heights. Connected components are then generated and small components are eliminated as trees. Rottensteiner & Briese (2002) propose a similar approach. After filtering the ALS data with robust interpolation (Kraus and Pfeifer, 1998), initial building regions are generated from the NDSM based on a height threshold. The analysis of the surface roughness of the DSM is then used to separate between the building and vegetated areas.

Besides such rule-based methods several other classification techniques are applied for the separation of buildings from other objects in ALS point clouds. Mallet & Bretar (2009) extract features from full waveform ALS data, such as the shape of the backscattered echoes or the number of echoes per emitted laser pulse, and classify buildings, trees, artificial ground, and natural ground, by support vector machines (SVM). Haala & Brenner (1999) use an unsupervised classification, whereas Rottensteiner et al. (2007) apply the Dempster-Shafer theory for the fusion of features from different data sources. The two latter approaches benefit from the combination of ALS and aerial imagery, because optical images provide more radiometric features than the ALS intensity. For example, healthy vegetation and buildings can be well distinguished based on the near infrared channel of multispectral imagery. Approaches only based on ALS data especially with a low point density have often problems to distinguish between trees and buildings.

In this thesis, context information from buildings is integrated in the image energy of active contours in order to act as repulsion force for the road and river objects. For that purpose only a 2D building mask is required. The approach of Rottensteiner et al. (2007) is applied to ALS data exclusively in order to generate the desired building outlines. Nevertheless, a building mask from GIS data bases or derived by other methods can be used as well.

2.2.3 *Snakes for the extraction of topographic objects*

In general, snakes are used in order to adapt the shapes and positions of objects modelled as parametric contours to features in some kind of sensor data. In other words, spatial data in a vector representation (the contour) are matched to another data set with a pixel-based description. Therefore, according to the two different adaptation strategies in section 2.2.1.1 snakes belong to the group of methods capable of dealing with different representation. Thus, an extensive pre-processing of the initial data sets is not required. GIS data represented by the vector model can be directly used for the initialisation of the contours, whereas the ALS data have to be converted into a pixel-based description by interpolation. Furthermore, the direction of adaptation based on the accuracy of the data sets fits to the objectives: shift vectors that can be easily derived from the initialisation and the final contour allow the determination of an adjusted solution.

Additionally, active contour models can be also classified based on the taxonomy of matching algorithms of Vosselman (1992) (cf. section 2.2.1.1). From the data perspective, the initialised contours are represented by the vector model (cf. section 2.1.2.1) and thus belong to the third level of abstraction containing features and their relations, whereas any grid of grey or height values corresponds to the lowest level. The energy functional corresponds to the evaluation function, which assesses the level of adaptation of the position and shape of the contour to the image data. The image energy represents the data term in the functional, whereas the internal energy includes the object model in the form of smoothness or other constraints. In image matching there are similar smoothness terms. One of the first papers that propose the use of the surface smoothness of real world objects for stereo vision applications is (Marr & Poggio, 1976). Finally, several optimisation methods can be used, such as variational calculus or dynamic programming, in order to find this contour that best fit to the image data and additional constraints.

The concept of parametric active contours is widely used in image and point cloud analysis as well as in GIS applications. Fua (Fua, 1996, Fua, 1998, Fua & Brechbühler, 1996, Fua & Leclerc, 1990) investigates the modelling of the Earth's surface and topographic objects from multiple images using constraint optimisation techniques in combination with snakes. They propose several new strategies for different aspects of the parametric active contour. For instance the representation of the snake is extended by additional parameters for the integration of the third dimension and also for the width of a linear structure, in order to model ribbon-like objects, such as roads, (cf. ribbon snakes in

section 2.1.2.2). Furthermore constraints are introduced that contain semantic properties of the modelled surfaces or objects. Such constraints are used for the connection of multiple snakes in order to generate network structures for buildings with rectangular corners (Fua, 1996). They also apply constraints for the physical properties of rivers. However, instead of using the original energy terms of Kass et al. (1988), which are able to describe soft constraints, they suggest a two-tier constraint optimisation method that exactly complies with hard constraints. This strategy avoids the complex tuning of weights for the additional constraint energies. Neuenschwander et al. (1997) are focused on the initialisation problem and suggest ziplock snakes for the extraction of roads from aerial images. In this strategy the user has to specify the two end points of a snake in the immediate vicinity of distinct image edges with clearly defined directions. Subsequently, the image energy is progressively turned on for consecutive nodes starting from the two well initialised end points. In an iterative optimisation process the two active snake parts from the head and the tail converge to the image features while they approach each other. Additionally, the ribbon model mentioned above is integrated in order to consider the image energy at the road borderlines.

Laptev et al. (2000) as well as Mayer et al. (1998) propose a similar snake approach for road extraction in open rural areas, exploiting the scale-space behaviour of these objects. They start with the extraction of lines in a coarse scale of an aerial grey value image using the approach of Steger (1998). This strategy is based on the assumption that the detection of linear road structures in low resolution images is more robust than the extraction based on regions in fine scale, where it strongly suffers from occlusions and shadows and the roads thus tend to be more fragmented. From the extracted lines salient road parts are separated from other object lines based on two features: the constancy of the width and the homogeneity of the related image region. These two criteria are determined in a coarse-to-fine strategy using ribbon snakes initialised by the extracted lines. The approximate width is taken from prior knowledge. The ribbon snakes refine the position of the centre line of the road hypotheses as well as the precise width of the homogeneous surface. Starting from the salient roads, road parts weakly defined due to occlusions or shadows are extracted using the connectivity property of the road network. Two salient road ends are connected by ziplock ribbon snakes if smooth edges indicate the presence of roads at least at one side (the other one could be occluded). Hypotheses with low intensity variations within the ribbon area are accepted as non-salient roads. During this step shadow areas and occluded road parts may be eliminated. Therefore, a second test is conducted that optimises the ribbon width while fixing the position of the road centre line. Small variations of the width indicate probable road surfaces. Crossings are modelled in the final step of the algorithm using two cues. Gaps in the already extracted road network and junctions in the line extraction indicate the presence of crossings. Closed contours are initialised at positions where both criteria are satisfied, and then they are optimised. Furthermore, connections are established between the closed contours and adjacent road ends. These connections are verified again based on the homogeneity of the intensities and a continuity of the road widths. The method provides a very high correctness (>95%) and accuracy (RSME <0.5m) in rural areas, but a lower completeness (72-84%). More complex environments, such as suburban or urban areas, may significantly decrease the accuracy as well as the completeness.

Ravanbakhsh (2008) is focused on the reconstruction of road crossings in aerial images. The method starts with the extraction of the road arms leading to the crossing by applying edge detectors. The edges are grouped and verified using parameters of road centre lines from a GIS data base, such as direction and width, homogeneous and bright intensity values between the edges, and possibly available lane markings. Afterwards, the extracted road arms are connected by applying a snake approach. In order to increase the robustness of the method, ziplock, balloon, and GVF snakes are combined.

Butenuth emphasizes the advantages of network snakes (cf. section 2.1.2.2) for the extraction of field boundaries (Butenuth, 2008) and roads in SAR data (Butenuth et al., 2011). Whereas Fua (1996) introduces hard constraints in order to concatenate multiple snakes, Butenuth (2008) connects different contour parts by integrating nodes of higher degree with a slightly changed internal energy. This modification enables the optimisation of entire networks and significantly increases the robustness of the algorithm in comparison to the application of single independent contours.

Parametric active contours are also applied to other tasks in photogrammetry, remote sensing, and cartography. For example, Burghardt & Meier (1997) suggest an active contour algorithm for feature displacement in automated map generalisation. Cohen & Cohen (1993) introduce a finite elements method for 3D deformable surface models, and Kerschner (2001) applies a twin snake model for seam line detection in orthoimage mosaicking. Borkowski (2004) shows the capabilities of snakes to detect break lines for the purpose of surface modelling (cf. section 2.2.2.2). Wolf & Heipke (2007) refine the positions and shapes of trees delineated from ALS data using a snake approach.

Parametric active contour models with the available extensions and modifications generally cover many aspects, which have certain relationships to our adaptation task. However, a unified strategy that combines these useful variations of the concept with respect to the objectives of this thesis is not yet available. As far as the initialisation problem is concerned, many algorithms rely on human interaction in semiautomatic applications or use the extraction results of a previous step. Methods that fully exploit the potential of GIS objects considering their geometry, topology, as well as the available attributes have not been developed. A suitable framework is provided by the network snakes of Butenuth (2008), which take advantage of the topology in the graph structure. Nevertheless, there remain quite a few unsolved problems if this concept is applied to objectives of this thesis. For instance, this modification of the internal energy cuts the smoothness term at crossings or t-junctions. This aspect may cause undesired geometric distortions at these important network parts due to strong image energies. Butenuth (2008) tries to counteract this effect by introducing a topology-preserving energy. This energy, which is established for two adjacent contour parts, increases if the distance between the two parts decreases. Therefore, this energy term prevents two contour parts from approaching the same image features. However, this term is deactivated at nodes of higher degree (>2) corresponding to crossings, in order to enable the convergence of the contours at this point. Therefore, this energy does not help to avoid distortions in the vicinity of crossings. Furthermore, the geometric object model prefers smoothness and straightness in any case. This model is not suitable for curved road parts and dead road ends. In these situations the image energy is often not able to compensate the smoothing and shrinking effect caused by the internal energy. This aspect hampers the determination of global weights for the entire network especially if the significance of the image features strongly varies. Therefore, the object model has to be modified. Another problem of the network snakes in the current formulation arises from the aspect that the image energy is only considered for linear structures, such as field boundaries. For road networks it is desirable to sample the image energy at the boundaries or even for the entire cross sections. For this purpose a combination with the ribbon snake model of Fua (1996) is useful. Attribute values of the GIS data, such as the road width, can be integrated to support the adaptation process.

2.3 Summary and conclusions of the literature review

As we have seen in the previous sections, three main strategies can be applied in order to adapt 2D vector data to ALS data. The most obvious concept starts with the extraction of suitable features or even objects from the ALS data. Afterwards, a vector-to-vector matching approach can be used in order to adapt the 2D GIS objects to the extraction results. The second strategy is based on the integration of the 2D vector data into height data modelled in TIN structures. The extension of Koch (2006) incorporates matching elements by least squares adjustment under certain constraints, which should ensure the semantic correctness of the integration result. The third idea arising from the literature review realises the adaptation of the two original data sets using parametric active contours. The main advantages and disadvantages of these three strategies are briefly summarised.

The feature and object extraction from ALS data is associated with a considerable loss of information. Using height data as well as the intensity values, completeness and correctness rates of up to 80% can be achieved for objects such as road and water areas. This means that 20% of the objects or object parts are not available for the subsequent matching to the GIS vector data. Additionally, some interesting vector-to-vector matching algorithms rely on the exploitation of network information. However, this aspect strongly suffers from fragmented extraction results and thus incomplete graph structures. Furthermore, incorrectly classified data may also affect the matching process. Areas with high misclassification rates may cause a lot of wrong matches or completely prevent the success of matching. An advantage of this approach arises from the fact that the search for the correct object class for matching becomes obsolete with a correct classification. However, the GIS vector data and the extracted ALS objects have to refer to the same object model, such as centre lines or boundary representation, and describe as accurately as possible identical object parts for a high quality matching with a subsequent derivation of the suitable transformation parameters. This aspect often requires the adaptation of the extraction methods to the model of the GIS data or at least some post processing. If no additional features, such as intensity values, are available, height values alone hardly provide enough information for object classification. Therefore, methods available in the literature only deal with the detection of distinct terrain features, such as break lines. In this case the assignment of the features to the desired object class increases the complexity of the matching task. Furthermore, the relationship of the frequently fragmented features to objects or object parts is unknown. This exacerbates the assignment problem in the matching algorithm. Many authors emphasise the complexity of the matching of network structures, even if two data sets with a similar modelling and an almost complete graph structure have to be matched. ALS data with fragmented objects or, even worse, only with unclassified unconnected terrain features would seem to provide an insufficient data basis for matching.

The methods combining height information and 2D vector data from GIS based on TIN structures firstly integrate the geometry of the DLM objects into the triangulation. Finally, the TIN structure is re-established in the vicinity of the object. This approach can be combined with optimisation algorithms in order to consider the semantic properties of the objects using constraints and accuracy measures for the observations. In the integration process the general accuracy of the initial vector data is assumed to be much higher than the accuracy of DTM with low resolution (typical grid size >12 m). Thus, the geometry and the position of GIS data are usually kept unchanged and the landscape objects are “dug” into the DTM by adjusting only the heights and simultaneously considering the constraints. Modifications that introduce the planimetric coordinates of the objects as additional observations, allowing a flexible geometry as well as position changes, are very sensitive to the setting of the weights. Another disadvantage of these approaches results from the fact that the implicit information about the vector objects in high resolution ALS DTM, such as break lines at road

embankments, is not yet considered. However, this is a crucial point of the method and has to be considered if the vector objects have to be adapted to ALS data. Additionally, the high resolution height data will increase the density of the TIN and thus the computational complexity of the integration and optimisation dramatically. This aspect makes this group of approaches insufficient for the adaptation of larger data sets. Additional features from ALS, such as intensity values, would further increase the complexity of the set of constraints. Finally, the integration of the two data sets based on TIN structures strongly changes the data representation of the vector objects. This is an undesired side effect the approach additionally suffers from. This strategy can be used for a semantically correct visualisation of the combined 2.5D data set, but it is not suitable for a geometric adaptation solving the existing inconsistencies.

The third strategy utilizes parametric active contours as a model-based concept for the adaptation of the GIS and ALS data sets. This method is applied by various authors to tasks related to photogrammetry and remote sensing, such as road extraction from aerial images or position refinement of extraction results. Parametric active contours seem to be suitable for the task of this thesis considering the various extensions and modification. After some pre-processing steps the original data sets can be used for the adaptation without loss of information. Object detection methods are usually not necessary and the information about the objects contained in the GIS data base can be easily incorporated in the initialisation or as additional constraints. Additionally, the potential of active contours to bridge areas with weak features is particularly important considering the often fragmented ALS features linking for example different road parts. The network extension of Buthenuth (2008) provides a suitable basis for the development of an adaptation method for road and river systems. Following these considerations, this thesis will design a parametric active contour approach for the adaptation of 2D vector objects from GIS data bases to ALS data sets

However, several aspects of the network snake concept have to be improved to realise the applicability to the objectives of this thesis. Firstly, the geometric object model of straightness and smoothness is not suitable for the objects of interest in any case. The shrinking effect at dead ends and the smoothing of curve structures can not always be compensated by the image energy derived from ALS data. Besides the topology, the geometry of the GIS vector data, such as the positions of curves or the intersection angles of cross roads, should also be exploited in the process. Secondly, the network snake model is originally designed for linear structures. However, the cross sections of roads and rivers carry semantic information, which is useful for the adaptation process and indispensable for a semantically correct result. The design of a suitable image energy from the ALS data represents the third important task towards an automatic adaptation process. The image energy should represent the objects of interest in the ALS data in an optimal manner and should fit to the geometric object model. Furthermore, semantic properties of these objects and also context objects carry valuable information and should be integrated in the image energy or as additional constraints. Finally, existing approaches of parametric active contours usually do not provide a suitable self-diagnosis in order to detect snake parts where the optimisation does not converge to a satisfying solution. Some work on this aspect was done by Kerschner (2003), who analysed the change of the width of the twin snake model for that purpose. However, a strategy for the general snake model is not available. Thus, another goal of this thesis is to derive suitable parameters from the algorithm for an internal evaluation.

3 A new method for the adaptation of GIS objects to ALS data by means of active contours

3.1 Basic concept and outline

In this section, the basic concept for the adaptation of GIS vector objects to ALS data based on active contours is presented. The general workflow of the method is shown in Fig. 5. This thesis is mainly focused on the adaptation of roads, but rivers are also taken into consideration. In the topographic GIS data bases of NMA, roads and small rivers are usually modelled by their centre lines resulting in linear networks. An attribute related to the width of the object is optionally assigned to each segment. For these objects a method based on a combination of network snakes (Butenuth, 2008) and ribbon snakes (Fua, 1996) is proposed. Larger (broader) rivers (width >12 m in ATKIS) are usually represented by areas in the GIS data bases. These objects hardly benefit from the network property and from the representation by their centre lines in the considered DTM resolution (<1.5 m) (Fig. 6). Thus, they will be treated in a different way using a twin snake approach (Kerschner, 2003). However, the general workflow in Fig. 5 is applied in both cases. Table 1 summarises the three considered object classes, their object models, and the proposed strategy for the adaptation to the ALS data. In the following sections different aspects of the adaptation strategy are explained in detail, such as the initialisation of the contours or the design of the energy terms. Not all aspects are relevant for each strategy. Thus, Table 1 is also a guideline that describes which section is relevant for a particular strategy.

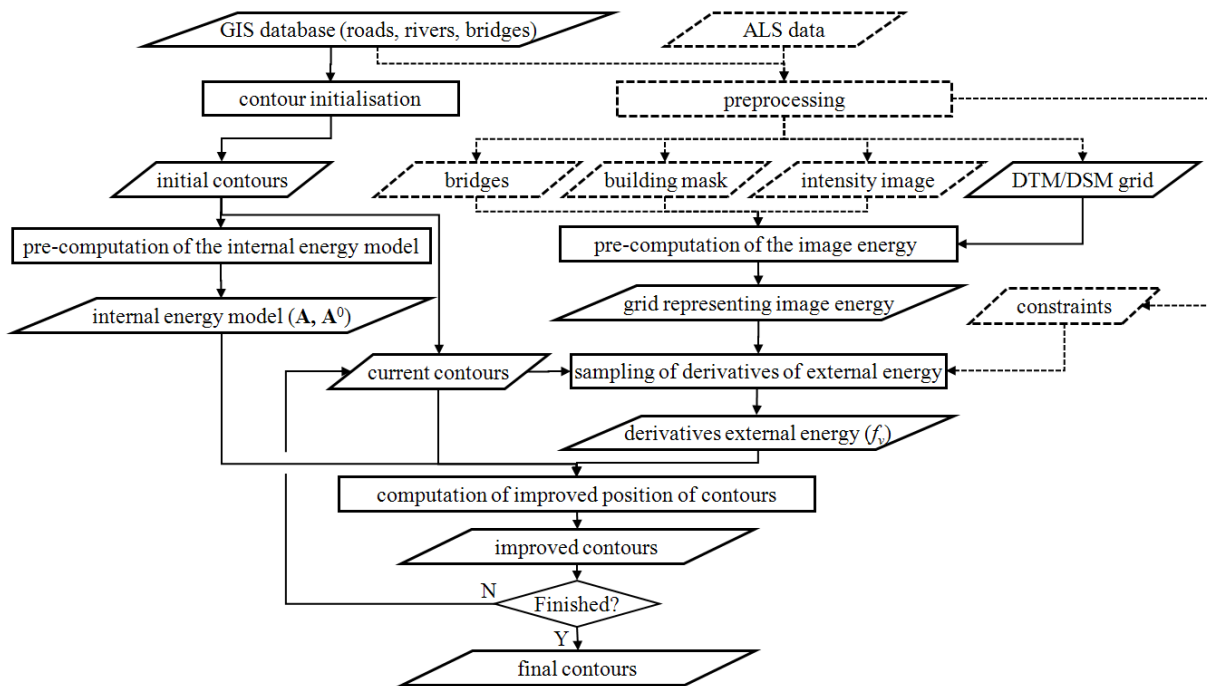


Figure 5. Work flow of the proposed method. Dashed lines indicate optional data or processes.



Figure 6. Different modelling of rivers and canals (background: orthophoto; dark blue: smaller rivers; light blue: large rivers)

Models	Roads	Rivers (Width < 12 m)	Rivers (Width > 12 m)
Object Model	Linear Network	Linear Network	Individual Regions
Proposed Snake Model	Network + Ribbon	Network + Ribbon	Twin
Sections			
Initialisation (3.2)	X	X	X
Pre-Processing Image Energy (3.3)	X	X	X
Rigid Snake Model (3.4.1.1)	X	X	
Network Snakes (3.4.1.2)	X	X	
Ribbon Network Snakes (3.4.1.3)	X	X	
Image Energy for Networks (3.4.2.)	X	X	
Image Energy for River Twins (3.5.1)			X
Constraints for River Twins (3.5.2)			X

Table 1. Object classes, corresponding models and relevant sections

The general workflow for the network snake (roads and small rivers) and the twin snake strategy (larger rivers) is described separately in the following.

Network snake strategy

First results of this strategy were presented in (Göpfert & Rottensteiner, 2009) and (Göpfert & Rottensteiner, 2010).

The minimum input of the method consists of a GIS data base containing the centre lines of the vector objects and a DTM. In addition, the user has to specify the weight parameters of the snake (not shown in Fig. 5). For the **initialisation** of the contours based on GIS vector data, nodes v_i are determined at a regular interval Δs along the vector polygons. Nodes at intersections are introduced once with identical coordinates in all adjacent segments. A list of all its neighbours is also generated for each node, which is a prerequisite for the network snake model. The contour initialisation will be explained in section 3.2.

The DTM is represented by a height grid having a spatial resolution sufficient for the relevant GIS objects, for example roads should appear as smooth bands of grid cells (e.g., 1.5 m or smaller for roads having a width $w \geq 5$ m). Optionally, the proposed method uses an ALS intensity image and information about context objects in the form of bridge and building data (dashed lines in Fig. 5). If the original ALS data are available, the DTM and the intensity image as well as the building and the bridge information can be derived automatically from these data in the **pre-processing stage** (cf. section 3.3). The latter case is considered to be the standard work flow, whereas the DTM is used as primary input data only if no original ALS information is available.

The core of any application of snakes is the definition of the energy terms. The basic model for the **internal energy** is represented by two matrices \mathbf{A} and \mathbf{A}_0 , which will be explained in section 3.4.1 and which can be pre-computed using the initialisation from the GIS data. The proposed model for the internal energy is based on a combination of the concepts of network (section 3.4.1.2) and ribbon snakes (section 3.4.1.3), which improves the accuracy of the final centre lines while preserving the network topology. The exploitation of the initial geometry for a template-like rigid snake model (section 3.4.1.1) enables the method to use global weights for the entire scene and deal with systematic and random errors in the original positions of the snake simultaneously. The initial shape of the snakes is also considered to support the convergence of the results in case of a large systematic displacement of the original GIS data.

The **image energy** forces the snake to move to salient features derived from the other input data. Assuming that the DTM is based on ALS data and because the optional input data can be derived from ALS as well, all features used for computing the image energy are called *ALS features*. The ribbon snakes additionally allow the integration of features at the borderline of the objects or even entire cross section models and require some modification of the image energy. Furthermore, context objects are incorporated in the definition of the image energy. Extracted buildings act as repulsion forces, whereas bridges are used to determine areas that attract the snake to its correct position. Based on all available ALS features, a grid representing the image energy can be pre-computed in order to generate the external force for the optimisation procedure. All aspects of the definition of the image energy are described in section 3.4.2

After the initialisation of the snake and the design of the different energy terms, the iterative **optimization process** is started. Whereas the derivatives of the internal energy are encoded in the matrices \mathbf{A} and \mathbf{A}_0 , the derivatives of the external energy are sampled along the curves in each iteration in order to compute the term f_v in Eq. 14. Solving Eq. 14, the positions of all parts of the network snake are modified simultaneously so that the total energy of the network is iteratively reduced. The iteration process is terminated when the change of position of the contours falls below a user-defined threshold t_{stop} or a maximum number of iteration Max_{iter} is achieved.

Twin snake strategy

First results of this strategy were presented in (Göpfert et al., 2010).

In the twin snake approach, two individual contours are initialised representing the left and right borderline of the GIS region-based river object. For the **initialisation** of the two separate contours, nodes v_i are again determined at a regular interval Δs along the vector polygons. The perpendicular distance to the opposite river borderline is computed for each snake node in order to initialise the distance between the twin partners, thus defining the reference object width.

The **pre-processing stage** (cf. section 3.3) is equivalent to the network snake concept. Context objects, such as bridges and buildings, are not yet considered for this approach.

In comparison to the network strategy, the **internal energy** is not modified for the twin snake approach and corresponds to the original formulation of Kass et al. (1988) (section 2.1.2.2). Some snake properties resulting from the modifications of the internal energy of the network snake concept are modelled by additional constraints.

The general design of **the image energy** (cf. section 3.5.1) is similar to the network snake strategy. However, the image energy of twin snakes is tailored to the representation of the object borderlines in the first place.

In contrast to the network snake concept, a **constraint energy** term E_{con} is considered in the twin snake approach for broader rivers. Three different terms are explained in detail in section 3.5.2. The *twin constraint* connects the nodes of one snake with an opposite line segment of an approximately parallel snake by pre-defined distances. This link to the twin partner avoids strong changes of the initial contour and thus has an effect similar to the rigid shape model of the networks snake concept (section 3.4.1.1). Equivalent to ribbon snakes, twin snakes allow the integration of an object width and thus of borderline features. Some comments on the relationship of these two snake concepts and a sound argumentation for their application to the different object classes can be found in section 3.6. A second proposed constraint models the downhill flow direction of rivers. The third constraint energy term exploits the fact that rivers usually flow in valleys and thus the terrain heights increase on each side with increasing distance to the river.

In contrast to the network snake concept, the **optimisation** of the energy functional for the twin snakes is conducted for each contour individually and alternates between the left and the right snake. The corresponding other snake is fixed in the meantime. In addition to the internal and image energy, the derivatives of the constraint energies with respect to the image coordinates have to be determined for the twin snakes. However, the general optimisation procedure based on Eq. 11 is similar to the one used in the network approach.

In section 3.7 an approach for the internal evaluation is proposed. The interpretation of the different energy terms after the optimisation process gives valuable cues for an automatic assessment of the final position of the snake. The statistical distribution of the energy values of all nodes after the final iteration can be used for outlier detection. However, single energy values of individual nodes are often not suitable to detect erroneous snake parts. Only the analysis of a combination of energy values and the consideration of a local neighbourhood provide reliable parameters for an internal evaluation.

The main parameters of the network and twin snake strategies are briefly summarised in section 3.8, where also some comments about their setup are given. A discussion of the entire method is carried out in section 3.9.

3.2 Contour initialisation from GIS data base

3.2.1 Description of the vector data provided by the NMA using the example of ATKIS

Because most experiments carried out in this thesis use the German Authoritative Topographic Cartographic Information System (ATKIS) as source for the vector objects, the specifications and the resulting conclusions for the initialisation of the active contours are exemplarily described for this topographic GIS. ATKIS was developed in order to provide a national digital topographic data base using different models of the Earth's surface. ATKIS was designed based on four components: the digital landscape model (DLM), the digital terrain model (DTM), digital orthophotos (DOP), and digital topographic maps (DTK). For the initialisation of the snakes in this thesis, the DLM of the finest scale (DLMBasis) is exploited. In general the DLM describes the objects on the Earth's surface using 2D vector objects, such as road centre lines or forest and urban regions, and additional attributes. The acquisition of the objects with respect to their size and importance is mainly based on the topographic maps. The corresponding criteria are summarised in the ATKIS object catalogue (ADV, 2011). This catalogue specifies which objects and which level of detail should be represented. In contrast to topographic maps, objects of the DLMBasis are not subject to cartographic generalisation. However, some kind of uncertainty results from the accuracy of acquisition and the modelling of the objects. The basis of the initial acquisition of the DLMBasis varies for the different federal states of Germany. In any case the main sources are topographic maps 1:5000 or 1:10000. In areas where maps of a scale of 1:5000 and additional large-scale orthophotos are available, the planimetric accuracy of the gathered objects achieves 3 m (e.g., Bremer et al., 1992). In contrast the digitization of the objects in maps 1:10000 results in an accuracy of 5-10 m. Some federal states manually improved the position of the objects in order to achieve an accuracy of 3 m. For the updating of the objects different data sources are exploited. For example, besides the digitisation of objects in orthophotos also coordinates of construction plans for roads are integrated. For objects of the highest importance, such as roads and rivers, the updating cycle is three months, whereas the updates of other objects is normally based on the regular acquisition interval of aerial photos (3-5 years). Thus, the entire process of acquisition and updating in different federal states results in a very inhomogeneous accuracy and up-to-dateness of the DLMBasis, which is used here for the snake initialisation. Generally, the objects in the DLMBasis are represented by the vector model (cf. section 2.1.2.1). The properties of roads and rivers with respect to the DLMBasis are briefly introduced in the next section.

3.2.2 Selected objects for the adaptation process

Roads

The Traffic Layer (3000) of the ATKIS DLMBasis contains road traffic objects in a sub layer (3100). The public road network in this sub layer mainly consists of the object classes "road" and "path". Whereas the class "road" includes the main traffic routes, such as highways or urban roads, the class "path" covers minor traffic connections, such as farmland roads. In general, road objects in GIS data bases are usually represented by their centre lines as a sequence of line segments connecting discrete nodes. The distances between the nodes vary with the curvature of the road parts and with the modelling accuracy. However, for a reliable approximation of derivatives of the contour with respect to the arc length s in the internal energy by finite differences, contour nodes v_i at a regular interval Δs along the line segments are required. Thus, the contour nodes are interpolated at a fixed interval Δs in the original GIS roads. This general node distance Δs determines the modelling accuracy of the road segment and crucially affects the quality of the snake optimisation, because the ALS features are sampled at these points. The node distance is usually set to the width of an ordinary two-lane road (5 m), because this is the standard road in the test data. Different road parts at crossings or t-junctions share a

common node in the GIS data base, whereas roads intersecting via tunnels or crossovers are not connected at this position. The common nodes of the road parts carry the topologic information of the network and are thus important for the snake initialisation. These nodes are also introduced once in the initialisation thus having identical coordinates in all adjacent segments. In order to generate the internal energy represented by matrix \mathbf{A} or \mathbf{A}_0 (cf. section 3.4.1.1) using the topology of the contours automatically, a list of all its neighbours is also generated for each node. Furthermore, various attributes describe the properties of the belonging road segment and can be used as additional information for the proposed snake algorithm. One of the relevant attributes is the actual width of the road. This attribute represents a suitable initialisation for the ribbon extension. Other interesting attributes, which can be exploited by further research, describe properties like the number of road lanes, the occurrence of cycle lanes or sidewalks along the road, or the surface material of the road. The latter attribute specifies the reflectance property of the road surface and can support the interpretation of the ALS intensity values, whereas the number of lanes and the availability of sidewalks can give information for the cross section model.

Rivers

In the example of ATKIS, rivers belong to the layer “water areas” (5100). In spite of its name the layer contains linear structures as well as region-based objects. Rivers are represented by two different object models corresponding to their widths. Narrow rivers (width <12 m) are modelled as a linear network similar to the roads and can be used for initialisation purpose in the same way. The original nodes of the network from the GIS data base are used to interpolate contour nodes at a predefined interval Δs in order to guarantee the robust computation of the finite differences in the internal energy term. Common nodes at river junctions determine the topology of the network and the adjacency graph is integrated in the matrix \mathbf{A} or \mathbf{A}_0 . Broader rivers (width >12 m) are usually represented as areas. For these objects the left and right borderlines of the elongated river areas are used in order to initialise two individual snakes. The nodes of the contour are again interpolated from the GIS vector objects in order to generate equidistant snake nodes. Additionally, for each node the perpendicular distance to the opposite borderline of the river is computed in order to determine the river width at this position, which is required for the initialisation of the twin constraint. This constraint connects the two snakes representing the opposite river sides by pre-defined distances during the optimisation process (section 3.5.2.1), so that the snakes are not able to move independently from each other. This is one of the aspects of the algorithm that exploits prior knowledge of the GIS data base in order to stabilise the optimisation process. Furthermore, attributes of rivers provide useful information for an adaptation to the ALS features. An important attribute for the applicability of the proposed method describes whether the river flows above or below the ground and can be thus detected in the ALS features or not.

Bridges

The approximate position of bridges can be derived from ATKIS either based on the given topology (crossings of roads and rivers without common nodes) or on explicitly modelled bridge objects. These positions are used as initial information for the bridge detection in the DTM.

3.3 Pre-processing of the ALS data

Pre-processing is required if the original ALS data are available rather than a derived DTM as the only data source. The ALS data can then be used to derive any of the four input data sets, namely a DTM, an intensity grid, buildings, and bridge information, used to define the image energy. The integration of all four data sets is considered to be the standard

workflow of the network snake strategy, whereas the bridge and building information has not yet been considered for the twin snake concept. The DTM represents the minimum input required for both strategies.

For **DTM** generation, the ALS points have to be classified as terrain or off-terrain points. It is important to note that the applied method should classify points on bridges as ground points. This aspect is necessary not only to detect bridges, but also to avoid large repulsive forces of the image energy at the end points of bridges affecting the motion of road centre lines. In principle, each filtering algorithm that assigns bridges as ground can be used for this pre-processing step (cf. section 2.2.2.1). In this study a simple method is used for filtering that is based on the classification of connected segments of points having a low local surface roughness as terrain segments (Niemeyer et al., 2010). The method estimates a plane for each point, taking into account its k (e.g., 9) nearest neighbours. Taking the R.M.S. error of the unit weight of the planar fit as a measure for the local surface roughness, we search for connected segments of points that have a low surface roughness. Using a morphological opening filter, a coarse DTM is generated from the DSM (Weidner & Förstner, 1995), and each segment is classified according to its average height difference from the approximate DTM. An improved DTM is generated from the points in segments classified as terrain segments, and the classification can be repeated taking advantage of the improved DTM from the first iteration. In order to also include terrain points that are characterised by a high surface roughness, a final classification of all ALS points is carried out based on their height differences from the improved DTM. The DTM grid is interpolated by kriging (Cressie, 1990) taking into account only the terrain points. Bridge points are assigned to the ground by the proposed method, because the road will correspond to a large segment with a low surface roughness that is situated on the terrain everywhere except at the bridge.

The **intensity** image is interpolated from the intensity values of the irregularly spaced ALS points by kriging (Cressie, 1990). Subsequently, a median filter is used to decrease the noise while preserving the object edges. For some ALS data sets the strong specular reflection of water surfaces results in streaking effects (Fig. 7) in the intensity values. This means that very high ALS intensities exist for small incidence angles, whereas there are low intensities or no suitable echoes at all at the borderlines of each flight strip. This effect makes it difficult to use the intensity image for the design of the image energy for rivers. The applicability of the intensity image is visually checked in the method in this thesis. If the check fails, the intensity image will not be considered in the workflow. Although there are methods that introduce a radiometric correction of the intensity values, for reasons explained in section 2.1.1.2 the uncorrected values are used in this thesis.

Buildings are detected in the ALS data by means of the method described in (Rottensteiner et al., 2007). This algorithm is used because building extraction is beyond the scope of this thesis and the method was available to the author. For the definition of the image energy (cf. section 3.4.2.3) only a binary building mask is required. The applied method starts with a morphological filtering in order to generate the DTM from the ALS point cloud. Afterwards, a two-stage Dempster-Shafer data fusion process is applied for classification. The height above the terrain, parameters of the surface roughness, and the difference between the first and last ALS echo are integrated as features in order to classify the data into buildings, bare soil, trees, and grassland. In contrast to the original approach, the NDVI is not used here, because colour infrared (CIR) images are not available. Rottensteiner et al. (2007) evaluate the influence of the NDVI on completeness and correctness rates of the building detection. The completeness hardly suffers from the missing NDVI feature, whereas the correctness is decreased by 20 % for small and medium-sized buildings due to more trees among the false positives. This aspect may affect also the quality of the adaptation process, because branches of trees hanging across the road or river will generate repulsive forces for the snake.

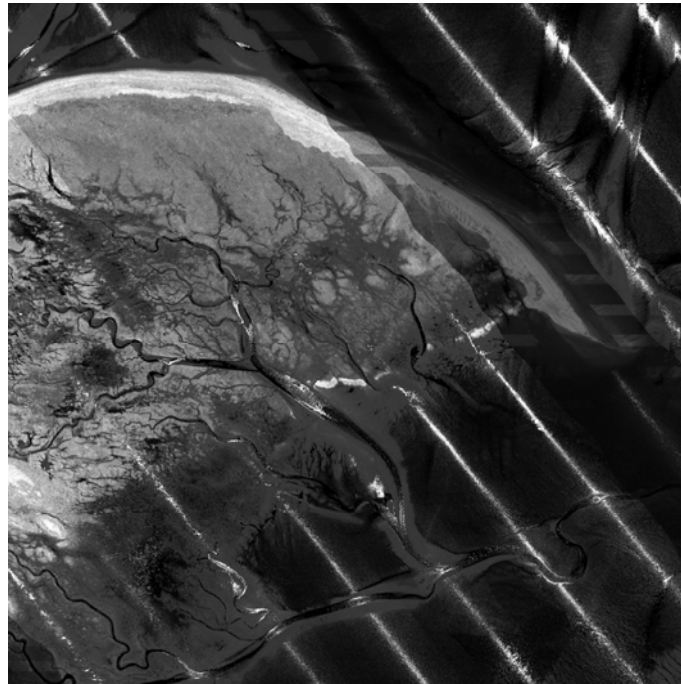


Figure 7. *Dependency of intensity values on the angle of incidence for water surfaces*

Bridge detection requires the approximate positions of bridges. This information is assumed to be contained in the GIS database, be it explicitly, e.g., in the form of bridge objects, or implicitly, e.g. by the fact that a road segment intersects a river in 2D. An edge amplitude image is generated from the DTM in the vicinity of the approximate bridge position (e.g., 100 m x 100 m). The largest edge amplitude corresponding to a local minimum in a smoothed version of the amplitude histogram is used as a threshold to mark edge pixels (Fig. 8a). The most dominant straight line detected by a Hough transform is considered to correspond to one of the bridge borderlines, and its line direction thus defines the direction of the bridge. The second edge of the bridge should correspond to a relative maximum in Hough space having the same direction, but a different offset (Fig. 8b). If no second significant relative maximum is found at this line direction within a certain distance from the first one, the procedure is abandoned and the bridge information is not taken into account. Otherwise, the offset difference between the two maxima defines the bridge width.

The length of the bridge is estimated by the maximum extent of the segmented edge pixels corresponding to the longer bridge borderline. The width, the length, and the direction of the bridge are then used to design a template in order to determine the coordinates of the bridge centre in the DTM by area-based matching. The template models the bridge to connect two horizontal planes separated by a trapezoidal valley (Fig. 8c). It is moved over the DTM, and the cross correlation coefficient is determined at each position. A small area around the maximum of the correlation image is segmented by thresholding (see red area in Fig. 8d). The bridge centre point is determined as the centre of gravity of the segmented area, and a distance transform of this area is determined (Fig. 8e) which will later be used to determine the image energy for bridges (cf. section 3.4.2.4).

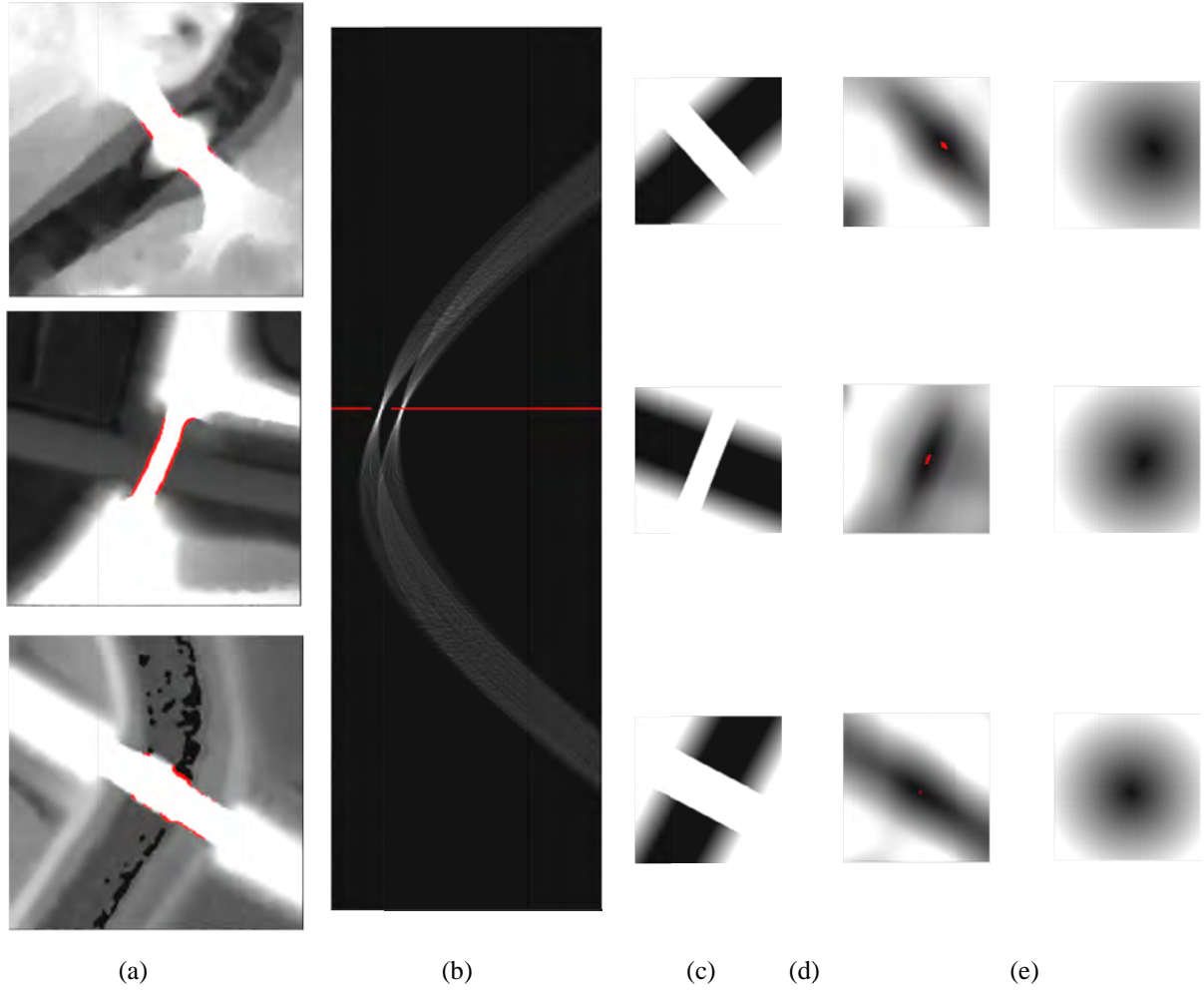


Figure 8. (a) Bridge borderlines in the DTM; (b) search for the second parallel borderline in Hough space for the first bridge (red: bridge direction); (c) bridge templates; (d) inverse correlation image (red: minimum); (e) E_{bridge} of the central bridge node after a distance transform.

3.4 Network snake strategy

This section describes the main aspects of the proposed network snake strategy using the example of roads. At the end of this section, the concept for roads is adapted to networks of narrow rivers by slightly modifying the image energy without changing the developed object model of the internal energy.

3.4.1 Internal energy

In this section, three modifications of the basic internal energy model described in section 2.1.2.2 are explained that are integrated into the proposed snake model in order to improve the applicability and robustness of the method. The expected positive effect of each individual modification on the quality of the adaptation results will be emphasized. Furthermore, synergy effects caused by the interaction of these modifications reveal the full strength of the proposed method and will be highlighted as well.

3.4.1.1 Rigid snake model

Due to the strongly varying reliability of the features in the ALS data, a well-balanced weighting between the internal and image energy for an entire scene is difficult to find. The original model of the internal energy in Eq. 5 (section 2.1.2.2) favours a smooth and straight shape of the snake in any case. However, this model is not well-suited for curves in the roads or rivers. Therefore, in the presence of weak ALS features, the image energy is often not able to compensate the smoothing and straightening effects of the internal energy, which changes the geometry of the roads in areas with a high curvature in an undesirable manner. On the other hand, in case of spurious edges and noisy data a strong smoothing is essential for convergence. One possible solution is to assign smaller weights to the internal energy for snake nodes with strong curvature in the initialisation. However, this modification may result in an overfitting of the curved road parts to the ALS data, and it weakens the stabilising effect of the significant geometry of these curved snake elements on the optimisation process. Therefore, another approach that was firstly introduced by Radeva et al. (1995) is preferred. Basically, the internal energy according to Eq. 5 increases with the deviation from a smooth and straight shape of the snake. In contrast, the new internal energy penalises the differences between the current and the initial geometry of the objects:

$$E_{int} = 0.5 \cdot \left[\alpha(s) \cdot |\mathbf{v}_s(s)|^2 - \alpha^0(s) \cdot |\mathbf{v}_s^0(s)|^2 + \beta(s) \cdot |\mathbf{v}_{ss}(s)|^2 - \beta^0(s) \cdot |\mathbf{v}_{ss}^0(s)|^2 \right] \quad (12)$$

In Eq. 12, \mathbf{v}_s^0 and \mathbf{v}_{ss}^0 are the derivatives of \mathbf{v}^0 , i.e., of the initialisation of \mathbf{v} , with respect to the arc length s ; α^0 and β^0 are the weights of the internal energy terms related to the initialisation \mathbf{v}^0 . Considering this alternative formulation of the internal energy in Eqs. 9 and 11 results in:

$$\mathbf{A} \cdot \mathbf{v} - \mathbf{A}^0 \cdot \mathbf{v}^0 + f_v(\mathbf{v}) = 0 \quad (13)$$

$$\mathbf{v}_t = (\mathbf{A} + \gamma \cdot \mathbf{I})^{-1} \cdot [\gamma \cdot \mathbf{v}_{t-1} + \mathbf{A}^0 \cdot \mathbf{v}^0 - f_v(\mathbf{v}_{t-1})] \quad (14)$$

If α and α^0 , β and β^0 (and, consequently, \mathbf{A} and \mathbf{A}^0) are identical, the geometric model of the snake according to Eq. 12 will penalise any deviation of the shape of the snake from the initialisation. Therefore, without any external energy neither the shape nor the position of the snake would change. By selecting α^0 and β^0 lower than α and β , an additional generalisation of the curve similar to the original formulation of the internal energy (Eq. 5) can be achieved, an aspect not considered in (Radeva et al., 1995). This is important for applications such as cartographic generalisation. However, a generalisation is not applied in the proposed approach, i.e. in all of the experiments in chapter 4 $\alpha = \alpha^0$ and $\beta = \beta^0$ are selected. Under these circumstances, the following advantages of the modified internal energy for the application dealt with in this thesis can be highlighted:

- The weights of the internal energy are directly connected to the GIS data. This fact facilitates the derivation of these parameters depending on the accuracy and reliability of this data set, which increases the transparency of the weight selection process. In the original formulation (Eq. 5), α and β just determine the weights of a generic geometric model of smoothness and straightness, which is not associated with the quality of the GIS data and may be inappropriate.
- Without any evidence in the ALS data for a discrepancy between the two data sets, the shape and position of the snake do not change. This fact is important mainly in areas of weak ALS features.

- The modified internal energy facilitates the fine-tuning of weights and allows new strategies for the iterative optimisation of the snake. For example, a large weight for the internal energy in the first iteration steps will result in a very rigid geometry of the snake, enabling the method to deal with systematic shifts between the data sets, whereas a smaller weight for the internal energy in the later iteration steps permits a local adaptation of the snake to the image energy.
- A large internal energy after the optimisation process indicates strong changes of the initial geometry. This fact can guide an operator to network parts which have to be checked in post-processing.
- The rigid object model stabilises the position of each node in the network structure. This aspect facilitates the direct determination of shift vectors from the change of the position of the nodes during the optimisation process.
- The shrinking effect of the internal energy is avoided, which is crucial especially at dead ends (nodes with degree = 1) of the roads.
- Constraints such as perpendicularity of road crossings are automatically integrated for network snakes (cf. Section 3.4.1.2) if they are contained in the initial data.
- Rapid changes with respect to the width of the ribbon snakes (e.g., at crossings of roads with different priority) can be preserved if they are available in the attributes of the GIS data as prior knowledge.

It may be considered a drawback of the modified internal energy that it increases the importance of a suitable initialisation. Whereas the original formulation (Eq. 5) requires an initialisation in the immediate vicinity of the object boundaries, the alternative term (Eq. 12) additionally relies on a good representation of the object shape by the initialisation. However, in many photogrammetric applications the model based on the initial shape, which is often taken from a GIS data bases, is expected to outperform the original model of straightness and smoothness.

3.4.1.2 Network snakes

The basic formulation of the energy minimisation of the snake is valid for closed contours. However, Butenuth (2008) extends this concept to networks of contours taking into account nodes of a higher degree. In Fig. 9 an example of a road network containing nodes of different degrees is shown. The extended topology of the network requires a few changes in the definition of the internal energy due to the lack of some finite differences. Because the nodes \mathbf{v}_{i+1} in Eq. 8 are not available for end nodes and for nodes of higher degree (>2), the first term of the internal energy defining the elasticity is not defined and, thus, not considered. The existing differences are used for the definition of the second term which controls the curvature and is weighted by β . For a node \mathbf{v}_n with a degree of three the energy is defined as:

$$\begin{aligned}
 \beta \cdot (\mathbf{v}_{a_n} - \mathbf{v}_{a_{n-1}}) - \beta \cdot (\mathbf{v}_{a_{n-1}} - \mathbf{v}_{a_{n-2}}) + f_{v_a}(\mathbf{v}_a) &= 0 \\
 \beta \cdot (\mathbf{v}_{b_n} - \mathbf{v}_{b_{n-1}}) - \beta \cdot (\mathbf{v}_{b_{n-1}} - \mathbf{v}_{b_{n-2}}) + f_{v_b}(\mathbf{v}_b) &= 0 \\
 \beta \cdot (\mathbf{v}_{c_n} - \mathbf{v}_{c_{n-1}}) - \beta \cdot (\mathbf{v}_{c_{n-1}} - \mathbf{v}_{c_{n-2}}) + f_{v_c}(\mathbf{v}_c) &= 0
 \end{aligned} \tag{15}$$

The three contour parts **a**, **b**, and **c** intersect in the common node $\mathbf{v}_n = \mathbf{v}_a = \mathbf{v}_b = \mathbf{v}_c$. Due to the definition of the internal energy according to Eq. 15, the shape of each part is controlled separately except for the intersection point. The rigidity and smoothness terms do not act beyond the intersection point. However, the initial topology of the network is taken into account and can be exploited during the energy minimisation process. Subsequently, the matrices \mathbf{A} as well as \mathbf{A}^0 in Eqs. 11 and 14 have to be reorganised by separating contour parts that are not connected as well as by adding entries for new

relations between adjacent nodes according to Eq. 15. For end nodes and nodes with higher degree (>3), a similar definition of the internal energy can be applied by adding or excluding equations in Eq. 15, depending on the degree of the considered node point. The combination of the network snake model with the rigid shape model (Eq. 12) changes Eq. 15 as follows:

$$\begin{aligned} \beta \cdot (\mathbf{v}_{a_n} - \mathbf{v}_{a_{n-1}}) - \beta^0 \cdot (\mathbf{v}_{a_n}^0 - \mathbf{v}_{a_{n-1}}^0) - \beta \cdot (\mathbf{v}_{a_{n-1}} - \mathbf{v}_{a_{n-2}}) + \beta^0 \cdot (\mathbf{v}_{a_{n-1}}^0 - \mathbf{v}_{a_{n-2}}^0) + f_{v_a}(\mathbf{v}_a) &= 0 \\ \beta \cdot (\mathbf{v}_{b_n} - \mathbf{v}_{b_{n-1}}) - \beta^0 \cdot (\mathbf{v}_{b_n}^0 - \mathbf{v}_{b_{n-1}}^0) - \beta \cdot (\mathbf{v}_{b_{n-1}} - \mathbf{v}_{b_{n-2}}) + \beta^0 \cdot (\mathbf{v}_{b_{n-1}}^0 - \mathbf{v}_{b_{n-2}}^0) + f_{v_b}(\mathbf{v}_b) &= 0 \\ \beta \cdot (\mathbf{v}_{c_n} - \mathbf{v}_{c_{n-1}}) - \beta^0 \cdot (\mathbf{v}_{c_n}^0 - \mathbf{v}_{c_{n-1}}^0) - \beta \cdot (\mathbf{v}_{c_{n-1}} - \mathbf{v}_{c_{n-2}}) + \beta^0 \cdot (\mathbf{v}_{c_{n-1}}^0 - \mathbf{v}_{c_{n-2}}^0) + f_{v_c}(\mathbf{v}_c) &= 0 \end{aligned} \quad (16)$$

The superscript zero again indicates that these nodes and weights belong to the initialisation.



Figure 9. Topology of a road network represented by its centre lines. The degree of the nodes is indicated by the node colour (background: DSM+ALS intensity).

3.4.1.3 Ribbon network snakes

Up to now the snakes were just represented by connected single polygons and the image energy is calculated at one point for every snake node per iteration. As the ALS features are particularly weak for road and river centre lines, the model has to be extended in order to integrate features at the borderlines or even along the entire cross section. For similar reasons, Fua (1996) proposed the ribbon snake model which introduces a width w in every node as an additional parameter. In contrast to Eq. 4, the parametric active contour is now represented by $\mathbf{v}(s) = [x(s), y(s), w(s)]$. If the same smoothing and straightening forces are valid for all three parameters including w , in order to determine w along with x and y , Eq. 7 corresponds to *three* (rather than two) Euler equations, namely one for x , one for y , *and* one for w . With respect to w , this formulation of the internal energy prevents a strong variation of the ribbon width in neighbouring nodes.

In the original ribbon snakes model, the image energy is sampled at two positions \mathbf{v}_{iR} and \mathbf{v}_{iL} on a line perpendicular to the snake direction at the distance w_i from the current node \mathbf{v}_i (Fua., 1996). That is, if \mathbf{n}_i is the unit normal vector to the snake at node \mathbf{v}_i with $\|\mathbf{n}_i\| = 1$, the image energy is sampled at $\mathbf{v}_{iR} = \mathbf{v}_i + w_i \cdot \mathbf{n}_i$ and $\mathbf{v}_{iL} = \mathbf{v}_i - w_i \cdot \mathbf{n}_i$. The curves consisting of the nodes \mathbf{v}_{iR} and \mathbf{v}_{iL} correspond to the object edges according to the original model, and $2 \cdot w_i$ is the width of the object at node i , more or less smoothly changing depending on the weight of the internal energy of the snake (Laptev et al., 2000). In order to combine this model with the concept of network snakes, the ribbon snake model needs to be modified for the intersections, that means for the nodes of a degree higher than 2 in the network. In the network snake concept, the contour parts linked to such a node are forced to intersect in a common node \mathbf{v} (cf. section 3.4.1.2). This is shown for three intersecting contour parts **a**, **b**, and **c** in Fig. 10. As there is a joint node \mathbf{v} and because \mathbf{v} also has a unique width w attached to it, all intersecting contours are forced to have the same width w in \mathbf{v} . As a consequence, the smoothing effect of the internal energy on the ribbon width is continued at nodes of higher degree, which may cause problems concerning crossings of streets with a different number of lanes. However, different ribbon widths can be initialised by attributes from the GIS database (if available). A change of the width at two neighbouring nodes leads to a strong curvature in the graph of w drawn against the parameter s . By applying the alternative internal energy (cf. section 3.4.1.1.) also to parameter w , this change of the object width is preserved. If the image energies for \mathbf{v} were sampled at the positions \mathbf{v}_R and \mathbf{v}_L according to the above definition for all intersecting contours, the areas defined by the intersecting ribbons would overlap. Thus, this definition for nodes having a degree higher than 2 is changed. For each pair l and m of contours that are neighbours in the ordered pencil of contours intersecting at \mathbf{v} , one common point \mathbf{v}_{lm} is determined where the image energy of both ribbon contours will be sampled (cf. \mathbf{v}_{ab} for the contours **a** and **b** in Fig. 10). This point is situated on the angle bisector of the two contours in \mathbf{v} (if $w_a = w_b$). If the intersection angle between these contours is θ_{lm} , the distance w_{lm} between \mathbf{v} and \mathbf{v}_{lm} is determined according to:

$$w_{lm} = \frac{w}{\sin\left(\frac{\theta_{lm}}{2}\right)} \quad (17)$$

This model causes the ribbons intersecting at the common node \mathbf{v} to have also intersecting edges. The modifications of the image energy for the ribbon snake model are explained in section 3.4.2.5. It has to be noted that the model in Fig. 10 and Eq. 17 has to be slightly modified for intersecting roads with a significantly different width. In principle, the method can deal with such asymmetric crossings due to the integration of the rigid snake model, which preserves discontinuities of the initial ribbon width. For the experiments it is assumed that smaller roads widen at such crossings. Thus, for the central node the width of the broadest road arms is used.

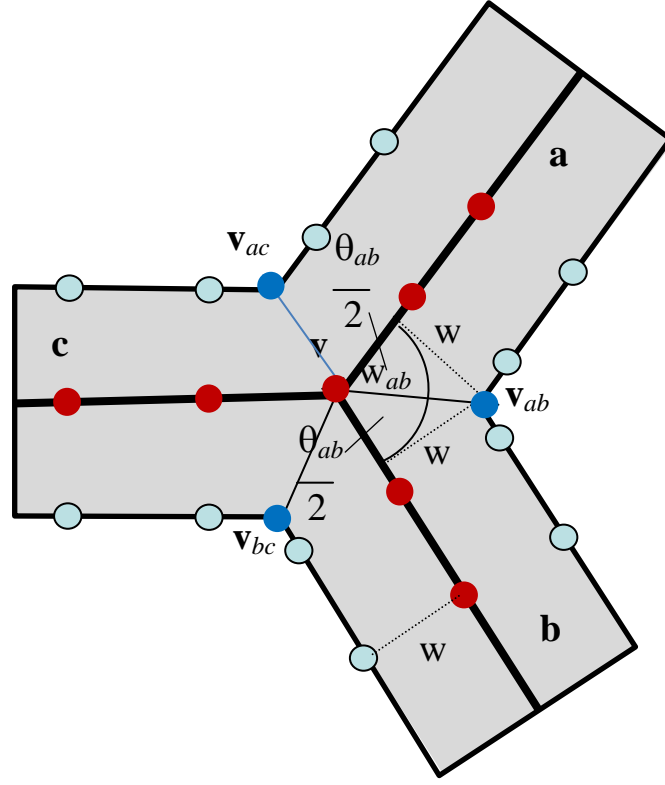


Figure 10. Ribbon snake model for a node v of degree 3. The ribbon area is shown in grey. **a**, **b**, **c**: the three intersecting contours. Red dots: the contour nodes. Blue dots: the positions where the image energy is sampled. w : the width parameter at node v . θ_{ab} : intersection angle of contours **a** and **b**. w_{ab} : the distance between v and v_{ab} .

3.4.2 Image energy

3.4.2.1 General image energy for network objects

The image energy E_{image} consists of three different components, namely a general ALS energy E_{ALS} , a building term E_{build} that repulses the snakes from buildings, and a bridge term E_{bridge} attracting the snake to bridges detected in the ALS data:

$$E_{image} = \kappa_I \cdot \left[\lambda(x, y) \cdot E_{ALS} + \mu(x, y) \cdot E_{build} + \nu(x, y) \cdot E_{bridge} \right] \quad (18)$$

In Eq. 18, κ_I is a weight for the entire image energy term, and $\lambda(x, y)$, $\mu(x, y)$, and $\nu(x, y)$ are weight functions for the individual terms that may vary over the image. More specifically, our method requires the consideration of buildings and bridges. Let $Build(x, y)$ be a binary image that takes a value of 1 to indicate the presence of a building and 0 otherwise. Analogously, let $Bridge(x, y)$ be a binary image indicating the presence of a bridge. Then we define

$$\begin{aligned} \lambda(x, y) &= [1 - Build(x, y)] \cdot [1 - Bridge(x, y)] \\ \mu(x, y) &= Build(x, y) \\ \nu(x, y) &= Bridge(x, y) \end{aligned} \quad (19)$$

In other words, in regions classified as a building, only E_{build} is taken into account, in regions classified as a bridge only E_{bridge} is considered, and in all other areas only E_{ALS} is used. Of course, Eq. 19 is only used if building and / or bridge data are available; otherwise, the corresponding weight functions $\mu(x, y)$ and / or $\nu(x, y)$ are set to zero.

The weighted sum of the general ALS and the building energies in Eq. 18 is pre-computed for every DTM grid point, resulting in a grid representing a part of the image energy (cf. Fig. 5), whereas for reasons explained in section 3.4.2.4, the binary image $Bridge(x,y)$ and thus E_{bridge} is updated in each iteration. In the subsequent sections, the individual energy terms in Eq. 18 are described in more detail.

3.4.2.2 ALS energy for road networks

The general ALS energy E_{ALS} consists of the sum of the *height variation energy* E_{Height} and the *intensity energy* E_I , weighted by a and b , respectively:

$$E_{ALS} = a \cdot E_{Height} + b \cdot E_I \quad (20)$$

Three different models for the height variation energy E_{Height} in Eq. 20 can be used, depending on the resolution of the point cloud:

- For data having a resolution of 1 m and smaller, we exploit the fact that roads are usually situated on smooth and nearly horizontal surfaces. Therefore, a plane is estimated in a 3 m x 3 m window for every grid point in the DTM, thus considering common values of the road width. The term E_{Height} is the sum of the absolute values of the plane slope in x - and y -direction. This definition of E_{Height} thus highlights strong slopes in the DTM; it should prevent the roads represented by the snakes from moving to surface areas having invalid height gradients.
- For data having a rather low resolution (> 1 m), the above definition was found not to be suitable. In this case E_{Height} is defined as the standard deviation of the DTM in a 3 m x 3 m window. The standard deviation increases with higher slopes as well as with a larger variation of the heights in flat terrain covered by vegetation (even in the DTM). These two facts indicate non road surfaces.
- For urban areas the lower ALS point density is not suitable to extract building outlines reliably (cf. Rottensteiner et al., 2007). Thus, the standard deviation of the unfiltered DSM is used for E_{Height} , in order to exploit the strong building edges in the DSM for the adaptation. However, local minima in smooth roof areas and branches of trees above the road disturb this part of the image energy.

Road surfaces such as asphalt generally appear dark in an intensity image (Clode et al., 2007). Therefore, the pre-processed intensity image is directly used for the image energy term E_I in Eq. 20, forcing the snake to low grey values. However, some other objects such as building roofs show a similar behaviour and disturb the optimization process related to E_I , which is the main motivation for using the building term E_{build} (Eq. 18). In case no intensity information is available, E_I is set to 0 and only the height variation energy E_{Height} is active. The weights (a , b) of the energy terms in Eq. 20 are determined empirically supported by the histograms of the intensity image and the DTM slopes or height variations. One of the weights (a , b) is redundant, because only the ratio is relevant to model the relative importance of the ALS intensity and the height variation on the image energy. Two parameters are introduced to facilitate the parameter setting.

3.4.2.3 Building energy

The second component, E_{build} , in Eq. 18 is required because E_{ALS} as defined in section 3.4.2.2 has local minima caused by nearly horizontal building roofs that additionally have reflectance properties similar to roads and rivers. On the other hand, buildings have strong relations to the adjacent road segments: they can be treated as “forbidden areas” for standard

roads, acting as a repulsion force. A distance transform is applied to the building mask (cf. section 3.3), and the binary image $Build(x,y)$ used to define the weight $\mu(x,y)$ of E_{build} (Eq. 19) is generated by thresholding the distance image at 1 m (to compensate for errors of the building outlines). Thus, E_{build} will be effective inside the building and within a distance of 1 m from the building boundaries. The building energy E_{build} itself is based on a distance transform of the negation of the binary image $Build(x,y)$. That is, E_{build} is zero outside the enlarged building area described by $Build(x,y)$, whereas in the interior of a building it is identical to the distance to the nearest non-building pixel. The skeletons of the building areas act as decision boundaries: if the initialisation of the road network is situated on the correct side of the building skeleton, the snake will slide to the correct “urban valley”. Fig. 11 shows a building mask and the corresponding building energy.

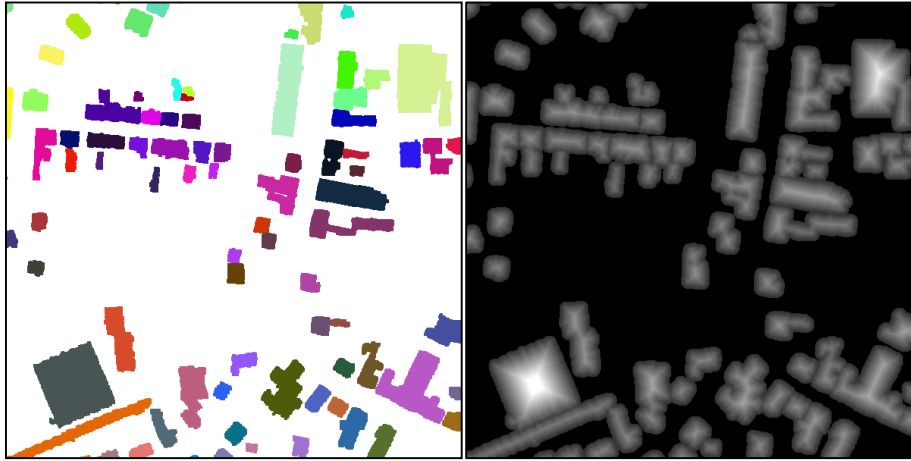


Figure 11. Left: building mask; right: building energy term E_{build} .

3.4.2.4 Bridge energy

Due to the fact that bridges indicate the course of roads with high confidence, the information about this object class should guide the snake optimisation process in the corresponding areas. Integrating the extracted bridge points as a constraint energy term would introduce new weights, which makes fine-tuning of the parameters more complex. Thus, a method is proposed that converts the information about bridges into a suitable image energy term for the related nodes of the road network.

At the end of bridge detection, a distance transform of the most likely bridge areas was determined (cf. section 3.3 and Fig. 8). E_{bridge} is determined by shifting the results of the distance transform in the bridge direction. More precisely, for any node \mathbf{v}_k on the bridge (according to the bridge length) having the coordinates (x,y) , E_{bridge} is defined as

$$E_{bridge}(x,y) = d[x - (k - c) \cdot \Delta s, y - (k - c) \cdot \Delta s] \quad (21)$$

In Eq. 21, c is the index of the node in the centre of the bridge, $(\Delta x, \Delta y)$ is the (normalised) direction vector of the bridge, Δs is the nominal spacing of nodes in the snake and $d(x,y)$ is the result of the distance transform. In case of two intersecting roads, for the underpass this energy is only used for the central node, i.e. for the node directly under the bridge. The binary image of bridge pixels $Bridge(x,y)$ used to define the weights $\mu(x,y)$ (cf. Eq. 19) thus is zero everywhere except in a narrow band of a few pixels width to the left and to the right of the approximate position of the snake from the last snake node before the bridge to the first node after the bridge. This implies that $Bridge(x,y)$ is updated

after each iteration in the optimisation process. That is, the final image energy at a position (x,y) is equal to the pre-computed combination of E_{ALS} and E_{build} where $Bridge(x,y) = 0$, whereas at positions where $Bridge(x,y) = 1$, E_{bridge} according to Eq. 21 is used in Eq. 18.

3.4.2.5 Image energy for ribbons

The image energy of regular snakes is determined exactly at the positions of the nodes, which in our application correspond to the object centre lines. Ribbon snakes were originally designed to determine the centre lines of objects that could more precisely be located by their edges.

The definition of the image energy for ribbon snakes used here is different and is exemplarily explained for roads. However, this definition can also be applied to rivers in a similar way. In Eq. 18, a model for the image energy E_{image} is defined. This image energy E_{image} is the basis for a new definition of the image energy for ribbon snakes E_{ribbon} that will then replace the original image energy in the energy functional of Eq. 4. Firstly we observe that E_{image} was defined based on model assumptions for road surfaces, so that its local minima should correspond to the road centre lines. A small local neighbourhood is taken into account for determining the ALS term in E_{image} . This local neighbourhood is so small that the local minima in E_{image} will be very flat for standard roads, i.e. the position of the centre line will not be very accurate.

Now let $\nabla E_{image}(\mathbf{p})$ be the gradient of E_{image} at a point \mathbf{p} . The component of $\nabla E_{image}(\mathbf{p})$ in direction of the normal vector \mathbf{n}_i at a node \mathbf{v}_i is the inner product $\nabla E_{image}(\mathbf{p}) \cdot \mathbf{n}_i$. Consider a profile of the absolute value of this component, $\|\nabla E_{image}(\mathbf{p}) \cdot \mathbf{n}_i\|$, that is perpendicular to the road at \mathbf{v}_i (Fig. 12). $\|\nabla E_{image}(\mathbf{v}_i) \cdot \mathbf{n}_i\|$, i.e. its value at the road centre line, will be close to 0. As \mathbf{p} moves along the profile towards the object edges in either direction, $\|\nabla E_{image}(\mathbf{p}) \cdot \mathbf{n}_i\|$ will remain close to 0 as long as the neighbourhood used to determine E_{image} is still entirely within the road surface. As \mathbf{p} moves further towards the edges, E_{image} will be more and more influenced by off-road points. Hence it will grow, and so will $\|\nabla E_{image}(\mathbf{p}) \cdot \mathbf{n}_i\|$. At the object edges, we expect $\|\nabla E_{image}(\mathbf{p}) \cdot \mathbf{n}_i\|$ to have a local maximum that can be caused by a change of material in the land cover and thus by a local maximum in the gradient of the intensity image, or by a change of the DTM slope at the road edge.

Thus, the classical way of defining the image energy for ribbon snakes would correspond to

$E = (-\|\nabla E_{image}(\mathbf{v}_{iR}) \cdot \mathbf{n}_i\| - \|\nabla E_{image}(\mathbf{v}_{iL}) \cdot \mathbf{n}_i\|)$. However, such a definition would require a good initialisation: if both road edges are initialised outside the actual object, in the optimisation process both edges could be attracted by the local minimum corresponding to the road border that is first crossed, yielding a ribbon snake of width 0. In order to make our method more robust with respect to the quality of the initialisation, we exploit the known different gradient direction of our image energy at the two object borders in a way similar to Laptev et al. (2000) (cf. Fig. 12 top). However, whereas the latter assume bright roads on a dark background, which is not always true in optical images, the U-profile of roads in our proposed image energy model is more reliable. Additionally, the original image energy for the object centre line is integrated into the ribbon image energy for faster convergence:

$$E_{Ribbon}(\mathbf{v}_i) = E_{image}(\mathbf{v}_i) - \nabla E_{image}(\mathbf{v}_{iR}) \cdot \mathbf{n}_i + \nabla E_{image}(\mathbf{v}_{iL}) \cdot \mathbf{n}_i \quad (22)$$

The original image energy $E_{image}(\mathbf{v}_i)$ does not depend on parameter w . Therefore, $E_{image}(\mathbf{v}_i)$ vanishes in the derivative of E_{Ribbon} with respect to this parameter in the third Euler equation (cf. Eq. 7).

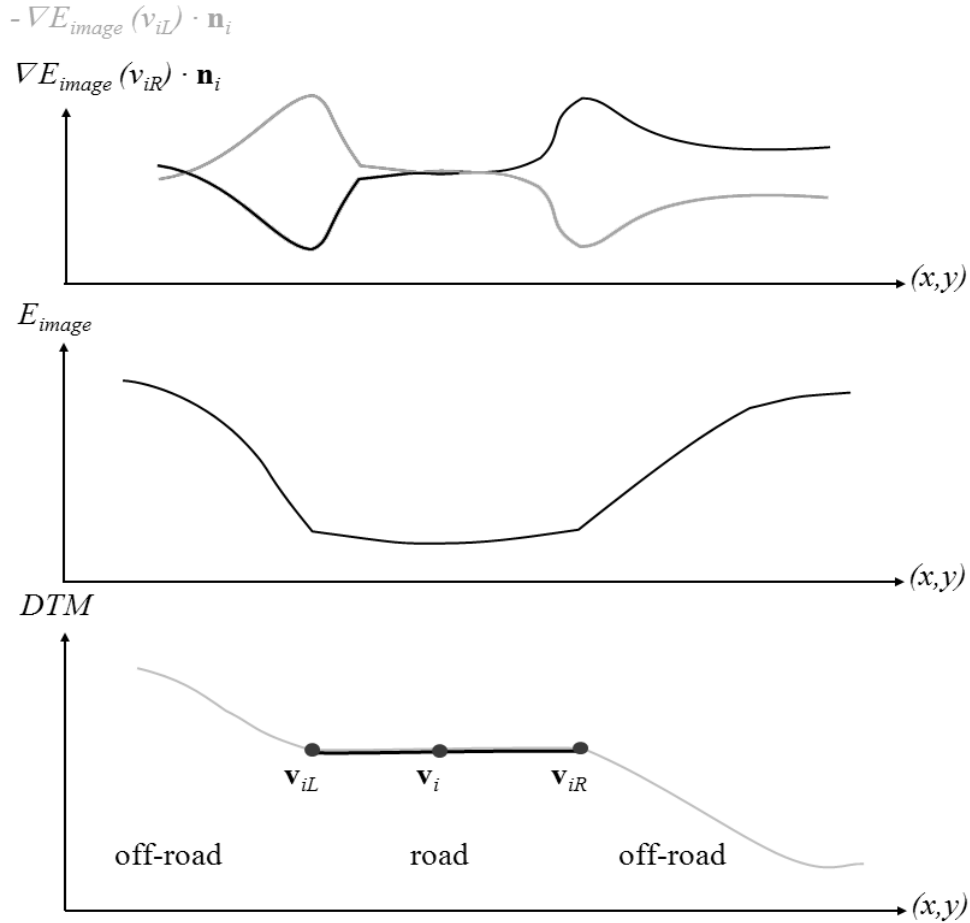


Figure 12. Bottom: A typical road profile through the DTM at node v_i with the road edge points v_{iL} and v_{iR} . The grey colour of the depicted profile corresponds to the ALS intensity. Centre: the corresponding profile of the image energy E_{image} according to Eq. 18. Top: Gradients of E_{image} in the direction of the normal vector \mathbf{n}_i of the road centre line with respect to the left and right position.

3.4.2.6 Modification of the image energy for river networks

Similar to the case of roads, the general ALS energy E_{ALS} for river networks is composed of the sum of one energy term derived from the DTM E_{Height} and the intensity energy E_I . Thus, Eq. 20 can also be applied. Due to the fact that rivers and ditches in the network are often very small and thus can not be represented by planar segments in the height data considering the available resolution (minimum resolution 0.5 m), the height variation energy E_{Height} for roads is not suitable here. In contrast to roads, rivers are always located in valleys and the terrain heights therefore increase on each side with increasing distance from the river. This valley in the original DTM heights may provide also a sufficient energy minimum, which is able to attract the snake to the correct position of the river. Thus, E_{Height} is simply represented by the unchanged DTM heights.

Due to the reflectance properties, water surfaces usually appear dark in the intensity images of most ALS data sets (Brzank et al., 2008). Therefore, the pre-processed intensity image can also be directly exploited for the image energy term E_I in Eq. 20 for river networks, forcing the snake to low grey values. In case no intensity information is available or if these values are not homogeneous due to the streaking effect of the specular reflection (cf. section 3.3), E_I is set to 0 and only the DTM energy E_{Height} is used. The weights (a, b) of the energy terms in Eq. 20 are determined empirically supported by the histograms of the intensity image and the DTM heights.

The slightly different definition of E_{ALS} for river networks results in some consequences for the interpretation of the ribbon image energy E_{ribbon} . For roads, E_{ALS} is derived from the slope or the height variation of the DTM, whereas the original DTM heights are introduced for rivers. The described definition of the ribbon image energy E_{ribbon} attracts the road edges to the position with the strongest change of the slope, i.e. the transition zone between flat and hilly terrain. If this definition of E_{ribbon} is not changed, the river edges will be attracted by the steepest terrain slope. In order to obtain the same representation for rivers, the gradients, i.e. the first derivatives, would have to be replaced by the second derivatives of the DTM (cf. Fig. 13). However, the fact that rivers and ditches are often very narrow compared to the resolution of the ALS data hampers the robust determination of the second derivatives. Furthermore, the general method is focused on the correction of the centre lines of the network objects (in contrast to the representation of broader rivers with the twin snake model) rather than on the exact determination of the edges of the objects. The edges should only support the adaptation of the object centre line. Thus, E_{ribbon} is not changed for rivers, resulting in different positions of the edges in the DTM for road and river networks.

It should be noted that the bridge and building energies are also considered for networks of small rivers.

3.5 Twin snake strategy

The following sections describe important aspects of the twin snake strategy. The internal energy for this approach is based on the original formulation of Kass et al. (1988). Thus, only the image energy and the proposed constraint energies are explained in detail.

3.5.1 Image energy for the twin snake model of broader rivers

Due to the region-based description of this object class, the approach is focused on the adaptation of the object edges rather than the centre lines. Therefore, it has to be discussed in more detail what the optimal positions of the borderlines of larger rivers in the DTM are. Fig. 13 visualises a cross section of a river bed in the DTM, the points of interest (black arrows), and the derivatives of the DTM. The points of interest mark the boundary between land and water, and it is assumed that they correspond to the maxima of the second derivative of the DTM. The cross section of the intensity data in the vicinity of a river is slightly different (Fig. 14b). Equivalent to the assumptions for small rivers, water surfaces of larger rivers also appear dark in the intensity image considering the typical laser wavelengths ($\lambda = 1000\text{-}1500\text{ nm}$). The transition zone between land and water is indicated by a sharp edge in the intensity image. Thus, it is assumed that the desired river borderlines correspond to the maxima of the first derivatives of the intensity image.

The ALS energy E_{ALS} , which represents the image energy for the twin snake strategy, is again determined by a weighted sum of two components, i.e. E_{Height} and E_I , according to Eq. 20 (section 3.4.2.2). Because this strategy is focused on the borderlines of the river, E_{Height} and E_I are computed in a different way considering the positions of the points of interest mentioned above. E_I is represented by the maxima of the first derivatives of the intensity image, calculated by a convolution with the corresponding derivatives of a Gaussian, whereas E_{Height} corresponds to the maxima of the second derivatives of the DTM, realised by a Difference of Gaussian operator (DoG). Analysing the histograms of E_{Height} and E_I , the weights (a , b) in Eq. 20 (section 3.4.2.2) are set in such a way that the two data sources have a similar range of values and thus a comparable influence. In order to generate local minima of the image energy for the border line nodes, the inverted ALS energy is used for E_{image} (Fig. 14c).

In contrast to the small rivers the determination of the second derivatives of the DTM is more suitable for broader rivers due to often only slightly tilted terrain at the river banks. The boundaries between land and water appear dark in the image energy, which forces the snake to move to these areas. However, due to the use of the second derivatives, many spurious edges in the vicinity of the desired borderline disturb the optimisation process (Fig. 14c). Therefore, some constraint energies are defined in the next section in order to increase the robustness of the algorithm.

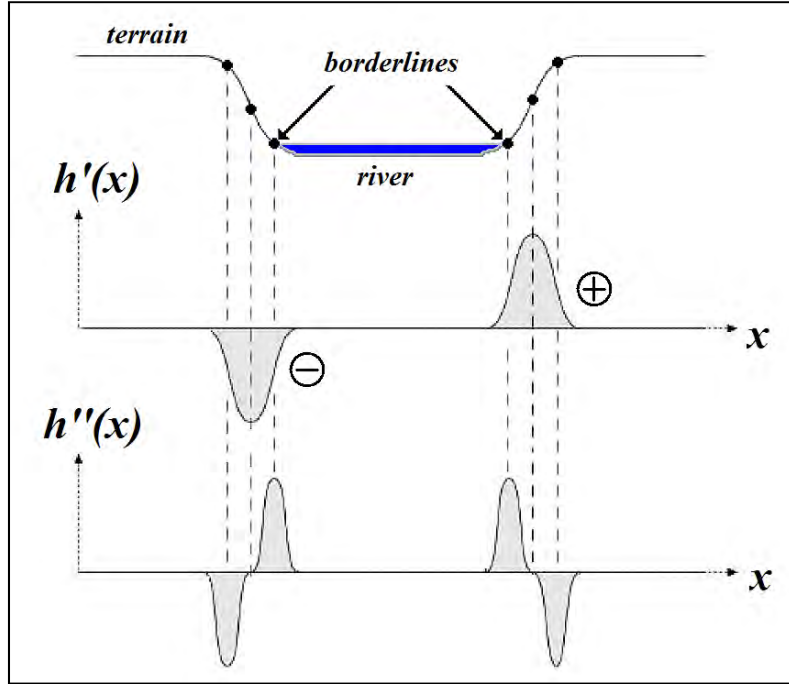


Figure 13. Cross section of rivers in the DTM; $h(x)$ represents the DTM height.

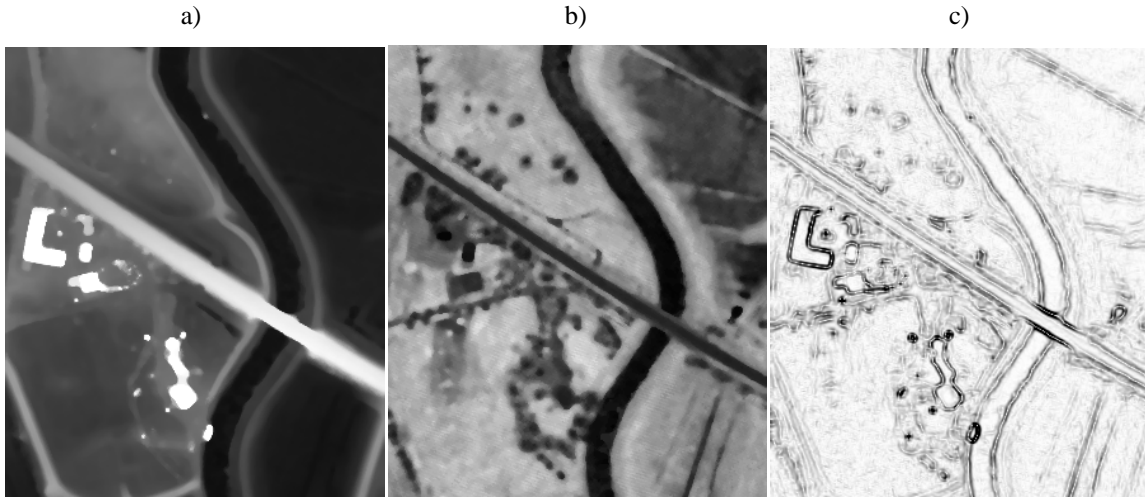


Figure 14. a) DSM b) intensity c) image energy.

3.5.2 Constraints for the twin snake model of broader rivers

The constraint energy E_{con} is computed as the sum of three components:

$$E_{con} = E_{Twin} + E_{Flow} + E_{Gradient} \quad (23)$$

The energy E_{Twin} is related to the concept of twin snakes (Kerschner, 2003) and is explained in section 3.5.2.1. E_{Flow} is related to the downhill flow direction and is explained in section 3.5.2.2. Finally, the term $E_{Gradient}$ takes into consideration the gradient direction of the terrain in the vicinity of the river bank; it is explained in section 3.5.2.3.

3.5.2.1 Twin snakes

Similar to the original constraint energy in Kass et al. (1988), which connects the contour to fixed points by spring forces, Kerschner (2003) developed the idea of twin snakes. In this concept two snakes are linked by a predefined distance d_0 . For that purpose the energy functional of each snake is extended by an additional term E_{Twin} that is minimised if the distance of the snakes fulfils this constraint:

$$E_{Twin} = \kappa_{Twin} \cdot (d(v_i) - d_0)^2 \quad (24)$$

In Eq. 24, $d(v_i)$ is the actual distance to the twin at node v_i and κ_{Twin} is the weight of this energy term.

The minimisation of the energy functional is carried out for each contour individually and alternates between the left and right snake. The corresponding other snake is fixed in the meantime. In the optimisation process the derivatives of Eq. 24 with respect to the image coordinates x and y have to be calculated (cf. E_{ext} in Eq. 7) in order to determine into which direction this energy term will move the contour. The twin energy acts perpendicular to the snake direction either with an attraction or repulsion force. Due to the fact that rivers vary in width a constant value for the predefined distance is not suitable for the proposed application. Assuming a relative quality that is higher than the absolute accuracy of the GIS data, this distance is derived from the 2D vector data for each node individually based on the distances of the GIS data. These values are calculated either as point-to-point or point-to-polyline distances. After each iteration the distances are updated. In order to find the inner edges of the bundle of edges along the rivers in the image energy (Fig. 14c), it is useful to decrease the value for river width taken from the GIS data base depending on the resolution of the DTM (one pixel). A smaller predefined distance increases the attraction force of the two corresponding snakes. Generally, the twin energy term supports the delineation of two image edges with a predefined adjustable distance and helps to overcome local minima in the image energy.

3.5.2.2 Flow direction

The downhill flow direction of rivers in the DTM is one of the physical properties which are integrated in the algorithm. Due to the effect of the Earth's gravity the nodes in flow direction should show a decreasing or at least a constant height. The flow direction can be usually derived from the order of the contour points in the GIS data base. Initially, a weight $w_{\Delta hi}$ depending on the differences between the heights of the upstream node h_{i-1} and the downstream node h_i of one snake is computed:

$$w_{\Delta hi} = \begin{cases} |h_{i-1} - h_i| & \text{if } h_{i-1} - h_i < 0 \\ 0 & \text{else} \end{cases} \quad (25)$$

The flow energy term is then defined by:

$$E_{Flow} = \kappa_{Flow} \cdot w_{\Delta hi} \cdot h(v_i) \quad (26)$$

In Eq. 26, $h(v_i)$ is the terrain height for node v_i and κ_{Flow} represents the weight parameter. In the minimisation process the derivatives of E_{Flow} at the nodes with respect to the image coordinates x and y have to be calculated (cf. E_{ext} in Eq. 7)

similar to the strategy used for the image energy. This approach attracts the nodes that do not satisfy the requirements of the flow direction to lower terrain heights. The height differences in $w_{\Delta hi}$ act as additional weights. The larger the deviation from the flow constraint for two nodes the stronger is the gradient descent force in the DTM for the node in downhill direction.

In principle this constraint energy can additionally be integrated for rivers also in the network representation. However, the river network of the GIS data base contains also ditches, where the flow direction is not well defined. Furthermore, the image energy of the river network includes the original DTM heights (cf. section 3.4.2.6). This definition of the image energy has an effect similar to E_{Flow} and attracts those parts of the snake centre line that have not yet reached a valley in the DTM to lower terrain.

3.5.2.3 Gradient direction

If the initialisations of the twin snakes are located far away from the corresponding edges in the DTM due to a low quality of the GIS data, the snakes are often not able to find their way to the range of attraction of the correct minima in the proposed image energy. Furthermore, many other edges at the river embankment (e.g., along a dike; cf. Fig. 15c) may disturb the detection of the correct snake positions. Thus, the range of attraction of reliable edge pixels has to be increased. For this purpose, the third energy term in Eq. 23 is introduced. The corresponding constraint exploits the fact that rivers usually flow in valleys and thus the terrain heights increase on each side with increasing distance from the river. Therefore, the horizontal components of the DTM gradient directions at the river borders should point away from the river centre, or, more precisely, into opposite directions for two opposite borderline points. Furthermore, we assume that the borders of the GIS river objects are approximately parallel to the corresponding edges in the DTM and the river width in the GIS data is approximately correct (see also the twin constraint). It is also supposed that the water surface is horizontal and has no significant edges in the DTM. According to these considerations, **two edge pixels** in the DTM corresponding to the opposite river borders have to be detected for each snake node which have the following properties:

- The horizontal components of their DTM gradient directions should point away from each other (difference approximately 180°) and should be approximately parallel to the river cross section at the corresponding snake node.
- Their distance should be approximately equal to the river width from the GIS data.
- There should be no edge pixels in between.

For this purpose, edge pixels in the DTM are calculated by using the Sobel operator with post processing steps (non-maxima-suppression and hysteresis threshold) following the strategy of Canny (1986). Afterwards, the horizontal components of the gradient directions of the edge pixels are computed. Fig. 15 visualises the DTM in the vicinity of a synthetic (Fig. 15a) and an actual river (Fig. 15c) and the corresponding grey value coded horizontal components of the DTM gradient directions (Fig. 15b and 15d). Due to the use of the unfiltered data vegetated areas disturb the edges depicted in Fig 15d.

A rectangular search buffer (blue in Fig. 15d) is created for every snake node, in which the two edge pixels of the opposite river borderlines are expected. The buffer is aligned with the snake direction. The width of the buffer q_{buffer} depends on the accuracy of the GIS data and the river width, whereas the size in snake direction l_{buffer} is set to a few pixels. If two edge pixels having the properties mentioned above are detected within the buffer, this constraint energy

term is considered in the optimisation process for the corresponding snake node. The related energy term is defined using the edge pixel on the correct river border (with respect to the considered snake node) in a similar way as E_{Twin} in Eq. 24. It is minimised if the distance between the current node and the extracted edge pixel is zero:

$$E_{Gradient} = \kappa_{Gradient} \cdot d(v_i) \quad (27)$$

In Eq. 27, $d(v_i)$ is the distance between the node v_i and the chosen edge pixel and $\kappa_{Gradient}$ represents the weight parameter. Due to the smoothing effect of the internal energy this constraint is already useful if the two edge pixels are detected for some nodes and if the predominant number of detections is correct.

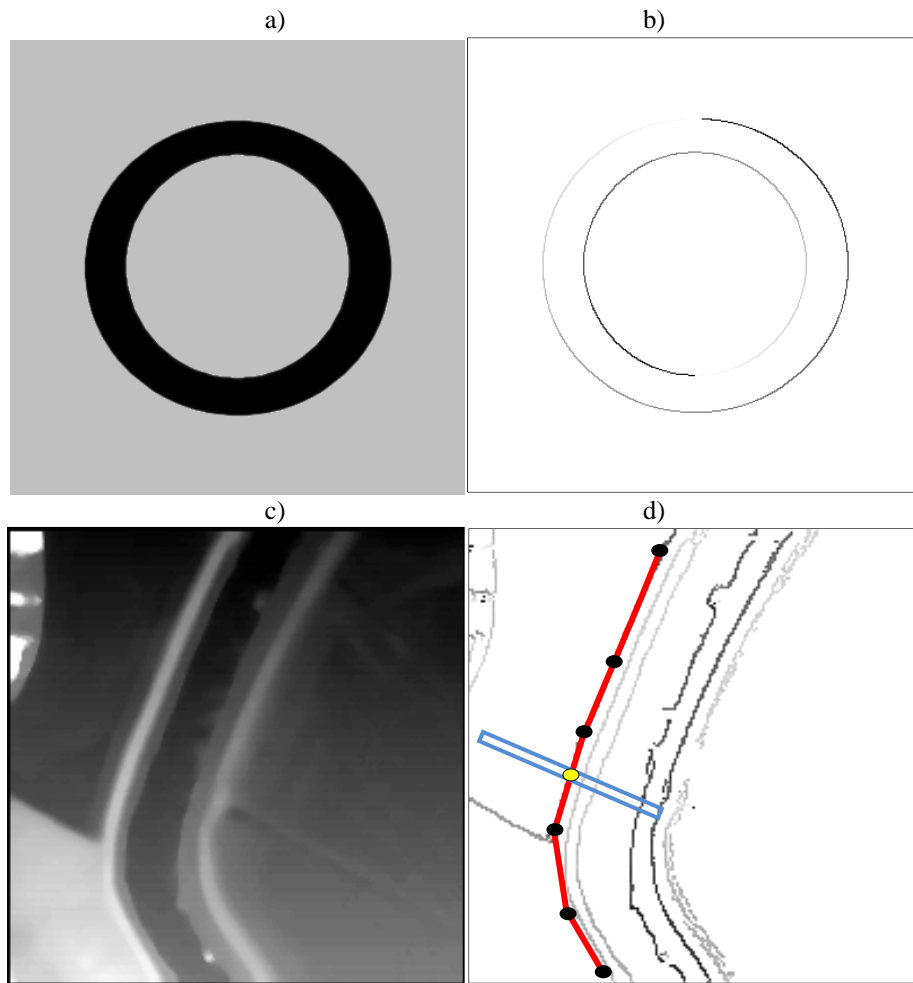


Figure 15. a) simulated DTM of a circular river; b) grey value coded gradient directions (horizontal component - 0-360°) of extracted edge pixels in the simulated DTM; c) DSM in the vicinity of a river; d) background: gradient directions (horizontal component) of extracted edge pixels using the same grey value code as before (Fig. 15b); red: left twin snake partner; blue: rectangular buffer for the yellow snake node

The influence of suitable edges depends on the size of the rectangular buffer. The gradient energy shifts the snakes to the correct gradients of the DTM (first derivatives) close to the desired positions and thus into the range of influence of the image energy (second derivatives).

In contrast to the constraint energy term $E_{Gradient}$ in this section, the gradient direction at the edges of river networks is implicitly considered in the ribbon image energy (cf. sections 3.4.2.5 and 3.4.2.6). However, the range of influence is limited to the position where the image energy is sampled. In comparison, the range of influence of $E_{Gradient}$ is determined by the search radius for suitable edge pixels (the size of the rectangular buffer) and can be easily extended.

The explicit extraction of edge pixels, the assignment to the snake nodes, and the design of the constraint energy $E_{Gradient}$ represent an adaptation strategy that is closely related to components of vector-to-vector matching approaches (cf. section 2.2.1.3).

3.6 On the relationship of ribbon and twin snakes

It seems that the ribbon model (Fua, 1996) and the twin snakes (Kerschner, 2003) have many features in common. Both concepts extend a linear object model by knowledge about the second dimension. In this context the *width of the ribbon* corresponds to the *distance between the twin snakes*. This section briefly discusses the differences of these approaches in the original version and points out how they can be designed to achieve a similar snake characteristic with respect to the analysed properties. Furthermore, this section also explains some reasons for the application of the ribbon snake for objects modelled by their centre lines in linear networks and of the twin snake for region-based GIS objects.

The twin snake model optimises two nearly parallel snakes that are connected to each other via a constraint energy term using predefined distances. During an iteration of the optimisation process the energy functional of one snake is minimised, while the other snake acts as reference polygon. This model strongly relies on the predefined distances between the snakes. The constraint is primarily used to stabilise the evolution of the two snakes. A slight change of the pre-defined distances is allowed during the optimisation, but a penalty is assigned to this deviation.

In contrast, the ribbon snake model physically consists of only one snake, but the image energy is sampled at the two borderlines of the ribbon. The width is introduced as third coordinate and is also affected by the internal energy, which prevents large differences of the width between neighbouring nodes during the optimisation process. If the features of the image data indicate large changes of the initial width for several consecutive nodes, the ribbon snake model in the basic design will allow these changes.

For the ribbon model the **smoothing of the width along the snake** is controlled by the weights α and β , which determine the elasticity and the rigidity of the width along the contour. Large weights only allow small changes of the width, resulting in a very smooth graph of this parameter with respect to the arc length s . In contrast, smoothness of the width between twin snakes can be obtained by introducing similar pre-defined distances for neighbouring nodes into the constraint energy E_{Twin} . Originally, twin snakes were developed for two approximately parallel contours and the pre-defined distance was usually kept constant for all nodes. This setting automatically leads to a smoothing of the distance between the two snakes.

Although an equal distance between to features along the contour is suitable for many applications, sometimes **rapid changes of the width along the snake** between neighbouring nodes are desired, such as for the occurrence of an additional road lane. Having in mind intersecting roads with different numbers of lanes, this aspect is also important for the network snake approach. The twin snake model is able to integrate such prior knowledge in the pre-defined distances

of E_{Twin} . However, a change in the distance of the twin snakes between neighbouring nodes influences the shape of the two individual snakes. Thus, the internal energy of each snake will counteract the twin force and the change of the distance. If the distance change is also present in the initial shape of the two snakes, the use of the rigid snake model (section 3.4.1.1) can preserve the changing of the distances. The original ribbon snake model is not able to support such changes in the width, because of the smoothing influence of the internal energy. However, the rigid snake model can also preserve a strong curvature in $w(s)$ if the initialisation of this parameter already contains the width change.

High weights for E_{Twin} result in an approximately **fixed distance** between the twin partners. However, due to the alternating optimisation of the two snakes this setting may completely prevent the evolution of the snakes if the actual distance is equal to the pre-defined distance. To avoid this effect the twin snakes are usually initialised with a larger distance from each other so that the corresponding image edges are situated between the two contours. On the contrary, the width of the ribbon model can be easily excluded from the optimisation by using a constant value. In this case the fixed ribbon width does not prevent the motion of the centre line. If the prior knowledge of the distance between the two linear features is very reliable, strongly fixing the distance between the snakes as well as the width of the ribbon results in a more robust convergence of the optimisation especially in case of poor initialisation. In particular the variability of the width across the snake direction in the ribbon approach introduces one additional free parameter, which can capture some of the uncertainty of the centre line position. However, the variability of this parameter is a prerequisite for the **simultaneous determination of the position and width of the snake**. Whereas the ribbon width can change in an almost unlimited fashion, the distances between the twin snakes usually slightly differ in a narrow range close to the initial value depending on the weight for E_{Twin} . The latter is caused by the penalty for any deviation from the pre-defined distance. For the ribbon width, a term similar to the rigid snake model can be additionally introduced in order to penalise large changes of the width during the optimisation process.

Roads and small rivers are represented by their centre lines in the GIS data bases and thus the optimisation has to be focused on these features. They are modelled as linear objects with an established network topology. The width of the objects is stored as an additional attribute. However, this attribute is often not very accurate, sometimes only available in classes of large intervals, or even completely missing. In any case it is not very reliable. The ribbon snake model fits well to these conditions. It is focused on the optimisation of the centre lines and the features at the border support this objective. Furthermore, the ribbon model can be combined with the networks without additional constraints and their corresponding weights. The ribbon snake is robust concerning poor initial object widths from GIS attributes and simultaneously determines the optimal position of the centre line and the optimal width. In contrast the twin snake model strongly relies on the initial distances and is more focused on the optimisation of the borderlines.

Larger rivers are represented by a region-based description and thus the optimisation has to be focused on the boundaries. Assuming that the relative accuracy of the GIS objects is better than the absolute accuracy, the distances between the two approximately parallel borderlines can be determined with high confidence. Thus, only small variations of the distances should be allowed. Considering the resolution of the ALS data the larger rivers are not well represented by their centre lines or small ribbons. They do also not really benefit from the network characteristic. All these conditions indicate that the twin snake model is more suitable for this object class.

3.7 Interpretation of the energy terms with respect to an internal evaluation

The lack of a suitable internal evaluation for active contours is one of the main drawbacks of the methodology and hampers its practical applicability. In this context the term *internal evaluation* means the assessment of the quality of the results only based on parameters that are derived by the algorithm itself without any reference data. In other words, the goal of this section is to find hints for those contour parts that are not situated at the correct positions after the optimisation process. Though Kerschner (2003) proposes the comparison of the actual distance between the twin snakes and the initial distance for that purpose, a more general concept of internal evaluation does not exist. The following section interprets the meaning of the different energy parts in the optimisation process and discusses their potential contribution to an internal evaluation.

Internal energy – rigid snake model

Generally, a low internal energy E_{int} after the optimisation process indicates small changes of the prior shape of the contour, i.e. the geometric object model fits well to the final shape of the corresponding contour part. This situation can be caused by

- (1) a good correspondence between the external energy (features in the image data) and the initial shape,
- (2) high weights of the internal energy in comparison to the external forces.

The first case represents a suitable solution and is not relevant for the purpose of error detection. In the second situation the large weights do not allow a strong adaptation of the contour to the image features and the final shape is thus highly correlated with the initialisation. Therefore, the absolute values of E_{int} after optimisation depend on the setting of the weights. This means that E_{int} of different contour parts can only be compared in case of the same parameter setting. This aspect is important for the internal evaluation. Assuming the same set of weights for all contour parts, large values of E_{int} indicate strong changes of the initial shape at the corresponding nodes. Two scenarios are able to explain these strong changes of the geometry:

- (1) The initial shape is approximately correct. Changes of the shape correspond to wrong contour parts. Fig. 16 (bottom – yellow circle on the left side) illustrates an example of this situation. Originally linear road parts (blue lines) are bent in the optimisation process (red lines) due to the influence of the image energy. The large gradients of the internal energy (derivatives of E_{int} in x- and y-direction) for the corresponding nodes (blue arrows on the right side of Fig. 16) also indicate these changes of the curvature.
- (2) The initial shape is not correct. The final shapes and positions of the contour parts can be correct or not according to the external forces (image energy). Fig. 16 (top - yellow circle) depicts an example for a correct solution despite high internal energy values. The larger curvature of the initialisation (blue line) has to be smoothed (red line) in the optimisation process in order to move the contour into regions of low image energy. In this case the large gradients of the internal energy indicate an incorrect initial shape.

E_{int} gives some indications for an erroneous contour part. However, this energy term alone is not sufficient in order to derive suitable parameters for an internal evaluation.

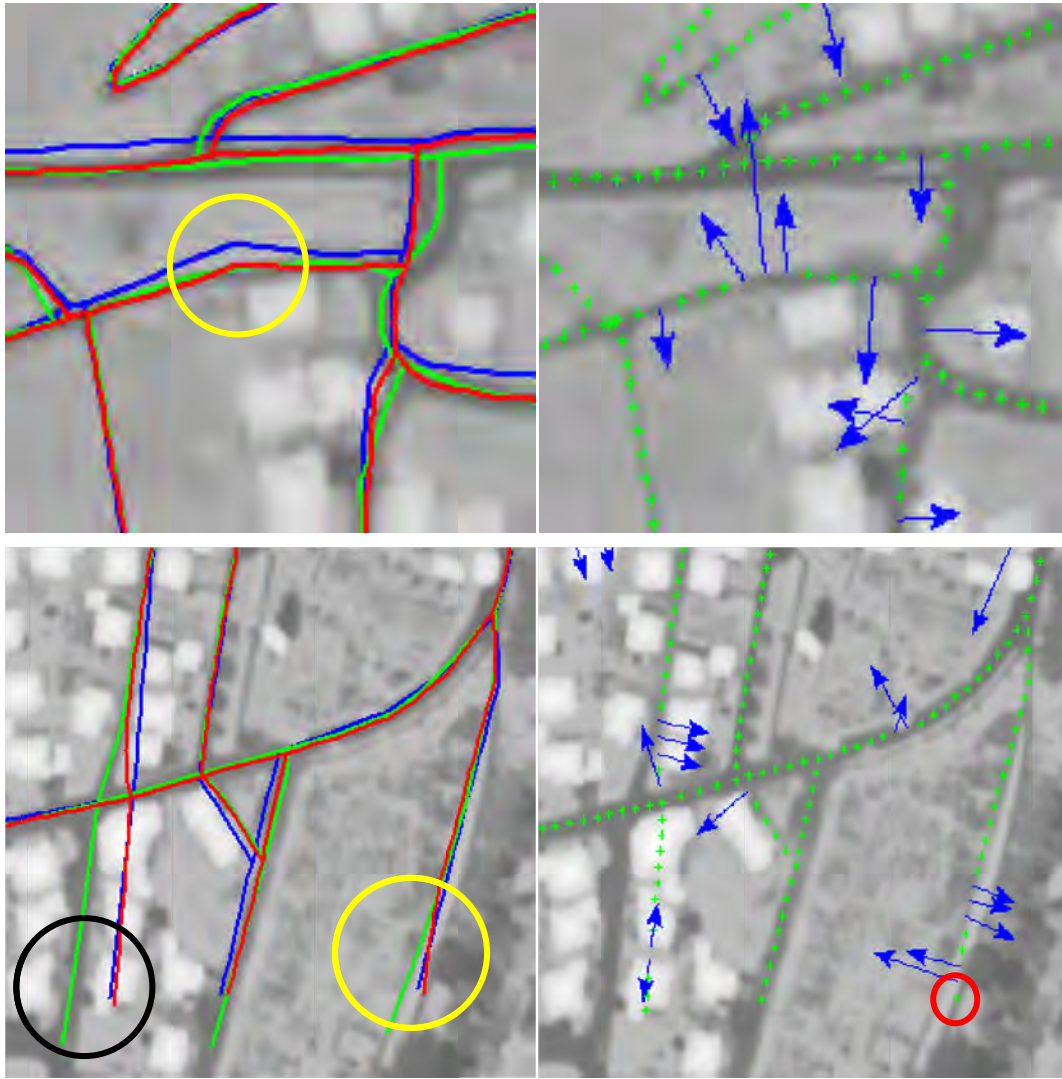


Figure 16. Two small optimised road networks (top and bottom); left: blue: initialisation, green: reference, red final solution; circles: areas of interest; right: green crosses: snake nodes, blue arrows: corresponding gradients of the internal energy ($> \mu + 2\sigma$; with μ, σ parameters of the normal distribution for all nodes)

The absolute values of the gradients of the internal energy do not contain any additional information, because a high internal energy causes large gradients in order to retain the initial shape. The direction of the gradients corresponds to the opposite direction of the gradients of the external energy and may provide some additional information (Fig. 16 right side). However, further research has to be carried out at this point.

Image energy

In contrast to E_{int} , the absolute values of the image energy are not affected by the setting of the weights and can thus be directly compared for contour parts with different parameters. In general, high values of the image energy will indicate inappropriate image features and probably a false position of the contour if the image energy is suitably designed for the desired object class. Thus, a large image energy is a valuable cue for the detection of outliers (see Fig. 17). However, the significance of the image features usually varies in larger scenes. For instance, the appearance of roads of different priorities in the ALS data strongly depends on parameters of the object, such as number of lanes or surface material, as well as on conditions during the ALS flight campaign, such as the angle of incidence. Therefore, the significance of a local minimum in E_{image} may also be crucially affected. This aspect decreases the comparability of the image energy of different contour parts.

The derivatives of the image energy in x- and y-direction, i.e. the gradients, correspond to the force that is generated by the image features. This force will change the position of the contours in the next iteration if no other energy terms counteract. In contrast to the internal energy, the absolute values of the image energy gradients provide information complementary to E_{image} . Strong gradients after the termination of the optimisation process indicate that the contour has not yet detected a suitable minimum in the image data and thus is probably not well located with respect to the image features. Thus, the gradients may be interesting for an internal evaluation. However, the influence of the image gradients will be fully compensated by the gradients of the internal energy if no other external force is introduced, and the process converges to equilibrium. Only the direction of the generated forces is opposed and the strength of the forces differs according to the weight factors for E_{image} and E_{int} . In this case the derivatives of the image energy do not provide additional information in comparison to the derivatives of the internal energy.

Conclusion for the internal evaluation

A simple approach for the automatic detection of erroneous contour parts is derived from the observations of the previous paragraphs. Very high image energies compared to the mean of E_{image} of all nodes of the contour reliably indicate outliers. Thus, assuming a normal distribution of the image energy values of all nodes, the parameters of this distribution are calculated. The first detector of errors d_{first} (green circles in Fig. 17) uses a simple threshold determined from the mean and the standard deviation of this distribution:

$$d_{first} = \{v_i: (v_i \in \mathbf{v}(s)) \text{ and } (E_{image}(v_i) > \text{mean}(E_{image}) + 2 \cdot \text{sigma}(E_{image}))\} \quad (28)$$

Furthermore, the above analysis shows that the gradients of the internal energy (equal to the gradients of the image energy) will often be high if the contour leaves the object outlines. Therefore, the absolute values of the image energy should be low at one side of the corresponding nodes and high at the other side¹. Thus, the second detector d_{second} (blue circles in Fig. 17) searches for nodes with high image energies and among their two neighbouring nodes for high internal energies. The two thresholds are again determined from the corresponding distributions:

$$d_{second} = \left\{ v_i: \begin{array}{l} (v_i \in \mathbf{v}(s)) \text{ and } [E_{image}(v_i) > \text{mean}(E_{image})] \\ \text{and} \left(\begin{array}{l} [E_{int}(v_{i+1}) > \text{mean}(E_{int}) + \text{sigma}(E_{int})] \\ \text{or} [E_{int}(v_{i-1}) > \text{mean}(E_{int}) + \text{sigma}(E_{int})] \end{array} \right) \end{array} \right\} \quad (29)$$

The second detector will usually find only the beginnings and the ends of wrong contour parts. If the contour part in between additionally converges to a wrong minimum in the image energy (e.g., a parallel road), the first detector won't help either (cf. the green cross in the red circle in Fig. 16 lower right image). Unfortunately, these contour parts have often the largest distance to the reference. However, the beginning and the end of wrong contour parts are usually sufficient in order to guide the user during a manual post processing. It should be noted that the two detectors will be applicable only if the majority of the contour nodes are located inside the object boundaries. This is necessary in order to determine suitable parameters of the energy distributions. In the experiments the two detectors are applied together.

¹ The direction of the image energy change between neighboring nodes is also useful, but is not considered in this thesis.



Figure 17. Detection of wrong contour parts in the two road networks of Fig. 16; crosses: image energy lower (green) or higher (red) than the mean value of all nodes, green circles: result of the first detector; blue circles: result of the second detector.

3.8 Parameters and setup

Table 2 summarises the main parameters that the user has to specify for both proposed snake strategies. The following section describes the influence of the parameters on the algorithm and gives some details with respect to the setup.

Parameters	Energy Term	Meaning	Network Snakes	Twin Snakes
α	E_{int}	Weight of the first order term of the internal energy	X	X
β		Weight of the second order term of the internal energy	X	X
γ		Step size (viscosity parameter)	X	X
κ_i	E_{image}	Weight for the entire image energy	X	X
$\lambda(x,y)$		Weight for E_{ALS}	X	
$\mu(x,y)$		Weight for E_{build}	X	
$\nu(x,y)$		Weight for E_{bridge}	X	
a		Weight for E_{Height}	X	X
b		Weight for E_l	X	X
κ_{Twin}	E_{con}	Weight for E_{Twin}		X
κ_{Flow}		Weight for E_{Flow}		X
$\kappa_{Gradient}$		Weight for $E_{Gradient}$		X
Δs		Sampling interval for the snake nodes	X	X
$w_{initial}$		Initial width for ribbon snakes (half width of the object)	X	
$l_{buffer} \quad q_{buffer}$		Size of the buffer (searching for suitable gradient directions)		X
t_{stop}		Sum of the position changes of all nodes in one iteration	X	X
Max_{iter}		Maximal iterations	X	X

Table 2. Most important parameters of the algorithm

Comments to the parameters for the network snake strategy

The weighting between the internal energy (here: the rigid shape model) and the image energy derived from ALS data is controlled by the parameters α , β , and κ_i . For the network snakes (without E_{con}) the parameters γ and κ_i are redundant, i.e. the setting $\alpha = 4$; $\beta = 4$; $\gamma = 1$; $\kappa_i = 4$ corresponds to $\alpha = 1$; $\beta = 1$; $\gamma = 0.25$; $\kappa_i = 1$. In general, the internal energy term E_{int} will be minimal if the current shape of the snake matches the initial shape. Thus, very high weights for E_{int} result in a rigid snake that is not able to locally adapt to the image features. A large parameter α preserves the initial node distances of the snake and thus results in a low elasticity of the corresponding contour parts. This parameter controls the ability of the method to compress and stretch the related contour parts. A large parameter β preserves the curvature of the initialisation. In contrast, a high weight for the image energy κ_i allows a strong adaptation of the contour to the ALS features. Thus, the user can derive the weight parameters from the accuracy of the GIS data and of the ALS features. Assuming a good quality of the geometry of the GIS objects, such as in the data of the NMA, the weights for E_{int} should be high in comparison to κ_i . In contrast, the accuracy of neighbouring road parts can be quite different in raw data from OpenStreetMap. Therefore, the initial shape can be distorted and the weights for E_{int} should be decreased for the adaptation of such data sets. The experiments in section 4.2.1.6 evaluate the influence of the weighting between E_{int} and E_{image} on the quality of the adaptation results and give recommendations for a suitable setup.

The parameter γ represents a factor that is used to amplify or damp all acting forces. If the parameter is doubled the forces will be simply divided by two and vice versa. This parameter determines the speed of the snake motion in a simulated liquid medium by changing the viscosity and is thus also called viscosity parameter. Another term for γ is the *step size* (actually, it is the inverse). A small viscosity supports jumps over wrong (but, unfortunately, also over correct) local minima and local maxima, which may be helpful in case of a poor initialisation, whereas a large viscosity enables the precise detection of the minimum. Increasing the viscosity during the optimisation is an interesting idea, but not yet tested. The parameter γ is set to constant during the optimisation for all the experiments. The selected value should be a compromise between a fast and robust convergence and an accurate detection of the local minima in the image energy.

The general image energy is derived from features of the DTM roughness and ALS intensity values, weighted by a and b . In the current implementation these parameters are derived by the analysis of the corresponding histograms in order to equally weight the two main source of the image energy. The other three parameters for the image energy $\lambda(x,y)$, $\mu(x,y)$, and $\nu(x,y)$ are simply set to one if the corresponding energy term should be considered or to zero if not. E_{build} and E_{bridge} are both derived by a distance transform. Thus, their influence linearly decreases with the distance to the object centres.

The parameter $w_{initial}$ determines the initial width of the ribbon snake. Experiments in section 4.2.1.4 demonstrate that the quality of the adapted centre lines is not very sensitive to the initialisation of this parameter. Thus, the ribbon width is set to a constant value for the entire network in the current implementation (e.g., 5 m for the road width). However, the attributes of the GIS road and river data often contain information about the object width, which can be used to initialise $w_{initial}$.

The sampling interval of the nodes Δs defines the approximation accuracy of the contour. Large values hamper a suitable representation of contour parts with high curvature, whereas small node distances increase the time that is required for the optimisation. Experiments (cf. section 4.2.1.1) show that the object width (6 m for standard roads) is a suitable compromise for the node distance.

The two criteria for the termination of the optimisation t_{stop} and Max_{iter} are alternatively applied. The parameter Max_{iter} determines the maximal iterations that will be carried out during the optimisation, whereas the parameter t_{stop} is derived from the position change of the entire contour during the last iteration, i.e. the sum of the position change of all nodes in [pixel]. The determination of a general setting for t_{stop} is difficult because this value depends strongly on the number of nodes in the network and on the weights for the energy terms in combination with the viscosity parameter γ defining the speed of the snake motion. However, a termination criterion based on the maximal position change of one individual snake node within one iteration is also not suitable, because some strong gradients of the image energy at a certain position may result in large alternating changes for the corresponding snake node for constant values of γ . The speed of the snake evolution influences also the setup for parameter Max_{iter} . Additionally, large inconsistencies between the two data sets that should be adapted require more iterations than smaller discrepancies. In many tests of section 4.2.1 the convergence behaviour is analysed for different termination criteria in order to find suitable parameters. Considering the inconsistencies in the original GIS data of the NMA the setting of $Max_{iter} = 200$ seems to be appropriate for the convergence of the algorithm.

Comments to the parameters for the twin snake strategy

The weighting between the internal energy and the image energy is different from the first strategy, because the original model of E_{int} is applied. This object model of straightness and smoothness is not suitable for every snake node. Thus, smaller values have to be assigned to the parameters α and β in order to avoid a strong smoothing of curved contour parts and the contraction of the general node distance. In contrast to the first strategy, the twin constraint is used to stabilise the shape of the two contours.

The comments for the general image energy derived from ALS mentioned above are also valid for the second strategy. However, E_{build} and E_{bridge} are not considered for the twin snake approach, but can be applied in future work.

Because of their quite different nature the derivation of well-founded weights for the constraint energies is difficult. In general, suitable parameters were empirically determined by several tests in order to weight the constraint energies with respect to each other and to set the relation to E_{int} and E_{image} . A brief insight of the influence of the constraints on the optimisation results is given in section 4.3.2.1. The reliability of the twin energy depends strongly on the accuracy of the pre-defined distances. These values are derived from the distances of the two opposite borderlines of the region-based GIS river object and are assumed to be quite accurate. Therefore, relatively large weights can be assigned to this constraint. The flow direction is well defined if the DTM quality is high. Thus, the weight should depend on the accuracy of the corresponding height information. The third constraint relies on the extraction of appropriate edge pixels and the related gradient direction. Therefore, the extraction quality should be used to define the corresponding weight for the gradient direction constraint. The search radius for suitable edge pixels is determined by the size of a rectangular buffer. The buffer size across the direction of the snake q_{buffer} depends on the inconsistencies between the GIS data and the ALS features as well as on the object width. The buffer size in the direction of the snake l_{buffer} is set to a few pixels.

The comments for the viscosity parameter γ , the node distance, and the termination criteria mentioned above are also valid for this second strategy.

3.9 Discussion

This thesis presents an approach for the adaptation of GIS objects to ALS data or height data by using active contour models. The main advantage of the proposed strategy compared to vector-to-vector matching approaches results from the aspect that feature and object extraction in the ALS data can be avoided. The active contour concept is able to directly process the implicit information about the objects in the ALS data without extensive pre-processing. This will be the crucial criterion if only height data as the required minimal input is considered. For instance, because of the weak and fragmented nature of the terrain features, a road extraction algorithm that relies only on the DSM or DTM does not exist at the moment to the knowledge of the author. Even the detection of suitable DTM features, such as break lines, that could be used as input for the vector-to-vector matching is difficult (cf. section 2.2.2.2).

The proposed algorithm for network objects (road networks and networks of small rivers) combines the properties of different active contour approaches. Besides the advantages of the individual methods, several synergy effects arise from this combination. The network snake approach (Butenuth, 2008) seems to be suitable for the adaptation of GIS objects with network characteristic. However, experiments have shown that the varying significance of the height features prevents a well-balanced weighting of the energy terms even for small networks. This problem is mainly caused by the geometric object model in the original formulation of the internal energy. Straight and smooth shapes are preferred in any case. In some regions a strong internal energy is required due to poor initialisation or in the presence of noisy ALS data. However, weak ALS features in road parts with high curvature or at dead road ends are not able to compensate the smoothing and shortening effect of the internal energy. The rigid snake model (Radeva et al., 1995) preserves the shape of the initialisation by penalising the change of the geometry and is thus a suitable extension. The combination of the two models results in several positive effects, such as the conservation of the intersection angles of cross-roads or the stabilising impact at dead ends. Furthermore, the ribbon snake model (Fua, 1996) is integrated in order to support the adaptation of the centre lines of the linear networks and to increase the range of influence of the image energy. Synergy effects with the other approaches result for instance from the preservation of changes of the ribbon width between neighbouring nodes and an improved modelling of network junctions.

The main drawback of the modifications of the snake approach results from the increased dependency on the initialisation, i.e. on the quality of the GIS data. In general, active contour models strongly depend on an initialisation that is close to the corresponding image features. The proposed approach additionally relies on the initial shape of the vector data. However, the geometric quality of the GIS data is assumed to be sufficient for this kind of strategy.

A second strategy adapts larger rivers based on a twin snake approach. This method is focused on the modelling of object knowledge by constraint energies. Whereas the network snake strategy primarily integrates the object knowledge via the internal energy, the constraint energy terms for larger rivers are able to establish similar snake properties. In this context, the twin constraint introduces a parameter for the object width similar to the ribbon approach. Furthermore, one twin partner, which is fixed during the optimisation of the other, acts as a supporting polygon stabilising the initial shape. Additionally, other semantic properties of rivers, such as the flow direction and the DTM gradients at the embankment, are modelled by constraints. The latter represents one possibility in order to incorporate matching components into the snake algorithm if the extraction of suitable features from the DTM is feasible.

Another strength of the proposed algorithms results from the design of the image energy from the ALS data. Besides features of the DTM and of the ALS intensity, context objects, such as buildings and bridges, are integrated as well in order to support the adaptation process. During the generation of the image energy also the semantics of the GIS objects are exploited. For example, the valid slopes in the DTM are considered in this part of the energy functional.

The algorithm also exploits the information of the GIS data base that can be useful for the adaptation process. The network snakes use the given topology and the shape is considered in the way mentioned above. Furthermore, attributes of the object from GIS, such as the road and river width or the flow direction, are introduced in the method.

One problem of the available active contour approaches results from the lack of a suitable internal evaluation. In this thesis, a method is proposed for this purpose that analyses the different energy terms in order to derive suitable evaluation parameters for each snake node. These parameters are able to guide the user to contour parts that have not reached an appropriate position and shape.

4 Experiments

The experiments in this chapter evaluate the applicability of the proposed new method with respect to the objectives in section 1.2. The tests are focused on various aspects, such as the general accuracy of the results, the transferability and robustness of the parameter setup, the requirements for the initialisation from GIS data bases as well as for the ALS data, and the comparison of different object models. Furthermore, the two proposed strategies (network and twin snakes) are evaluated using different larger data sets in order to show the general applicability and transferability of the new algorithm. A detailed description of the methodology of the experiments and an overview about the test data can be found in the next section.

4.1 Overview

4.1.1 Description of the test methodology

The experiments are structured based on the three considered objects, namely road networks, networks of small rivers, and broad rivers. The tests are carried out using four test data sets. The specifications of these data sets are described in the **section 4.1.2**. The geometric accuracy of the results is determined by the root mean square point-to-line distances (called R.M.S. errors in the following) of the contour nodes to a reference (external evaluation). The reference consists of road and river centre lines for the network objects, and border lines for the large rivers. These reference lines were manually digitised in the corresponding orthophotos (resolution: 0.2 m-0.4 m; cf. Table 3). The vector data for the initialisation of the contours are taken from different GIS data bases. For some experiments the GIS data are shifted and rotated to simulate larger inconsistencies.

Section 4.2, representing the main part of the experiments, is focused on road objects. In this context the effects of the interaction between the network, the ribbon, and the rigid snake model are emphasized based on several tests. This section is divided into the following parts:

(1) Sensitivity analysis

Fundamental analyses are conducted using a small road network in order to evaluate the performance of the proposed active contour approach with respect to various aspects. In addition to the geometric accuracy mentioned above, the tests also consider the speed of convergence of the optimisation process under different conditions. Unless otherwise stated, the rigid snake model is always applied. For some tests the differences between the standard and ribbon network snakes are highlighted. In particular the impact of following factors on the R.M.S. errors as described above is investigated:

- Influence of the initialisation:
 - ❖ Sampling interval of the snake nodes Δs
 - ❖ Shifted initialisation
 - ❖ Rotated initialisation
 - ❖ Initial width of the ribbons
- Influence of different control parameters
 - ❖ t_{stop} , Max_{iter} , and γ (convergence of the algorithm)
 - ❖ α , β , and κ_i (balanced-weighting between E_{int} and E_{image})

At the beginning of every test the most important parameters that are not changed during the experiment are summarised. The impact of the different image energy terms is not tested in this subsection because of the small significance of this experiment. However, several aspects with respect to the image energy are analysed for the larger test sites in section (4).

(2) *Rigid snake model*

Some examples highlight the necessity to change the original internal energy term of parametric active contours for the general applicability of the method. A visual comparison between the original geometric model of straightness and smoothness and the rigid snake model is performed.

(3) *Bridge energy*

A set of experiments illustrates the integration of the bridge detection results as one part of the image energy. This aspect exemplarily demonstrates how reliably detected context objects decrease the dependency of the algorithm on the quality of the initialisation.

(4) *Optimisation of larger road networks*

This part exemplifies the general applicability of the method based on five larger road networks. At least one example is selected from each test data set in order to apply the method with respect to different conditions concerning the quality of the GIS data, different topography, as well as various ALS specifications. Furthermore, the impact of the design of the image energy on the results is highlighted.

(5) *Internal evaluation*

The considerations about the analysis of the energy terms for an internal evaluation are examined based on two examples. The goal of this part is to evaluate whether the developed detectors are able to guide the user in a post processing step to contour parts that have not reached a suitable minimum in the image data.

Section 4.3 is generally focused on the adaptation of river objects. **Section 4.3.1** is dedicated to networks of small rivers. Two examples illustrate that the geometric object model designed for roads is also suitable for rivers or ditches. The only change that was made is related to the term E_{ALS} of the image energy.

In **section 4.3.2**, the twin snake model is applied to broader rivers. Initially, the effects of the three proposed constraint energy terms representing the semantics of rivers are briefly discussed using simulated initialisations. Afterwards, two river sections are optimised to highlight the properties of this approach.

4.1.2 *Test data*

The specifications of the four ALS data sets used in this thesis are summarized in Table 3. Larger details of the corresponding orthophotos are illustrated in Fig. 18. Three of the data sets have comparable point densities as well as vertical and horizontal accuracies, whereas the data from Emmental (Switzerland), captured at the beginning of this century, are of lower quality, and additional features, such as the ALS intensity are not available. Thus, this data set specifies the minimum input for the following experiments. The DTM grid width in Table 3 also determines the resolution of the image energy for tests with the respective data set.

Test data set	Point density	Horizontal accuracy	Vertical accuracy	FP / LP recorded	Intensity recorded	DTM / DSM grid width	Resolution orthophoto
1. Kellinghusen	3-4 pts/m ²	<0.50 m	<0.15 m	FP + LP	Yes	0.5 m	0.4 m
2. Oldenburg	3-4 pts/m ²	<0.50 m	<0.15 m	FP + LP	Yes	0.5 m	0.4 m
3. Emmental	0.5 pts/m ²	<0.50 m	<0.30 m	LP	No	1.0 m	0.25 m
4. Vaihingen	4-6 pts/m ²	<0.50 m	<0.15 m	FP + LP	Yes	0.5 m	0.2 m

Table 3. Specifications of the ALS data and of the orthophotos for the four test data sets. FP/LP: First Pulse / Last Pulse.

The **first test data set** is situated near the village of Kellinghusen in the federal state of Schleswig-Holstein (Germany). It covers the village and its surrounding area and is characterised by flat terrain. The ALS data were acquired by the company TopScan during a countrywide flight campaign between 2005 and 2007 using the Optech ALTM 3100 system. The topographic data base used was the German Authoritative Topographic Cartographic Information System (ATKIS). For some experiments, the road network was intentionally shifted. The following **test sites** belong to this data set and contain:

- 1a) a small road network (urban part of 1b) used for the sensitivity analysis (section 4.2.1) and for the test of the internal evaluation (section 4.2.5). (253 nodes, 380 x 470 m²)
- 1b) a large road network (urban and rural) optimised in section 4.2.4. Details of this network are used in order to illustrate the advantages of the rigid snake model (section 4.2.2) and of the bridge energy integration (section 4.2.3). (2115 nodes, 1700 x 1100 m²)
- 1c) a larger network of small rivers and canals (rural) that is optimised in section 4.3.1. (538 nodes, 1200 x 800 m²)
- 1d) a broader river (urban and rural). Parts of this test site are used to demonstrate the effects of the constraint energies for the twin snake strategy (section 4.3.2.1) and to optimise the borderlines of two larger river segments (first: 124/120 nodes, 750 m; second: 101/104 nodes, 600 m) (section 4.3.2.2).

Some parts of the city of Oldenburg in the federal state of Lower Saxony (Germany) and the surrounding rural area are covered by the **second test data set**. This data set is also characterized by flat terrain. The ALS data was again captured by the company TopScan during a flight campaign in 2008 using the Optech ALTM 3100 system. ATKIS was the data source for the vector objects. Note that some specifications, such as the original data source and thus the quality, may vary for different federal states of Germany (cf. section 3.2.1). The following **test sites** belong to the second data set and contain:

- 2a) a road network (urban) optimised in section 4.2.4. (416 nodes, 400 x 600 m²)
- 2b) a network of small rivers and canals (rural) optimised in section 4.3.1. (384 nodes, 750 x 1200 m²)



Figure 18: Orthophotos (larger details) of the test data sets: a) Kellinghusen (RGB) b) Oldenburg (RGB) c) Emmental (RGB) d) Vaihingen (CIR)

The **third test data set** is located in the Emmental valley in Switzerland. It covers a rural area with villages in the valleys, but also mountainous regions. As the point density was too low for building or bridge detection and because no intensity data were available, only the term E_{Height} could be used for the image energy. The related experiments have the goal to emphasize the applicability of the geometrical model with a minimum configuration with respect to the ALS data. For reasons explained in section 3.4.2.2, a DSM was used for defining E_{Height} in urban areas, whereas a DTM was used in mountainous areas. The vector data are those of the Swiss DLM. They are directly used for initialisation. The following **test sites** belong to this data set and contain:

- 3a) a larger road network (urban) optimised in section 4.2.4. (987 nodes, 750 x 1000 m²)
- 3b) a small road network (mountainous) optimised in section 4.2.4. (261 nodes, 500 x 500 m²)

The **fourth test data set** is situated close to the town of Vaihingen in the federal state of Baden-Wuerttemberg (Germany). Some agricultural areas and vineyards are located in the surroundings of the town. The ALS data set was

acquired by the company Leica Geosystems using a Leica ALS50 system in 2008 (for detailed information see Haala et al., 2010). The ALS data has the highest point density of all data sets, but the acquisition time in the leaf-on period decreases the proportion of ground points in vegetated areas. The initialisation for the snakes was taken from the OpenStreetMap data base provided by the company Geofabrik GmbH. Furthermore, the network topology was established manually by integrating common nodes at the crossings. The OpenStreetMap data are characterised by a very inhomogeneous accuracy due to their patch-work character. Parts of the road network with a high and a low quality may be located in an immediate neighbourhood. This aspect decreases also the reliability of the shape of the vector objects. These facts cause large inconsistencies between the GIS and ALS data sets, resulting in a challenging input for the test of the method. The following **test site** belongs to this data set and contains:

- 4) a large road network (rural and urban) optimised in section 4.2.4. (1782 nodes, 1000 x 600 m²)

4.2 Test of the adaptation of roads

4.2.1 Sensitivity analysis

The experiments in this section are carried out using the small road network of test site 1a (Fig. 19) (253 nodes with a distance of $\Delta s = 6\text{m}$). Generally, this section evaluates the performance of the proposed network snake strategy with respect to various aspects. In addition to the geometric accuracy the tests also consider the speed of convergence of the optimisation process under different conditions. Table 4 shows the standard parameter setup for the following experiments. These standard parameters were found empirically. At the beginning of each experiment the fixed parameters are shown in a similar table. Unless otherwise stated, the rigid snake model is always applied. Thus, the relatively large weights for the internal energy ($\alpha = \beta = 15$) result in a very rigid object model, assuming a high quality of the shape of the initialisation. For many tests the differences between the standard and ribbon network snakes are highlighted (specifically marked by “std.” and “rb.”, respectively, in the tables).



Figure 19: Road network used in the sensitivity analysis (background: orthophoto; yellow lines: original GIS data)

α	β	γ	κ_i	$w_{initial}$ (m)	Δs (m)
15	15	1	10	2.5	6

Table 4. Most important parameters for the optimisation of the reference and the original road network of the GIS data

4.2.1.1 Quality of reference data

In this section the accuracy of the reference network with respect to the correct local minimum in the image energy derived from ALS data is estimated. This analysis gives an idea about which accuracy level the GIS road networks in the following experiments can achieve if they detect the same minimum. For this purpose the reference of the road network of test site 1a is adapted by the proposed algorithm. The applied parameters are those summarised in Table 4. The results of the optimisation of the reference data are depicted in Table 5. The R.M.S. error between the optimised reference and its initialisation is smaller than 0.8 m and comparable for both snake models. This error primarily consists of three components:

- 1) the definition of the correct position of the centre line in the orthophoto by the human operator
- 2) the registration of the orthophoto and the ALS data to each other
- 3) the influence of the design of the image energy from ALS data.

Considering the resolution of the orthophotos (0.4 m) and assuming an uncertainty of the determination of the correct position of one and a half pixel, the error of the digitisation results in 0.6 m. By analysing the registration between the orthophoto and the ALS data at corresponding points well-defined in both data sets, an approximate registration error of 0.2 m was determined. We suppose that the remaining R.M.S. error of the reference optimisation (error propagation: $\sigma_{snake} = 0.5$ m) is caused by the definition of the image energy. This value corresponds to the used grid size of the image energy. The original reference data (and not the optimised) are used for the external evaluation in the following experiments for two reasons: First, the reference should be independent (particularly from the influence of the optimisation algorithm and the parameter setup). Second, the influence of the image energy design on the performance of the algorithm has to be preserved, because it is one of the main error sources of the proposed method. Generally, the R.M.S. error of the reference optimisation (0.8 m) should be kept in mind for the analysis of the following optimisation results with respect to this reference.

t_{stop} (pixel)		Iterations		R.M.S. error (m) of the centre line		Max. error (m) of the centre line		w (m)
std.	rb.	std.	rb.	std.	rb.	std.	rb.	rb.
1	1	148	107	0.71	0.71	1.49	1.43	4.28
0.14	0.60	1000	1000	0.79	0.78	1.60	1.58	4.40

Table 5. Optimisation results for the reference (bold letters indicate the termination criterion: first row: $t_{stop} = 1$; second row: $Max_{iter} = 1000$).

Other interesting results of the optimisation of the reference data can be observed in Table 5. The average width of the reference road network converges to 8.8 m (twice the ribbon parameter w). The maximal error is slightly larger for the standard model. The ribbon snake converges faster for $t_{stop} = 1$ pixel (sum of all node changes is 0.5 m – the resolution of the grid of the image energy), but the standard snake nodes move slower at iteration 1000 ($t_{stop} = 0.14$ for std. and

$t_{stop} = 0.60$ for rb.). This is caused by the fact that the image energy for ribbons is sampled at three points instead of one, i.e., at the centre line and the two edges. For iteration 1000 a more or less stable status is achieved for both variants except for some nodes jumping left and right with respect to the local minimum. This jump is larger for the ribbon snake model due to the additional free parameter w and the changed image energy.

4.2.1.2 Quality of the original GIS data

Table 6 illustrates the optimisation results of the original small road network from the GIS data base (R.M.S. error = 1 m) using the parameters in Table 4. This result should be kept in mind for the comparison with experiments starting from a changed initialisation (sections 4.2.1.3 - 4.2.1.6). A suitable solution is obtained for $t_{stop} = 5$ pixel after less than 80 iterations. Due to the high quality of the initialisation, the improvement is small in this experiment. The deviation from the results of the reference in Table 5 is caused by a slightly different shape of the two initial networks (reference and GIS data) and a very rigid geometry model. The rigid shape model will be the standard for the experiments, because errors that are additionally introduced by the algorithm itself due to inappropriate local image energies should be avoided. The slightly increasing maximal error for ribbons (red column in Table 6) arises from the later convergence of the width for the related node (last column of Table 6 - $w = 3.82$ m for $t_{stop} = 5$ pixel; $w = 4.35$ m for $t_{stop} = 1$ pixel). The road edges in the image energy corresponding to this node are not well-defined (asymmetric to the centre line), which also affects the quality of the centre line. The performance of the standard and the ribbon models is comparable. The ribbons converge slightly faster.

t_{stop} (pixel)		Iterations		R.M.S. error (m) of the centre line			Max. error (m) of the centre line			w (m)
std.	rb.	std.	rb.	init	std.	rb.	init	std.	rb.	rb.
5	5	78	72	1.61	0.97	0.97	3.36	2.85	2.54	3.82
1	1	234	183		1.00	1.02		2.76	2.69	4.35
0.40	0.78	1000	1000		1.01	1.02		2.81	2.76	4.37

Table 6. Optimisation results for the original GIS data (bold letters indicate the termination criterion).

4.2.1.3 Node distance

In this experiment the impact of the sampling interval of the nodes Δs on the performance is analysed in order to find a suitable value for this parameter. Table 7 summarises the main parameters of the experiment. The ribbon model was not used for this experiment. The initialisation from the original GIS data is shifted by 5 m in x- and y-direction to simulate larger inconsistencies.

α	β	γ	κ_i	xShift (m)	yShift (m)
15	15	1	10	5	5

Table 7. Most important parameters for the optimisation with different node distances Δs .

The optimization results of the experiments for different node distances Δs are depicted in Table 8. The quality of the polygon approximation is reflected by the errors for the initialisation and is comparable for all node distances. The

difference for $\Delta s = 2$ m, $\Delta s = 6$ m, and $\Delta s = 12$ m are even smaller than 1 cm. Using $t_{stop} = 5$ pixel, the small number of nodes for $\Delta s = 24$ m results in the fastest convergence, but also in the lowest adaptation quality. The use of the sum of all node changes during one iteration (t_{stop}) is not really suitable, because the number of iterations that are performed varies strongly for networks with a considerably different number of nodes. However, an average value is also not sufficient in any case. Considering a large network whose majority of nodes has already detected a suitable position, large changes in a small contour part result in a very small average change. Thus, this part won't be able to converge to the correct position. In order to make the results for different parameter settings more comparable, the number of iterations may provide a more suitable termination criterion (Max_{iter}).

Δs (m)	t_{stop} (pixel)	Iterations	R.M.S. error (m) of the centre line		Max. error (m) of the centre line	
	std.		init	std.	init	std.
2	5	356	4.29	1.05	8.45	2.82
6	5	174	4.29	1.33	8.31	3.52
6	0.733	356		1.05		2.95
12	5	114	4.29	1.73	8.31	4.08
12	0.219	356		1.10		3.22
24	5	61	4.47	2.44	8.31	5.99
24	0.089	356		1.13		3.52

Table 8. Optimisation results for shifted GIS data ($\Delta x = \Delta y = 5$ m) with different node distances Δs (bold letters indicate the termination criterion – white rows: $t_{stop} = 5$ pixel; grey: $Max_{iter} = 356$; identical for $\Delta s = 2$ m).

Choosing $Max_{iter} = \text{const.} = 356$ instead of $t_{stop} = \text{const.}$, the overall accuracy slightly decreases with the node distance, but the maximal error increases significantly at the same time. These errors occur often at dead road ends, which do not benefit from the network topology during the optimisation process. In this case a finer sampling of the image energy along the contour supports the adaptation, because more features in the ALS data are considered. A sampling distance of $\Delta s = 6$ m seems to be an appropriate compromise between the quality of the results and the computational time, which significantly decreases with the node distance. In comparison to the unchanged initialisation (Table 6 - R.M.S. error = 1.0 m; max. error = 2.8 m) the results for $\Delta s = 6$ m seems to be acceptable. Whereas the R.M.S. error for $\Delta s = 12$ m and $\Delta s = 24$ m is still sufficient, the maximal error increases significantly by 0.4 m and 0.7 m, respectively (cf. Table 6).

4.2.1.4 Shifted initialisation

In order to assess the robustness of the algorithm with respect to poor initialisations the method was applied to the GIS data that were shifted by different values for this experiment. The results are illustrated for shift values of 5 m and 10 m in x- and y-direction. The smaller value is selected because it corresponds to typical errors in the GIS data of the NMA (usually 3-5 m, sometimes up to 10 m). For 10 m shift in x- and y-direction the algorithm starts to fail. This fact is an important aspect in order to evaluate the general applicability of the proposed method. The parameters for the tests can be found in Table 9. Again a very rigid shape model is used during the optimisation process, because we strongly rely on the shape of the GIS data. Due to the same number of nodes in all experiments $t_{stop} = 5$ pixel is suitable for comparable results in this case.

α	β	γ	κ_i	$w_{initial}$ (m)	Δs (m)	t_{stop} (pixel)
15	15	1	10	2.5	6	5

Table 9. Most important parameters for the optimisation of shifted initialisations.

Table 10 illustrates the results of this experiment. If the initialisation is shifted by ± 5 m in x- and y in four different directions, the algorithm always converges to a reasonable minimum in the ALS data for both snake models (cf. Table 6). The ribbon model slightly outperforms the standard model with respect to the speed of convergence and the maximal error. Using a constant termination criterion $t_{stop} = 5$ pixel, the results for $|\Delta x| = |\Delta y| = 10$ m indicate that the final solution seems to be direction-dependent. The ribbon snake does not reach a suitable position for an x-shift of 10 m and an y-shift of -10 m by applying $t_{stop} = 5$ pixel, because the evolution of the snake already becomes very small after 65 iterations. The additional free parameter w may be the reason for this difference compared to the standard model. If the termination criterion is set to $t_{stop} = 2$ pixel, the ribbon snake continues the movement and finally achieves a suitable position (values in brackets in Table 10). However, both shape models fail for an x- and y-shift of -10 m and do not recover by using smaller values for t_{stop} (see the lower red row in Table 10 and Fig. 20 left for the ribbon model). Indeed, some road parts in vertical direction detect suitable positions in the image data. Nevertheless, most contour parts stop the evolution in the wrong minimum. They are often not able to cross the buildings along the roads due to the strong gradients of the building energy term and the initialisation at the wrong side. However, if the bridge energy is introduced into the process, both models converge to a correct solution (green line in Table 10 and right side of Fig. 20). At first the road part on the bridge starts to move to the right position and due to the rigid shape of the network, other contour parts having a similar orientation like the bridge follow.

In general the rigid shape model is robust against a shifted initialisation. If the building energy term is used, the main limitation for the shift is specified by the distance between the building skeletons and the road centre lines. In case of a shifted initialisation the image energy generates homogeneous gradients for many nodes of the network (same gradient direction), which allows a fast convergence to the correct local minimum (Fig. 21 left).

x-Shift (m)	y-Shift (m)	Iterations		R.M.S. error (m) of the centre line			Max. error (m) of the centre line		
		std.	rb.	init	std.	rb.	init	std.	rb.
5	5	174	151	4.28	1.33	1.23	8.81	3.86	3.49
5	-5	244	205	6.34	1.18	1.20	9.89	3.32	3.19
-5	5	167	139	4.13	0.93	0.89	6.90	2.48	2.13
-5	-5	287	249	5.49	0.86	0.90	10.08	2.37	2.14
10	10	497	526	8.58	1.32	1.25	13.83	3.85	3.49
10	-10	674	65 (865)	11.15	1.18	10.75 (1.04)	16.88	3.33	15.93 (2.74)
-10	10	397	385	8.99	0.93	0.89	13.38	2.46	2.06
-10	-10	391 (592)	405 (493)	9.86	8.67 (8.32)	9.59 (9.69)	16.89	15.06 (14.02)	16.71 (16.66)
-10	-10	507	498		1.05	0.95		3.61	2.67

Table 10. Optimisation results for shifted GIS data; red: final solution not suitable (in brackets: $t_{stop} = 2$ pixel), green: bridge energy is used.

Considering the typical errors of the road centre lines in the GIS data bases of the NMA (usually 3-5 m, sometimes up to 10 m) the results of this section verify the applicability of the proposed algorithm to the adaptation task. The shift of the initialisation by 14 m (10 m in two directions) may define some kind of limit of the method in urban areas. This limit may change with the average distance between the building skeletons and the road centre lines.

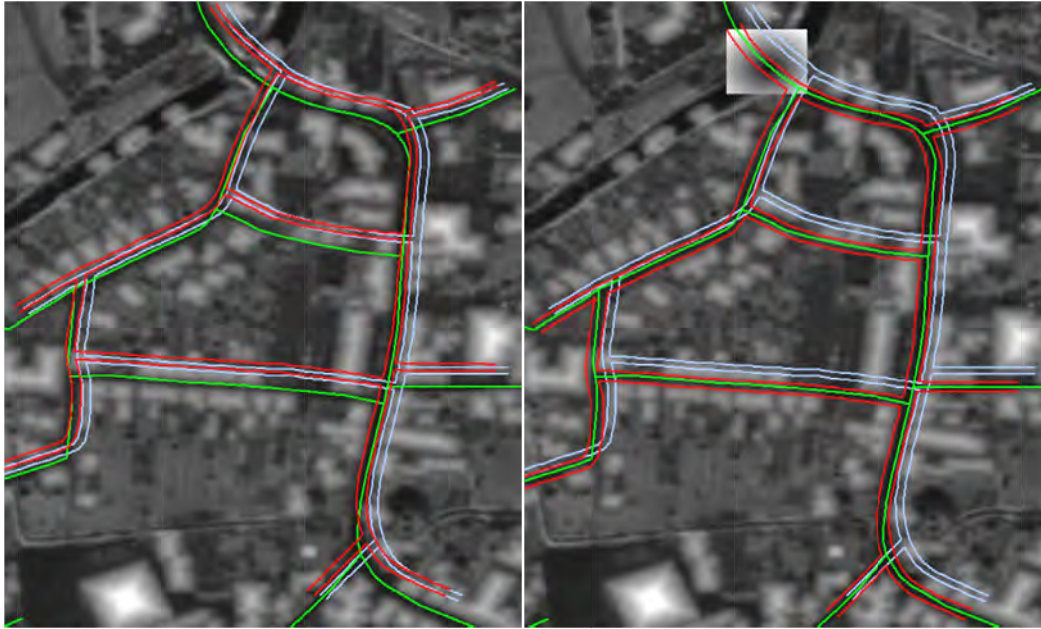


Figure 20: Optimisation results of the ribbon model for shifted GIS data (-10 m x-and y-shift) (background: image energy; blue: initialisation; red: final position; green: reference centre line); right: bridge energy of one bridge (bright rectangle) is used



Figure 21: Distribution of the gradients of the image energy after 100 iterations: left: shifted initialisation (5 m; 5 m); right: rotated initialisation (0.05 rad) (background: image energy)

4.2.1.5 Rotated initialisation

In order to assess the robustness of the algorithm with respect to poor initialisations the method was applied to the GIS data that were rotated by different angles. Although rotated data were more common in the period of analogue maps, a rotation of smaller parts of a GIS road network is not unusual. The parameters for this experiment are summarised in Table 11. The centre of the rotation is defined by the centre of gravity of the network. Therefore, large contour parts in the centre of the initial network are almost correctly located with respect to the ALS data. For these parts only small gradients of the image energy exist. This fact results in a slow evolution of the snake, which influences the applicability of t_{stop} . In order to allow a larger number of iterations comparable to the previous experiment, the termination criterion was therefore set to $t_{stop}=1$ pixel. Table 12 illustrates the results for the rotated initialisations. The ribbon snake converges faster than the standard model and often achieves a smaller R.M.S. error. The integration of the bridge energy amplifies this trend. In general the bridge energy in the upper left corner acts as a lever and improves the results significantly. However, such strong features are not often available. Thus, the experiments were also carried out without the bridge energy in order to assess the performance of the algorithm using the standard features.

α	β	γ	κ_i	$w_{initial}$ (m)	Δs (m)	t_{stop} (pixel)
15	15	1	10	2.5	6	1

Table 11. Most important parameters for the optimisation of rotated initialisations.

Rot (rad/deg)	Bridge	Iterations		R.M.S. error (m) of the centre line			Max. error (m) of the centre line		
		std.	rb.	init	std.	rb.	init	std.	rb.
-0.05/-2.86	no	270	200	5.57	3.96	3.91	12.48	10.98	11.47
-0.05/-2.86	yes	419	221		3.61	3.29		9.30	10.98
-0.03/-1.72	no	227	170	3.50	2.10	2.15	7.55	6.85	8.16
-0.03/-1.72	yes	1000	166		2.01	1.56		5.80	4.39
0.03/1.72	no	317	240	3.98	2.10	1.67	9.85	5.32	5.19
0.03/1.72	yes	373	237		1.84	1.37		5.45	3.20
0.05/2.86	no	648	325	6.09	3.86	3.52	14.46	9.33	11.10
0.05/2.86	yes	485	400		3.37	2.47		10.15	9.36
0.05/2.86	no	1000	1000		3.78	2.85		9.14	8.64
0.05/2.86	no	500	500		1.24	1.15		3.28	3.04

Table 12. Optimisation results for rotated GIS data; red: no convergence for $t_{stop}=1$ pixel, green: termination criterion

$Max_{iter}=1000$; blue: $\kappa_i=50$

Despite a similar number of iterations and an equivalent initial R.S.M. error, the algorithm performs worse for the rotated road network in comparison to the shifted initialisation (Table 10). Acceptable results in comparison to the optimisation of the original GIS data (Table 6) are only obtained for smaller angles ($\pm 1.72^\circ$) by using the ribbon extension and the bridge energy. The gradients of the image energy are not so homogeneous for rotated initialisations. They often point into different directions even for nodes of the same contour part (Fig. 21 right side). Thus, the force created by the image energy is small for the entire rigid network. Furthermore, the errors of the rotated initialisations increase with the distance

to the centre of the rotation. Dead ends, which do not benefit from the network characteristic and additionally have often weak image features, are located at the largest distances and have the largest errors. The adaptation of these points takes many iterations. Due to the inhomogeneous and small gradients of the image energy, the results are improved by considerably increasing Max_{iter} (green line in Table 12) as well as the weight of the image energy $\kappa_i = 50$ (blue line in Table 12). The good performance for large weights of the image energy and the significantly higher quality of the results for the ribbon model (remember: the image energy is sampled at three points instead of one) indicate that this very rigid setting is not really suitable for the rotated initialisations. However, nodes at dead ends, which additionally are far away from the centre of rotation, (having the largest errors) are often located on the wrong side of the buildings. They thus need the help of neighbouring contour parts and therefore require a rigid setup in order to move to a correct position.

Generally, the algorithm is also able to deal with rotated initialisation, because the errors of the initialisations are significantly decreased for all the demonstrated experiments. Due to the more inhomogeneous distribution of the image energy gradients for the entire network, the adaptation takes longer as for shifted vector data using the same parameter set and the results are significantly worse than those of the optimised original GIS data set (cf. Table 10).

4.2.1.6 Variation of initial ribbon width

This experiment evaluates the influence of the initial ribbon width on the accuracy of the optimised centre lines. Table 13 summarises the main parameters of the test and Table 14 illustrates some results. Despite a quite different initialisation of the ribbon width the algorithm always converges to a suitable position of the centre line (cf. Table 6).

α	β	γ	κ_i	Δs (m)	t_{stop} (pixel)
15	15	1	10	6 (253 nodes)	5

Table 13. Most important parameters for the experiments concerning the ribbon width.

Initial road width (m)	Optimised road width (m)	Iterations	R.M.S. error (m) of the centre line	Max. error (m) of the centre line
1	6,16	79	0,96	2,74
3	7,50	82	0,96	2,63
5	7,84	72	0,96	2,54
7	8,29	69	0,98	2,55
9	8,81	63	0,99	2,62
11	9,32	62	0,98	2,65
13	9,72	72	0,98	2,66

Table 14. Influence of the initial road width (twice the ribbon width) on the performance of the algorithm.

The differences in the average width of the ribbons after the optimisation show that this parameter is not correctly determined for the applied termination criterion (except maybe for an initial width of 9 m, c.f. the reference $2w = 8.80$ m in Table 5). Generally, the algorithm converges slightly faster if the initial ribbon width is close to the optimum. The roads of the network have an actual average width between 6-8 m and a corresponding sidewalk (1-2 m) on both sides in most cases. This may be a hint that the design of the image energy forces the borderline of the ribbon to a position in the middle of the sidewalk (see Fig. 22). However, this snake approach was not created for the exact determination of the

road borderlines. The ribbon model is primarily used for the more accurate delineation of the object centre line. In this context asymmetric road features may be a considerable error source. In order to avoid such errors, a more sophisticated cross section model has to be integrated considering for instance additional attributes of the GIS data (e.g., sidewalks only on the left road side).



Figure 22: Position of the optimised ribbon borders (yellow points) superimposed to an orthophoto

4.2.1.7 Convergence behaviour

This section compares the convergence behaviour of the ribbon and the standard snake model. Table 15 depicts the main parameters for this test. The initialisation was slightly shifted in order to simulate larger inconsistencies between the data sets. The parameter γ represents a factor that is used to amplify or damp all acting forces. If the parameter is doubled the forces will be simply divided by two and vice versa. Increasing the viscosity parameter γ during the optimisation is an interesting idea, but has not been tested yet. A small viscosity supports jumps over wrong (but, unfortunately, also over correct) local minima and local maxima, which may be an advantage in case of a poor initialisation, whereas a large viscosity enables the precise detection of the minimum. The parameter γ is set to constant during the optimisation for all the experiments. The setup in Table 15 is found to be a suitable compromise between a fast and robust convergence and an accurate detection of the local minima in the image energy.

α	β	γ	κ_i	xShift (m)	yShift (m)	Δs (m)
15	15	1	10	5	5	6

Table 15. Most important parameters for the optimisation with different iterations.

Fig. 23 highlights the convergence characteristic of the small road network for the ribbon and the standard snake model. The small sum of the position changes of all network nodes (green graphs) for the iteration 500 (less than 0.25 m corresponding to half a DTM pixel) indicates the detection of a significant and stable minimum of the energy functional for both models. This sum of position changes is used as one termination criterion (t_{stop}). The transferability of this parameter decreases with the difference in the number of snake nodes in the network.

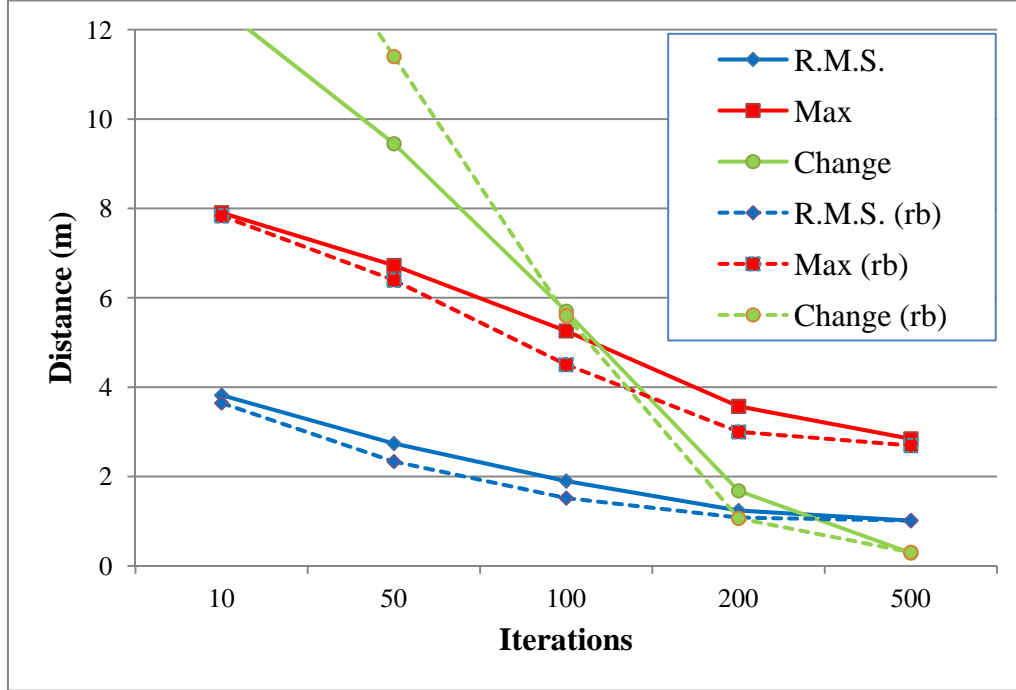


Figure 23: Influence of the number of iterations on the distance to the reference and on the sum of the position changes of all network nodes (distance to the previous iteration) (green) for the standard and the ribbon model (rb)

Due to the sampling of the image energy at three positions for each snake node, the ribbon model moves faster into the direction of the minimum than the standard model for the first 100 iterations (green lines in Fig. 23). Thus, also the R.M.S. error and the maximal error decrease faster for the ribbon model. For the iteration 500 both models have approximately the same (very slow) speed. The ribbon model performs slightly better than the standard model with respect to R.M.S. error and the maximal error at the end of the optimization.

4.2.1.8 Weighting between E_{int} and E_{image}

This experiment evaluates the performance of the algorithm using a different weighting between the internal and the external energy in order to find a suitable parameter setup. Table 16 summarises the main parameters of the test. The initialisation is again slightly shifted in order to simulate larger inconsistencies between the data sets.

γ	κ_i	Δs (m)	xShift (m)	yShift (m)
1	10	6	5	5

Table 16. Most important parameters for the optimisation with different weights for the internal energy.

Figs. 24 and 25 illustrate the influence of the weights of the internal energy on the performance of the algorithm while using a fixed weight for the image energy. In Fig. 24 the termination criterion $t_{stop}=5$ pixel is used for the determination

of the convergence. In general the performance of the algorithm is satisfactory for a wide range of weight parameters of the internal energy according to Eq. 12. Even for the most rigid setting ($\alpha = \beta = 1000$) the R.M.S. error (1.30 m) is improved considerably in comparison to the initialisation (4.28 m) for the standard and the ribbon model. The R.M.S. error for this stiff geometry is mainly caused by the errors of the initial shape with respect to the reference and the difference of the reference to the image energy (cf. Table 5), i.e. the original shape fits well to the reference shape. Of course this aspect is generally important for a good quality of the results when applying the rigid shape model. In comparison to the results of the original GIS data (Table 6) these errors are also acceptable.

For the weakest internal energy ($\alpha = \beta = 0.01$) an overfitting of the contour to the ALS data can be detected and the quality of the results decreases considerably. In this context the largest errors can be observed for road parts, for which the centre lines are not well defined in the image energy. Such situations occur if roads open into a square or if a courtyard is close to the road (yellow circles in Fig. 26). Also the ribbon width changes rapidly from node to node for small weights of the internal energy (Fig. 26 centre). The R.M.S. error graph in Fig. 24 shows a flat local minimum for $\alpha = \beta = 1$, and the smallest maximal error can be observed for the parameters $\alpha = \beta = 0.5$ for both models. However, for these settings also the highest number of iterations was required until termination. In comparison to the standard model, the ribbon network snakes suffer from small weights of the internal energy (Fig. 24 left for $\alpha = \beta = 0.1$). The additional free parameter may introduce some new uncertainties in this weakly weighted object model. For more rigid shapes ($\alpha > 0.5$ and $\beta > 0.5$) both models show a comparable performance, but the ribbon model converges faster (cf. Fig. 24 right).

Using the same number of iterations for each setting (Fig. 25 left), which is the standard for the tests with larger data sets, the ribbon model performs better than the standard model for more rigid object models ($\alpha > 0.5$ and $\beta > 0.5$). In contrast, the standard model is more robust for setups with a weak internal energy. The best results for the ribbon model (R.M.S. error = 1.1 m) are achieved by using a quite rigid shape ($\alpha = \beta = 10$). This insight will be used in order to set the parameters for the tests with larger data sets.

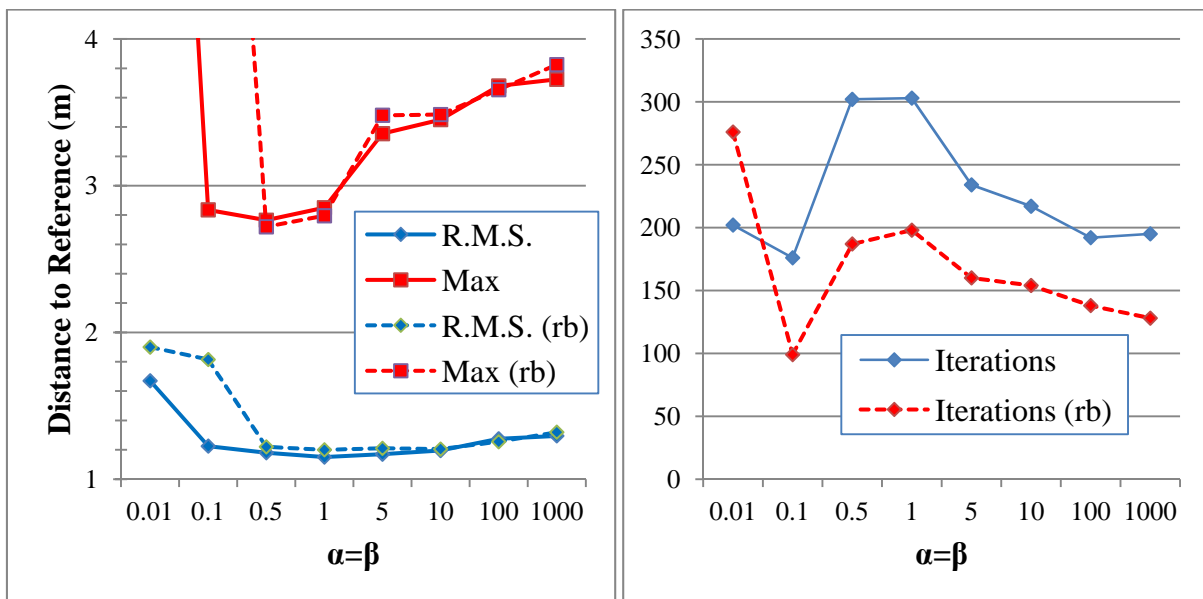


Figure 24: Optimisation results using different parameters for the internal energy and $t_{stop} = 5$ pixel; rigid snake model

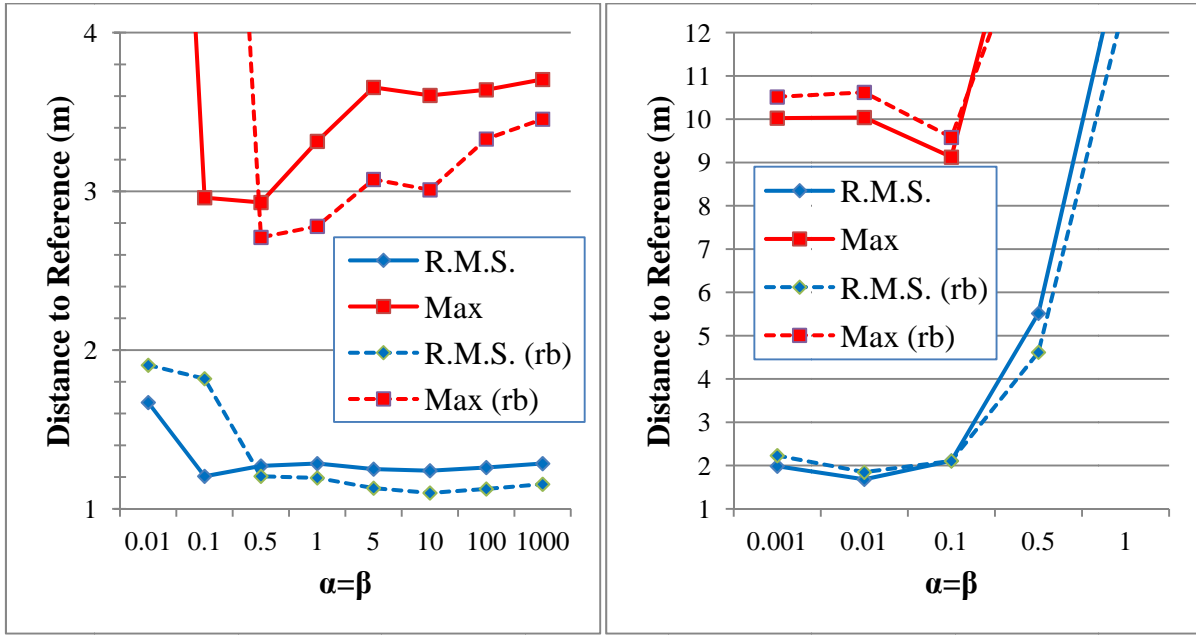


Figure 25: Optimisation results using different parameters for the internal energy and $Max_{iter}=200$; left: rigid snake model (Eq. 12); right: original E_{int} .

The right graph of Fig. 25 shows the performance for the original model of the internal energy defined by Kass et al. (1988) (Eq. 5) using different weights. If the influence of the internal energy is weak ($\alpha = \beta = 0.01$), there will be almost no difference between the accuracy of the results of the original object model and the rigid snake model. By increasing the weights of the internal energy and thus the impact of the object model, the rigid snake model further improves the R.M.S. error of the road network, whereas the quality of the results is decreased using the original model of smoothness. The largest errors for the original model occur at road parts of high curvature and at crossings, where the object model obviously does not fit well. The examples in section 4.2.2 will illustrate these findings in more detail.



Figure 26. Optimisation results for the standard (left) and the ribbon model (centre) using very small weights for the internal energy ($\alpha = \beta = 0.01$) (left and centre: background: image energy; blue: initialisation; red: final position; green: reference centre line, yellow circles: large errors) (right: background: orthophoto; green: reference centre line)

4.2.1.9 Summary of the sensitivity analysis

In this section the main conclusions of the sensitivity analysis are briefly summarised. These findings will also influence the parameter setup for the experiments with larger test sites.

Quality of the reference

- The manually digitised reference data are subject to different error sources. Thus, they do not represent very accurate positions of the centre lines in the ALS data. The optimisation of the reference data resulted in a R.M.S. error = 0.8 m. This value should be kept in mind for the evaluation of the results of larger test sites.

Initialisation:

- A **node distance** of $\Delta s = 6$ m is a suitable compromise between the quality of the results and the computational time.
- The initial **width of the ribbon** snake hardly influences the quality of the optimised centre lines ($w = 2.5$ m is suitable for roads having two lanes).
- Using the rigid snake model, the algorithm can cope **with shifted initialisations** quite well. Due to the defined building energy, the distances of the building skeletons from the road centre lines represent a limit for the shift in urban areas (test site 1a: approximately 10 - 14 m except if strong features such as bridges are present).
- Due to inhomogeneous gradients of the image energy, the method performs worse for **rotated initialisations** in comparison to the shifted ones. In order to deal with rotated initialisations, the algorithm requires more iterations or a larger weight for the image energy. For rotations up to 2 degree the results are sufficient for the analysed small road network using the standard setup.

Parameters:

- The determination of a suitable **termination criterion** is difficult. The parameter t_{stop} is not really suitable especially for the transferability to networks with different error characteristics or different numbers of snake nodes. $Max_{iter} = 200$ seems to be a suitable value for the optimisation of larger test sites, which are not synthetically shifted or rotated, in order to obtain comparable results.
- The rigid snake model is very robust with respect to a change of the **weighting between the internal and external energy** if the initial shape has a good quality. Assuming the latter for the topographic GIS data of the NMA, in general a relatively rigid setup ($\alpha = \beta = 15$, $\kappa_i = 5$) is preferred for the tests with larger test sites. These test sites contain a high percentage of rural areas. Assuming a lower quality of the ALS features in rural areas (no building energy, problems with strongly vegetated areas), the weight for the image energy is reduced in comparison to the sensitivity analysis. For GIS road networks of lower quality the weights for the internal energy should be reduced.

4.2.2 Tests of the rigid snake model

In this section, three tests are carried out in order to highlight the advantages of the rigid snake model in comparison to the original internal energy. After the primarily quantitative considerations of the sensitivity analysis, the results of this section are only interpreted visually. The original GIS data are again shifted for each test in order to simulate larger inconsistencies with random and systematic errors. The identical parameters for the three tests are shown in Table 17.

γ	κ_i	Δs (m)	Max_{iter}
1	5	6	200

Table 17. Most important parameters for the tests in this section.

The first test site is known from the previous section (test site 1a). The GIS road data is shifted by -8 m in x- and y-direction. The standard image energy (buildings, intensity, and height variation) is applied. Fig. 27 visualises the results for the original internal energy (top) and the rigid snake model (bottom) using small (left: $\alpha = \beta = 0.5$) and large (right: $\alpha = \beta = 15$) weights for the particular object model. In order to counteract the shortening effect of the original E_{int} , a constraint is introduced that allows the nodes at dead road ends to move only across the snake direction. This direction is determined from the neighbouring nodes of the previous iteration. The end nodes are thus somewhat fixed. This procedure is able to improve the results for this object model in many cases; but it also fails sometimes (yellow circle in Fig. 27) if the corresponding snake part is distorted during the optimisation process due to strong image energy gradients.

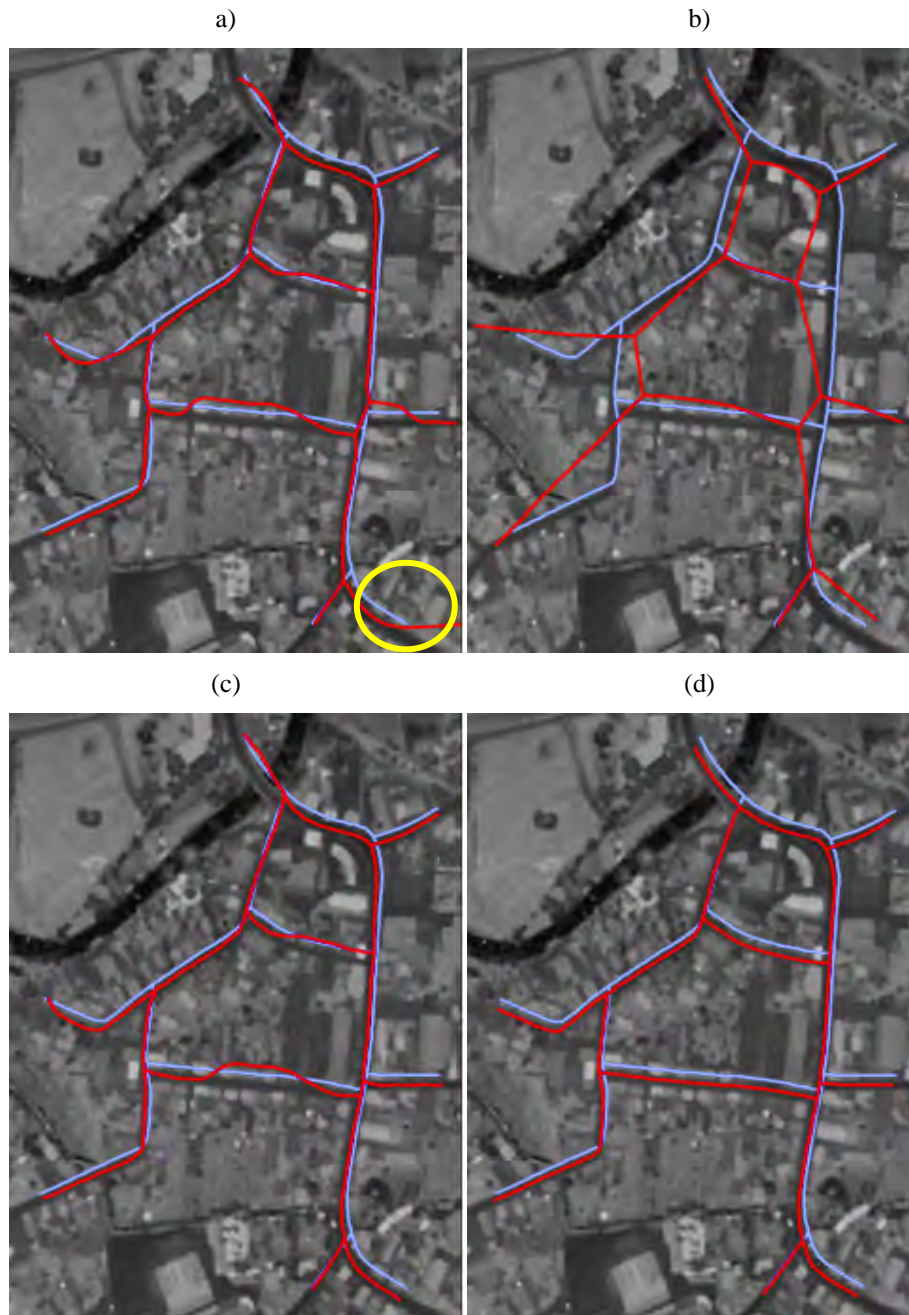


Figure 27. Optimisation results of a small road network for the original E_{int} (top - a, b) and the rigid snake model (bottom - c, d) (background: DSM; blue: initialisation; red: final position; yellow circle: area of interest) (left (a,c): $\alpha = \beta = 0.5$; right (b,d): $\alpha = \beta = 15$)

For a small internal energy (Figs. 27a and 27c) the snakes of both object models are often not able to cross local maxima in the image energy caused by buildings. Due to the weak influence of the object models, correct contour parts can not support the inaccurate nodes. If the weights for the internal energy are increased, the rigid snake moves to the correct solution (Fig. 27d). In contrast, the snake with the original internal energy completely fails (Fig. 27b). The next example illustrates this behaviour in more detail.

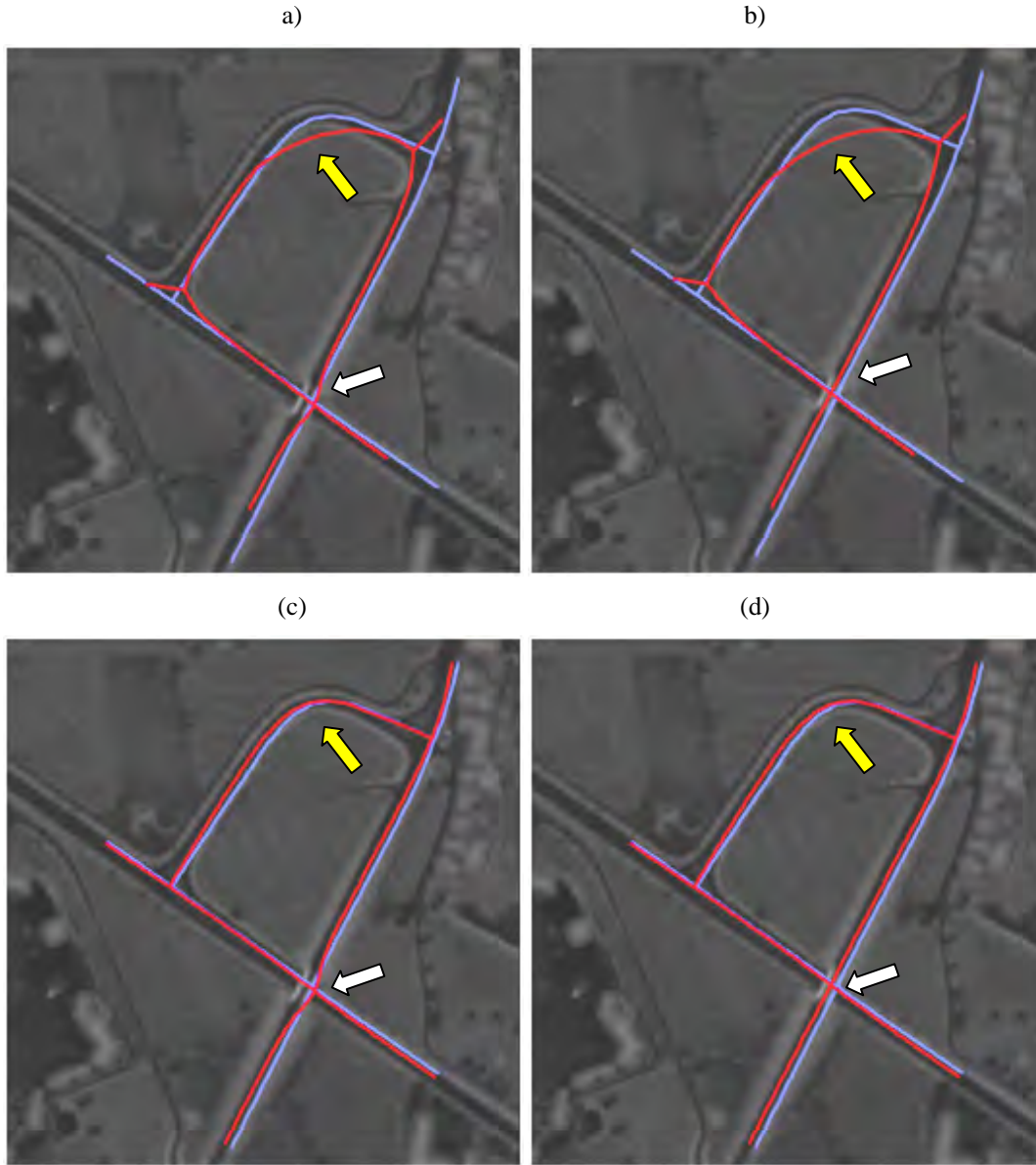


Figure 28. Optimisation results of a small road network for the original E_{int} (top - a, b) and the rigid snake model (bottom - c, d) (background: image energy; blue: initialisation; red: final position; white arrows: bridge; yellow arrows: a road segment with relatively high curvature) (left (a,c): $\alpha = \beta = 0.5$; right (b,d): $\alpha = \beta = 50$).

A small road network (part of test site 1b) containing a bridge was adapted to the ALS data under different conditions in the second test. The original GIS data, shifted by 5m in x- and y-direction, are used for the initialisation. Fig. 28 shows the results for the original internal energy (top) and the rigid snake model (bottom) using small (left: $\alpha = \beta = 0.5$) and large (right: $\alpha = \beta = 50$) weights for the particular object model. The image energy in Fig. 28a is not able to compensate the straightening force of the original formulation of the internal energy in curves even with small weights α and β for the smoothness term in Eq. 5. In addition, this force is not strong enough to guarantee the straightness of the road in the

vicinity of the bridge edges in the lower part of the image. The use of large values of α and β (Fig. 28b) ensures the smooth passing of the bridge, but increases the straightening effect in curves. Obviously, there are no global values for the weights that at the same time preserve the road shape in curved regions and guarantee the straightness of the road on the bridge without additional knowledge or constraints. In contrast, the alternative term of the internal energy maintains the curvature by applying small (Fig. 28c) as well as large values of α and β for the smoothness term in Eq. 12 (Fig. 28d), though only in the latter case the road passes the bridge correctly after optimisation.

The example in Fig. 29 (part of test site 1b) illustrates that the new object model preserves the perpendicularity of crossings and underpasses using relatively small weights for the internal energy ($\alpha = \beta = 1$). The original GIS data, shifted by 5m in x- and y-direction, are again used for the initialisation. The standard image energy for ALS data with a low resolution (height variation of the DSM and ALS intensity) is applied. Using the standard internal energy with an optimal parameter setup ($\alpha = 0.1$, $\beta = 0.2$) (Fig. 29a), the shape at crossings and underpasses may change during the optimisation. Exploiting the initial shape (Fig. 29b) maintains geometrical constraints implicitly contained in the initialisation.

In order to reduce the smoothing effect of the original internal energy in curved road parts, it is possible to assign smaller weights to this energy term for snake nodes with strong curvature in the initialisation. However, this modification may result in an overfitting of the corresponding road parts to the ALS data, and it weakens the stabilising effect of the significant geometry of these curved snake elements on the optimisation process. Furthermore, this strategy increases the complexity of the parameter setup. Due to its robustness with respect to the weight parameter, the rigid shape model increases the transferability of the entire method.

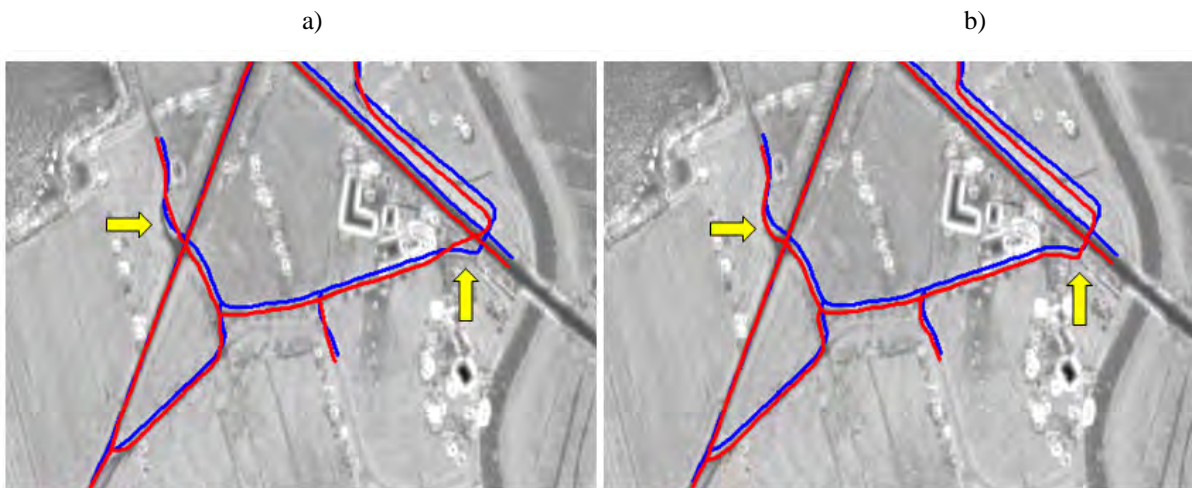


Figure 29: Maintenance of curvature and intersection angles of road crossings (background: image energy; blue: initialisation; red: final position; yellow arrows: points of interest). (a) original E_{int} using $\alpha = 0.1$ $\beta = 0.2$; (b) rigid snake model using $\alpha = \beta = 1$.

4.2.3 Bridges

The next four examples adapt a small road network (parts of test site 1b) in the vicinity of one bridge both without and with the bridge energy E_{bridge} in order to show the benefits of using this information (Fig. 30). The standard internal energy (Eq. 5) is applied in these cases in order to separate and emphasize the effects. The parameters for the test, which

were determined empirically, are depicted in Table 18. Table 19 shows the R.M.S. errors of the results for the examples in Fig. 30. It is obvious that if the initialisation is located within the borderline of the bridge, the bridge energy has hardly any influence on the quality of the results, though the algorithm converges faster if the bridge energy is considered. However, if the initial position of the road network is outside the bridge due to large differences between the DLM and the height data, the snake is not able to jump across the strong edges along the bridge using only E_{ALS} and E_{build} and thus cannot move to the correct position. In order to illustrate this effect, the initialisation from the original GIS data is shifted so that the snake nodes are located outside the bridge for all experiments of this section. Due to different bridge widths these shift values can vary.

α	β	γ	κ_i	Δs (m)	Max_{iter}
0.1	0.2	1	5	6	200

Table 18. Most important parameters of the experiments for the bridge energy.

In the first example (Fig. 30a) a straight road is adapted. For the simulation of inconsistencies the initialisation was shifted by 6 m both in x and y . Without using the bridge energy the snake nodes that should be on the bridge are not able to cross the strong gradients of the image energy at the bridge border (Fig. 30a left). A larger weight of the internal energy would help to force these nodes to the bridge centre due to the smoothing effect. However, this limits the range of possible parameter setups for the network connected to this bridge. Fig. 30a (right) shows that the integration of the bridge energy results in an accurate solution (R.M.S. error = 0.6 m).

The examples in Figs. 30b and 30c show a similar behaviour. Each initialisation was shifted by 5 m both in x and y . Integrating the bridge energy significantly improves the quality of the results. Obviously, the bridge energy affects only the network nodes in a certain vicinity if the weights of the internal energy are small. Because the example in Fig. 30b is significantly smaller (62 vs. 252 nodes for Fig. 30c), the quality improvement in this example is larger (without bridge: 3.95 m; with bridge: 1.87 m) than in example in Fig. 30c (without bridge: 2.42 m; with bridge: 2.06 m).

In the example in Fig. 30d (initialisations also shifted by 5 m in x and y) the underpass road is not located in the centre of the bridge. Therefore, the assigned new image energy forces this road segment to the bridge centre, which is in this case not the correct position. For this situation the bridge detection method has to be extended by position and direction information of the underpass road.

Examples		Fig. 30a		Fig. 30b		Fig. 30c		Fig. 30d	
Bridge		no	yes	no	yes	no	yes	no	yes
R.M.S. error (m) of the centre lines	init	8.24		5.63		5.11		4.84	
	std.	6.00	0.61	3.95	1.87	2.42	2.06	3.77	2.13

Table 19. Evaluation of the results: R.M.S. errors for the examples in Fig. 30 without and with the bridge energy.

The examples in Figs. 28 (section 4.2.2) and 30c were achieved for the same road network. This illustrates the ability of the method to deal with problems using different strategies (integration of E_{bridge} or of the rigid shape model). The combination of these approaches facilitates the setting of suitable weights and increases the robustness of the algorithm. For instance, the integration of the bridge energy enables the reduction of the values of the smoothness weights α and β .

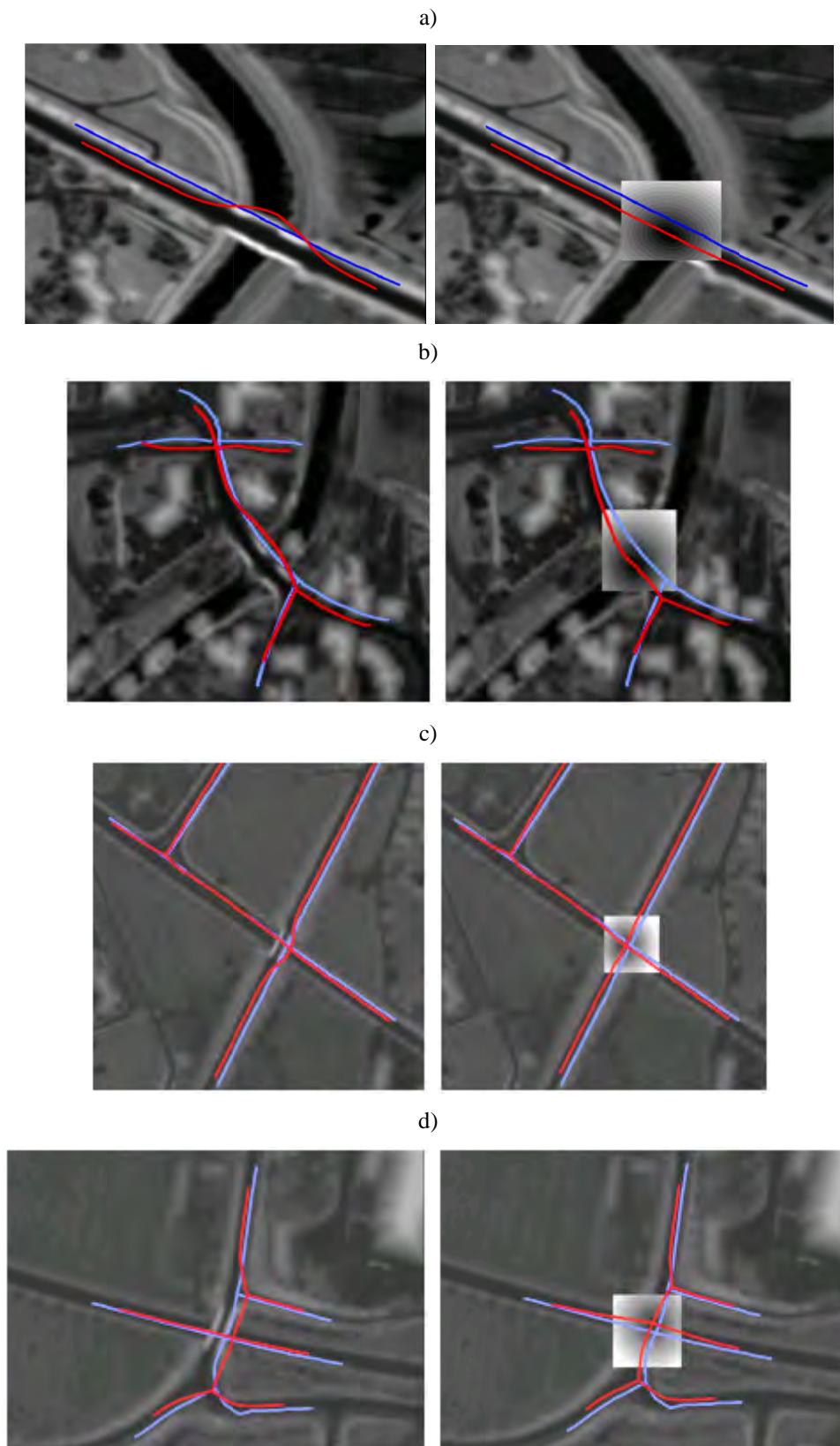


Figure 30. (a)-(d): Adaptation of four small road networks to ALS data near single bridges (blue: initialisation; red: final position); left/right: without / with bridge energy.

In general the design of the bridge energy by a distance transform generates gradients in the image energy that move the nodes step by step to the desired position during the optimisation. This gradual process enables the neighbouring nodes to continue this motion. Thus, the bridge energy does not immediately change the shape of the contour at the beginning and end of the bridge. This is an important property for the iterative optimisation process. Furthermore, due to a similar design, the bridge and the building energy have similar gradients. This aspect facilitates a well-balanced parameter setup.

4.2.4 Evaluation of larger road networks

In this section five larger road networks (Fig. 31) are adapted to the ALS data using the proposed network snake strategy in order to evaluate the general applicability of the method. Furthermore, some results of the sensitivity analysis, which was carried out for one small road network, should be confirmed using larger data sets. The original GIS data are used for the initialisation of the network snakes. Accuracy information of the respective GIS data set can be derived from the specified R.M.S error and the maximal error of the initialisation with respect to the reference. The specifications of the ALS data sets, such as the point density or the availability of intensity values, and of the GIS data vary strongly (cf. section 4.1.2) and allow an assessment of the transferability of the algorithm.

α	β	γ	κ_i	$w_{initial}(\text{m})$	$\Delta s(\text{m})$	Max_{iter}
15	15	1	5	2.5	6	200

Table 20. Most important parameters for the optimisation of the larger road networks (for test site 4 the weights for the internal energy are decreased to $\alpha = \beta = 2$).

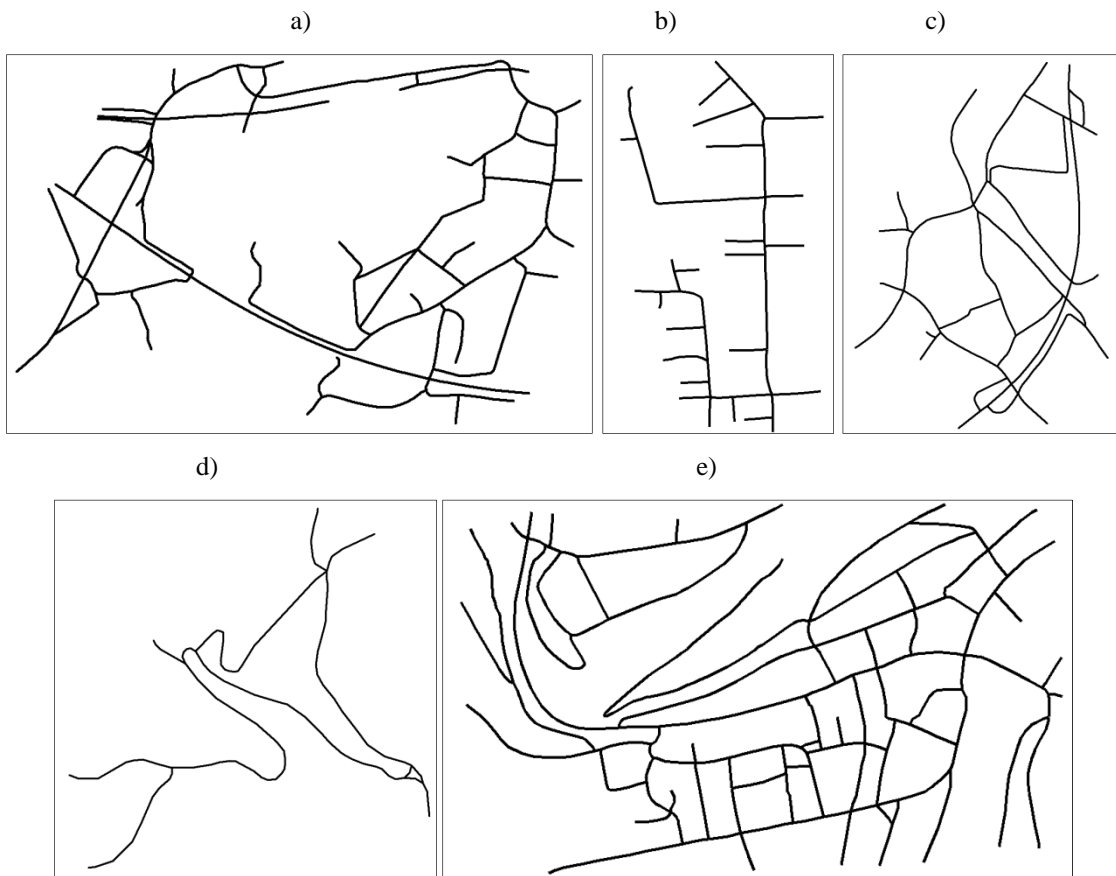


Figure 31. Larger road networks (different scales): a) test site 1b; b) test site 2a; c) test site 3a; d) test site 3b; e) test site 4.

In order to check the transferability of the setup, the parameters for the first four examples in this section are identical. Because the GIS data of these examples are provided by the corresponding NMA, it is assumed that the shapes of the networks have a high quality. Thus, a relatively strong influence of the rigid snake model is preferred (Table 20). This setup should avoid an overfitting to the sometimes spurious ALS features and thus preserves the shape of the vector data. In addition to urban areas studied in the sensitivity analysis, the data sets of this section contain also large rural regions. The image energy of these regions is not so reliable compared to the urban environment. For example, large vegetated areas disturb the filtering of the ALS heights resulting in some spurious features in the DTM. Thus, the weight for the image energy is reduced in comparison to section 4.2.1.

Test site 1b

Fig. 32 shows the results of the entire test site 1b (data set Kellinghusen), covering an area of 1700 x 1100 m². For this test area, all terms of the image energy, including features of terrain slope, ALS intensity, building outlines as well as bridges, are integrated. The overall R.M.S. error with respect to the reference decreases from 1.8 m for the initialisation (in this case based on the actual ATKIS data base) to 1.4 m for the standard network snake and to 1.2 m for the ribbon extension considering all of the 2115 centre line nodes (Table 21). A comparison to the results of the sensitivity analysis shows that the algorithm performs well for this example. Although the road width in the scene varies between 3 m and 14 m and the initial width for the ribbon snake was set to 6 m for all the road segments, the method is able to adapt the road borderlines to the ALS features and thus detect the correct position of the middle axis in most cases. Only 42% and 71% of the initial nodes are situated within a distance of 1 m and 2 m from the reference, respectively. These values increase to 57% and 85% for the standard snake and to 68% and 91% for the ribbon extension, respectively (cf. Fig. 34 left). The node with the maximum distance to the reference both in the initialisation (6.70 m) and after optimisation (7.47 m) is located at a curved dead road end and, thus, does not benefit from the network solution (yellow arrow in Fig. 32). This fact and the poor initialisation are the reasons for the large remaining error.

Fig. 33 shows a part of test site 1b. After the optimisation the ribbon snakes coincide with highway as well as farm road borderlines even when using an initial road width of 6 m for all roads. The snakes fit well also to the orthophotos except on the bridge. This indicates that the bridge height was not considered during the generation of the orthophoto.

	Test site 1b (2115 nodes)			Test site 2a (416 nodes)		
	init	std.	rb.	init	std.	rb.
R.M.S. error (m)	1.82	1.41	1.24	1.58	0.92	0.84
Max error (m)	6.73	7.47	7.09	4.25	2.67	2.65

Table 21. Evaluation of the results for the test sites 1b and 2a.

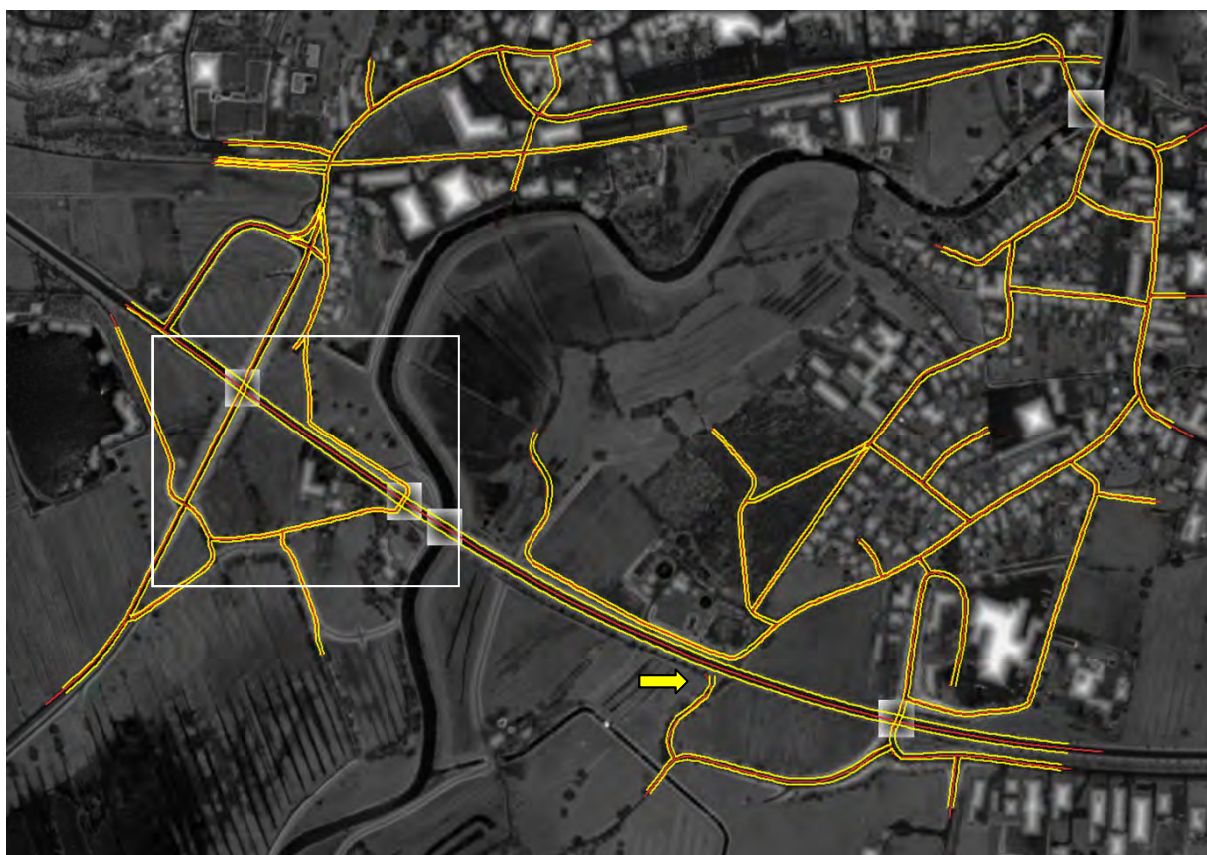


Figure 32. Test site 1b (Kellinghusen): Comparison of the reference centre line (red) and the final ribbon snake (yellow); background: image energy with buildings and bridges; yellow arrow: largest error; white rectangle: detail in Fig. 33.



Figure 33. Detail of test site 1b: final ribbon snake (red and black dots); background: image energy from ALS (left); orthophoto (right).

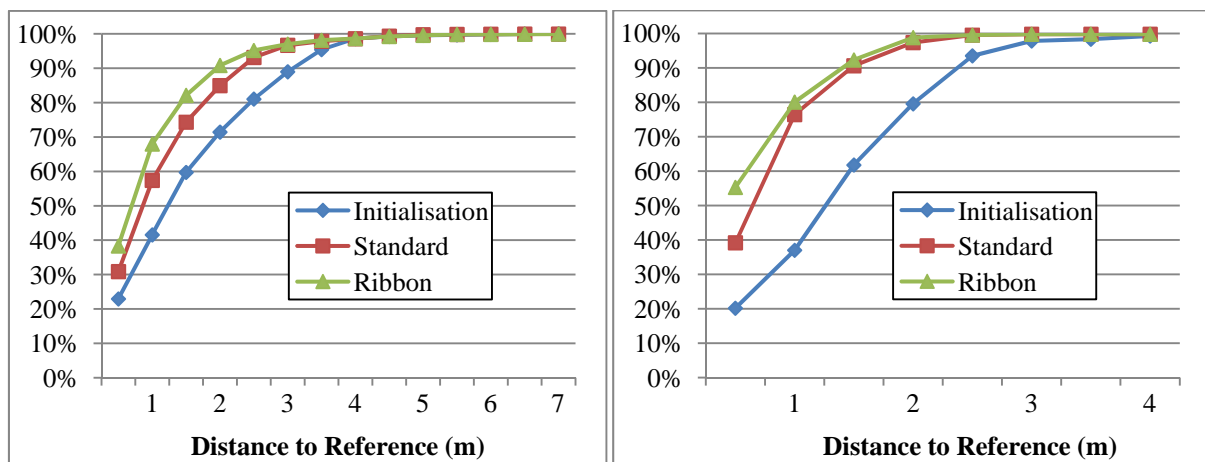


Figure 34. Cumulative histogram of the orthogonal point-to-line distances of the snake nodes from the reference: left: test site 1b; right: test site 2a.

Test site 2a

Fig. 35 illustrates the results for a part of the test site 2a (data set Oldenburg), covering an area of $400 \times 600 \text{ m}^2$. For this test area, all terms of the image energy, including features of terrain slope, ALS intensity, building outlines as well as bridges, are available, too. The overall R.M.S. of the orthogonal point-to-line distances with respect to the reference decreases from 1.6 m for the initialisation (in this case again based on the actual ATKIS data base) to 0.9 m for the standard network snake and to 0.8 m for the ribbon extension considering all of the 416 centre line nodes (Table 21).

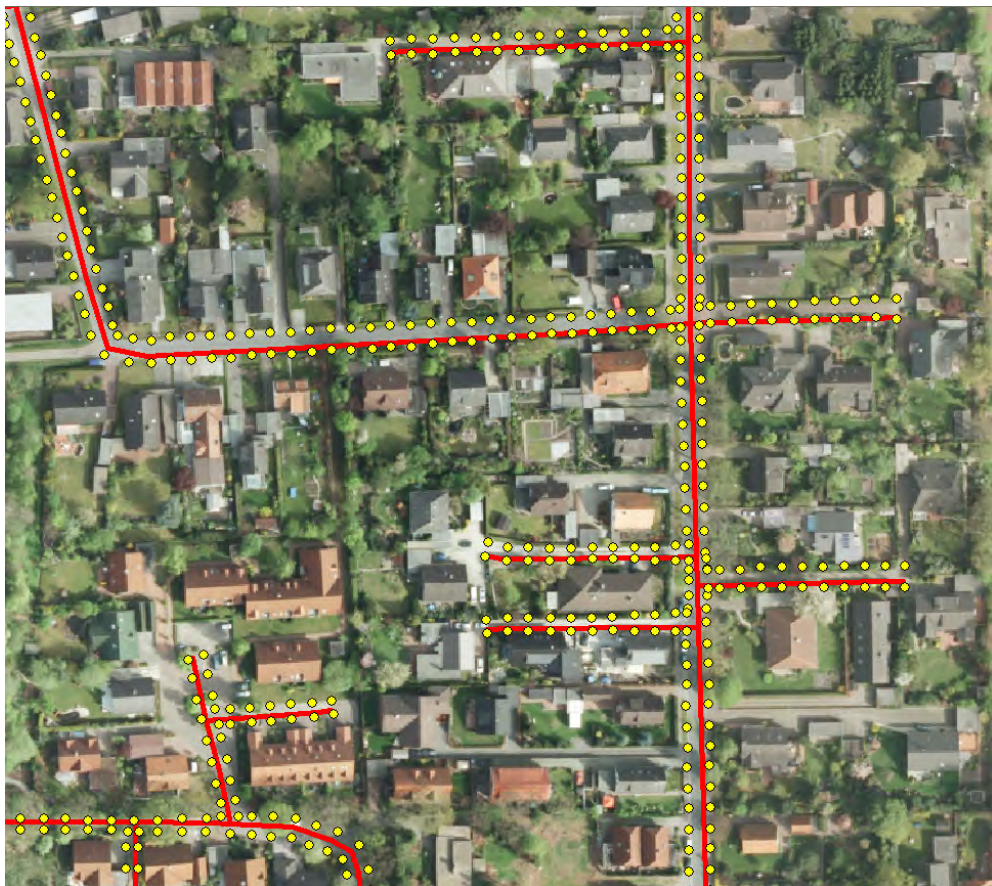


Figure 35. Part of test site 2a (data set Oldenburg, urban): ribbon snake borders superimposed to an orthophoto. red: original vector data; yellow points: optimised ribbon nodes.

Only 37% and 62% of the initial nodes are situated within a distance of 1 m and 2 m from the reference, respectively. These values increase to 76% and 97% for the standard snake and to 80% and 99% for the ribbon extension (cf. Fig. 34 right). The percentage of nodes with a difference smaller than 0.5 m even increases from 20% to 39% and 55%. For this interval also the largest difference between the ribbon and standard model can be recognised. In general the algorithm performed very well for this test site due to a good initialisation, both with respect to the accuracy as well as to the shape and to the high quality of all parts of the ALS features. Errors larger than 3 m could not be observed.

Test site 3a

The results for a part of test site 3a, an urban site in Emmental (Switzerland) covering an area of 750 x 1000 m², are shown in Fig. 36. In this case, no building and bridge energy terms were used. The reason is that for building detection, the point density was not high enough, in particular because the majority of the buildings in the scene are rather small. There are only two bridges in the scene, and one of them is covered by a saddleback roof, so that the bridge detector failed. As described in section 3.4.2.2, in this case the image energy was generated from the standard deviation of the unfiltered ALS points in order to preserve features from buildings. Homogeneous areas inside building roofs creating local minima in the image energy and branches of trees hanging across the roads increasing the image energy disturb the optimisation process. Nevertheless, the adaptation algorithm is successful in improving the geometrical accuracy of the road centre lines. The overall R.M.S. error with respect to the reference decreases from 3.5 m for the initialisation to 2.2 m for the standard network snake and to 1.9 m for the ribbon extension, considering all of the 987 centre line nodes (Table 22).

The cumulative histogram (left side of Fig. 37) also shows that the integration of the cross-section information of the ribbon snake model improves the accuracy of the road centre lines compared to the standard snake approach. Only 28% and 59% of the initial nodes are situated within a distance of 1 m and 3 m from the reference, respectively. These values increase to 40% and 80% for the standard snake and to 46% and 88% for the ribbon extension (cf. Fig. 37 left). The maximum error can be observed in an area with dense vegetation (yellow arrow in Fig. 36). It is caused by a poor initialisation and the effects of trees on the image energy described above, so that the optimisation does not converge to the correct position.

	Test site 3a (987 nodes)			Test site 4 (1782 nodes)			
	init	std.	rb.	init	std. without buildings	std.	rb.
R.M.S. error (m)	3.52	2.24	1.87	3.40	2.60	2.22	2.25
Max. error (m)	8.13	7.16	7.50	18.30	18.37	19.22	19.49

Table 22. Evaluation of the results for the test sites 3a and 4.



Figure 36. Part of test site 3a (data set Emmental, urban): centre line of ribbon snake model superimposed to an orthophoto. red: original vector data; yellow: reference; blue points: optimised snake nodes, yellow arrow: largest error.

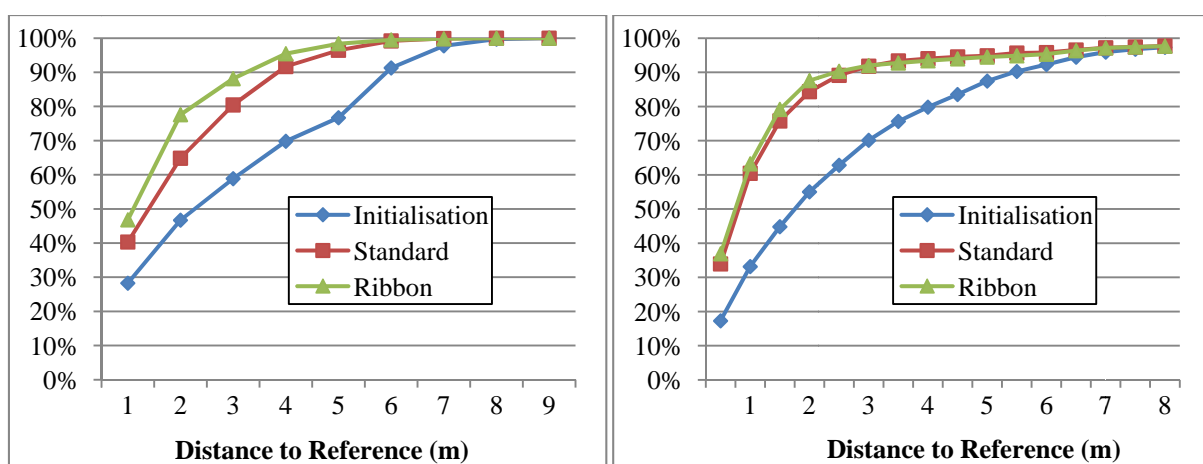


Figure 37. Cumulative histogram of the orthogonal point-to-line distances of the snake nodes from the reference: left: test site 3a; right: test site 4.

Test site 3b

The results for the test site 3b, a mountainous test site in Emmental, which covers an area of 500 x 500 m², are depicted in Fig. 38. Besides a very rough terrain, considerable differences between the initial vector and the ALS data of up to 13 m can be observed. The image energy was only based on the standard deviation of the DTM. For lack of orthophotos reliable ground truth could not be generated, but a visual inspection of Fig. 38 indicates a successful adaptation of the road network. After the optimisation, the borderlines coincide with the ALS features, and the nodes representing the centre line cover smooth and horizontal DTM areas (e.g., yellow arrow in Fig. 38).

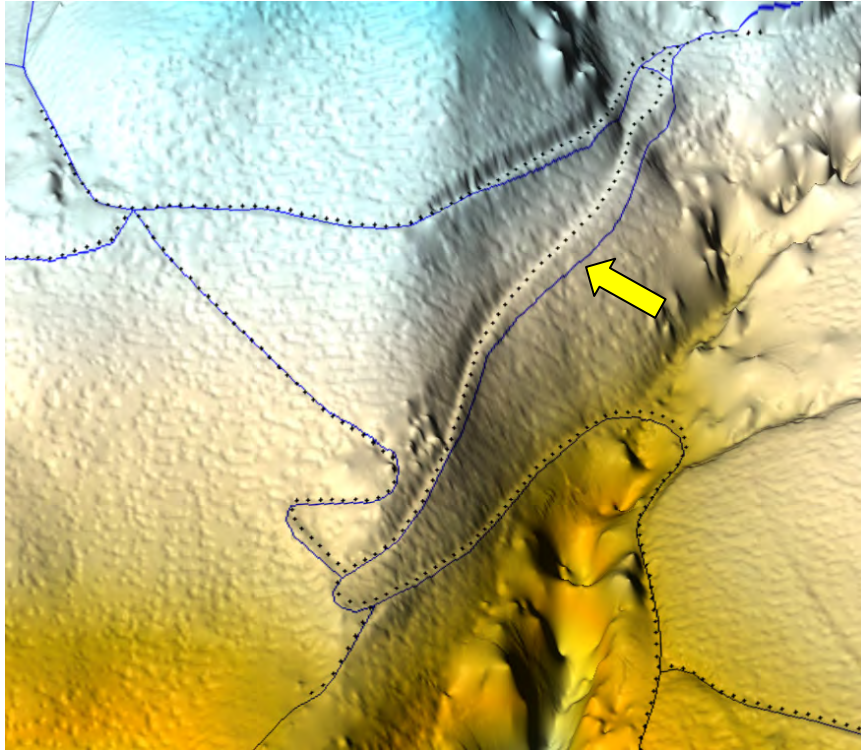


Figure 38. Test site 3b (data set Emmental, mountainous): background: shaded and colour-coded DTM; blue lines: initialisation; black dots: optimised snake nodes; yellow arrow: significant quality improvement (difference: 13 m)

Test site 4

For the test site 4 (Fig. 39, data set Vaihingen, urban and vineyards), the initialisation was not taken from one of the NMA, but from OpenStreetMap. The quality of the roads is very inhomogeneous due to the patch-work character of this data base. Roads of high quality are adjacent to roads with low accuracy. Thus, the initial geometry of the network strongly suffers. Therefore, the setting of the parameters ($\alpha = \beta = 2$, $\kappa_i = 15$) is changed for this case in order to weight the ALS features higher. This example shows how the rigid shape model supports the interpretation of the weights and thus facilitates a well balanced setting: The weights for the internal and image energy can be directly related to the two input data sets, whereas the original term of the internal energy attaches weights to a generic model of smoothness.



Figure 39. Test site 4 (data set Vaihingen, urban and rural): green: reference centre line; blue: initialisation; red dots: optimised snake nodes (central nodes of the ribbon); black rectangles: details in Figs. 40 and 41



Figure 40. Details of test site 4: two images on the left: without building energy; two images on the right: with building energy (blue line: initialisation; red line: final position; green line: reference centerline; circles: errors detected by the internal evaluation (green: first detector; blue: second detector) ; crosses: image energy lower (green) or higher (red) than the mean value)

The test site 4 covers an area of $1000 \times 600 \text{ m}^2$. For this test area, all terms of the image energy including features of terrain slope, ALS intensity, building outlines as well as bridges could be used. The overall R.M.S. of the orthogonal point-to-line distances with respect to the reference decreases from 3.4 m for the initialisation to 2.6 m for the standard network snake without building energy, to 2.2 m for the standard network snake with building energy, and to 2.3 m for the ribbon extension with building energy, considering all of the 1782 centre line nodes (Table 22). The ribbon extension performed slightly worse, probably because of the high amount of large errors in the initialisation. The ribbon width is an additional free parameter and sometimes hampers the detection of the correct minimum in these cases. Only 33% and

55% of the initial nodes are situated within a distance of 1 m and 2 m from the reference, respectively. These values increase to 58% and 82% for the standard snake without buildings (not shown in Fig. 37 right), to 60% and 86% for the standard snake with buildings, and to 64% and 88% for the ribbon extension (cf. Fig. 37 right). The ribbon model again performed best in the intervals of high quality. The building energy supports the optimisation in case of poor initialisation (Fig. 40). Nevertheless, wrong contour parts generated by the image energy without considering the building outlines could be well detected by the proposed internal evaluation. The nodes with the maximum distances to the reference both in the initialisation and after optimisation belong to a contour part located at a dead road end (black circle in Fig. 16 – section 3.7). However, many of these nodes could be also detected by the internal evaluation (black circle in Fig. 17 – section 3.7). In general, the algorithm performed well also for this test site. However, some problems occur due to the low quality of the initial shape of the GIS data (Fig. 41). One poorly initialised road segment is located between two more or less accurate road parts. The algorithm is not able to stretch and compress the node distances for the corresponding road segments due to the low elasticity (relatively high weight of α). The original formulation of the internal energy would not be able to fix this problem either. Indeed, the compression of one road segment would be easier on the one hand, but on the other hand the stretch of the other road segment would be much more difficult. In order to achieve better results for this part of the road network, the elasticity has to be increased (smaller values for α) for both object models. Of course, this would affect the optimisation result of other network parts if a global setup is applied. The internal evaluation recognises again some nodes of the inaccurate contour part (Fig. 41 right). A quantitative analysis of the internal evaluation is carried out in the next section.

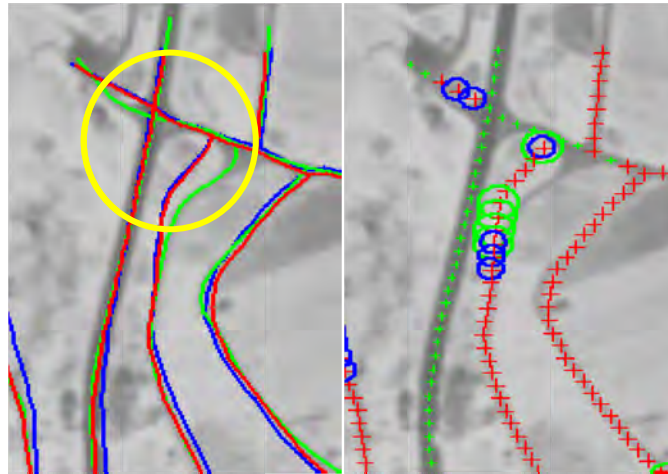


Figure 41. Detail of test site 4: problems with the initial shape (relative accuracy) of the OpenStreetMap data (left: blue: initialisation; red: final position; green: reference center line; yellow circle: wrong shape of the initial contour); (right: circles: errors detected by the internal evaluation; crosses: image energy lower (green) or higher (red) than the mean value)

4.2.5 Internal evaluation

The experiments of test site 4 have already shown some visual results of the two error detectors of the proposed internal evaluation. In this section the effect of these detectors is analysed on the small road network from section 4.2.1 (test site 1a) for a rotated initialisation (0.05 rad) and a shifted initialisation (-10 m; -10 m). The results are depicted in Fig. 42. The graphs at the bottom of this figure show the evaluation results for the two examples. The green graph illustrates the cumulative histogram of the orthogonal point-to-line distances of the snake nodes from the reference for contour parts that are detected as errors.

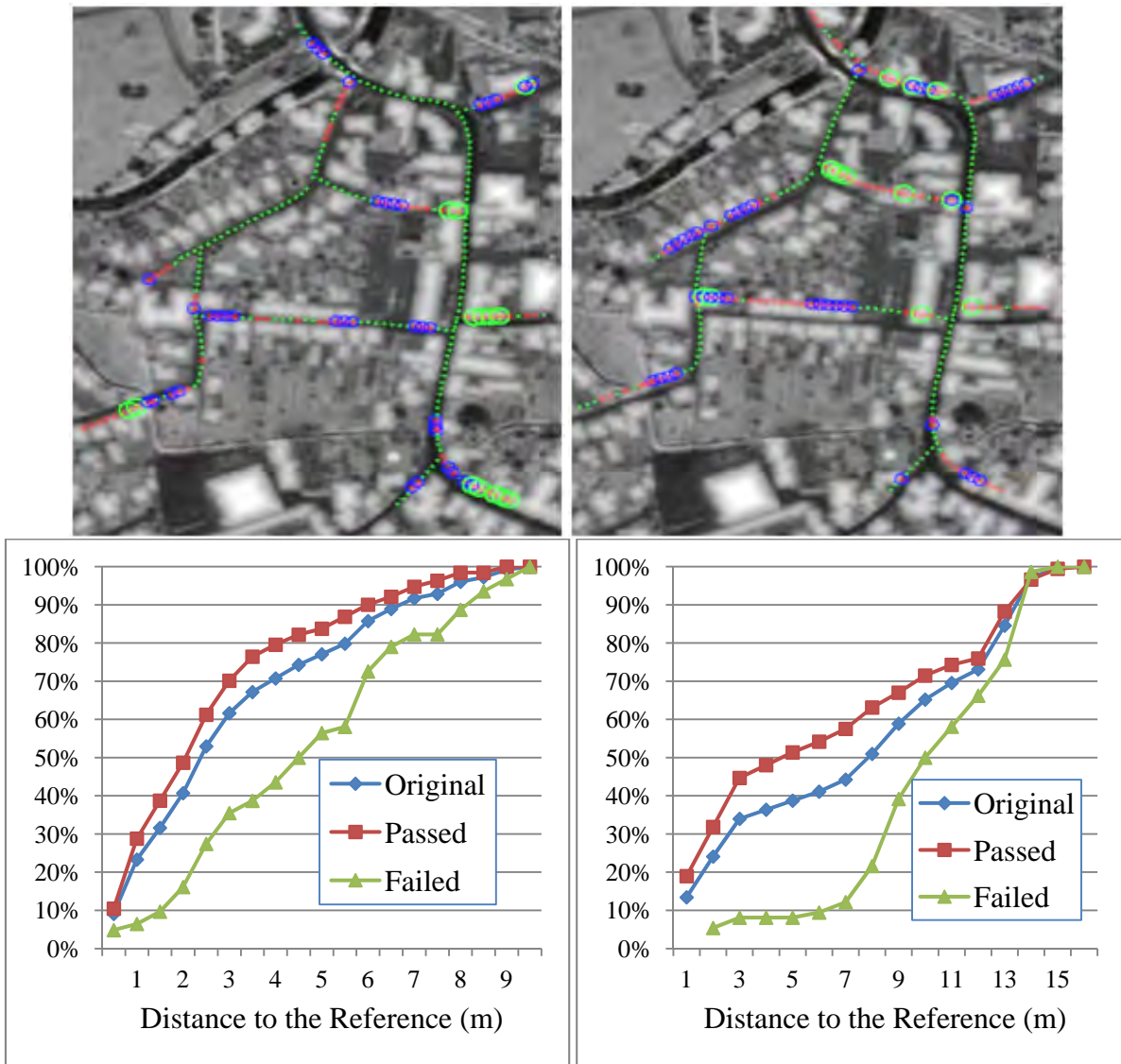


Figure 42. Error detection using the example from section 4.2.1; top: the green and blue circles are the output of the internal evaluation (green circles: first detector; blue circles: second detector, dots: image energy lower (green) or higher (red) than the mean value); bottom: cumulative histogram of the orthogonal point-to-line distances of the snake nodes from the reference; left: rotated initialisation (0.05 rad); right: shifted initialisation (-10 m; -10 m)

For the rotated initialisation 62 nodes and for the shifted initialisation 74 nodes (entire network: 253) were detected. As mentioned in section 3.7 the second detector is primarily able to detect those nodes that mark the point where the snake leaves the object boundaries. Unfortunately, these nodes do not have the largest errors in the network. However, they indicate the beginning and the end of the erroneous contour part and are thus useful for manual post-processing. The detected nodes in the graphs of Fig. 42 show a good characteristic for the shifted initialisation. Many nodes with large errors are detected while preserving the nodes of high quality. The detectors performed worse for the rotated initialisation on the left side of the figure, but the accuracy characteristic of the preserved nodes is significantly increased (red graph in comparison to the blue graph).

Generally, the proposed internal evaluation relies on the analysis of the image energy. Therefore, snake nodes in wrong local minima of the image energy, which have usually the largest errors, could not be reliably detected. For these nodes other indicators have to be derived from the algorithm in order to detect outliers fully automatically. However, the detection of the beginning and the end of inaccurate contour parts provides valuable information for the user.

4.3 Test of the adaptation of rivers

4.3.1 Evaluation of river networks

In this section two smaller networks of ditches and small rivers are optimised in order to show the transferability of the method to other linear GIS objects. For this purpose the parameter setup of the larger road networks provided by the NMA are used ($\alpha = \beta = 15$, $\kappa_i = 5$). The first network (test site 2b - Fig. 44 left) is located in the data set of Oldenburg and covers an area of $750 \times 1200 \text{ m}^2$, whereas the second network (test site 1c - Fig. 44 right) is situated in the data set of Kellinghusen and covers an area of $1200 \times 800 \text{ m}^2$. Fig. 43 depicts a detail with inconsistencies between the ATKIS vector data and the Orthophoto close to the city of Oldenburg. The results of both networks are illustrated in Fig. 45 and Table 23. In general the accuracy is comparable to the results of the ATKIS road networks. The R.M.S. error could be reduced by 0.7 m and 0.5 m, respectively. The cumulative histogram in Fig. 45 shows for the first river network that 47% and 72% of the initial nodes are situated within a distance of 1 m and 2 m from the reference, respectively. These values increase to 76% and 90% for the standard snake and to 79% and 93% for the ribbon extension. For the second river network a considerable improvement can be observed as well. The values mentioned above increase from 56% and 86% for the initialisation to 81% and 100% for the standard snake and 87% and 100% for the ribbon extension. A good initialisation and suitable ALS features in the DTM as well as in the intensity data support the optimisation process in an optimal manner. The ribbon snake model slightly outperforms the standard snake. For the first example, larger errors could be observed due to disturbed intensity values under trees. In general, the optimisation of the two river networks in this section illustrates that the proposed object model performs well also for other network objects. The transferability is achieved only by slightly modifying the image energy.

In Tables 24 and 25 the influence of the different image energy parts are depicted. The significance of the intensity values alone is not sufficient in order to adapt the river networks, whereas suitable results can be obtained for the DTM. By combining the two data sources the quality of the results can be further improved in comparison to the exclusive use of the height information.



Figure 43. Errors in the GIS river network (test site 2b - detail); background: orthophoto; yellow: ATKIS data



Figure 44. River network and DTM of test site 2b (left); river network and DTM of test site 1c (right) (different scales).

	Test site 2b (384 nodes)			Test site 1c (538 nodes)		
	init	std.	rb.	init	std.	rb.
R.M.S. error (m)	1.75	1.04	1.01	1.38	0.79	0.71
Max. error (m)	3.86	3.00	3.50	3.82	2.16	1.88

Table 23. Evaluation of the results of the two river networks using the standard and ribbon model.

std.	Test site 2b (384 nodes)			Test site 1c (538 nodes)		
	All	DTM	Intensity	All	DTM	Intensity
R.M.S. error (m)	1.04	1.12	1.87	0.79	0.80	1.15
Max. error (m)	3.00	3.93	4.92	2.16	2.43	4.98

Table 24. Evaluation of the results of the two river networks using the standard model and different image energies.

rb.	Test site 2b (384 nodes)			Test site 1c (538 nodes)		
	All	DTM	Intensity	All	DTM	Intensity
R.M.S. error (m)	1.01	1.18	1.79	0.71	0.71	0.84
Max. error (m)	3.50	4.14	5.00	1.88	1.91	2.05

Table 25. Evaluation of the results of the two river networks using the ribbon model and different image energies.

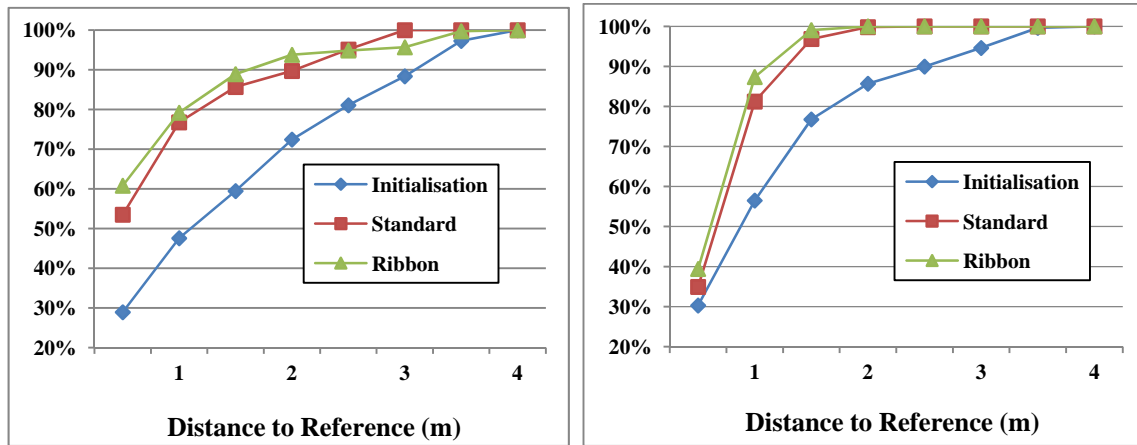


Figure 45. Cumulative histogram of the orthogonal point-to-line distances of the snake nodes to the reference: left: test site 2b; right: test site 1c

4.3.2 Evaluation of the twin snake strategy for broader rivers

In this section the applicability of the twin snake strategy is evaluated for broader rivers. First, the effects of the three constraint energies are qualitatively illustrated using a small river part of test site 1d (data set Kellinghusen) and simulated initialisations. In the second part of this section, larger segments of broader rivers in test site 1d are optimised. In order to highlight the ability of the method to deal with poor initialisations, the original ATKIS data shifted by different values are used. For all experiments the original internal energy is applied. Although this section emphasizes that the proposed constraint energies have also a geometry stabilising effect during the optimisation, some errors caused by the changed shape of the contour show that the integration of the rigid snake model would be advantageous also for this strategy. In the last experiment the influence of different image energies on the quality of the optimisation results is analysed. In this context, the image energy is designed using the DSM or the DTM in order to demonstrate the differences.

4.3.2.1 Effects of the constraint energy terms

The first four experiments in this section emphasize the advantages of the constraint energy terms. For that reason, a higher weight is assigned to the respective constraint and the initialisation is manually changed in order to highlight the different effects (cf. Table 26). The parameters were determined empirically.

The example in Fig. 46a visualises the behaviour of the original pair of snakes without constraints, i.e. they evolve independently. If the initialisation is situated close to the desired edge (upper part of the left snake), the snake moves to the river borderlines. However, with a poor initialisation either the influence range of the image energy is too small to

attract the contour (lower part of the left snake) or other edges along the river disturb the final position of the snake (right snake). This problem is tackled by integrating the three constraint energy terms.

Figs.	α	β	κ_i	κ_{Twin}	κ_{Flow}	$\kappa_{Gradient}$
46a	0.1	1	2	0	0	0
46b	0.1	1	2	0.2	5	0.02
46c	0.1	1	2	0.1	40	0.02
46d	0.1	1	2	0.1	5	0.05

Table 26. Weights for the energy terms used for Fig. 46.

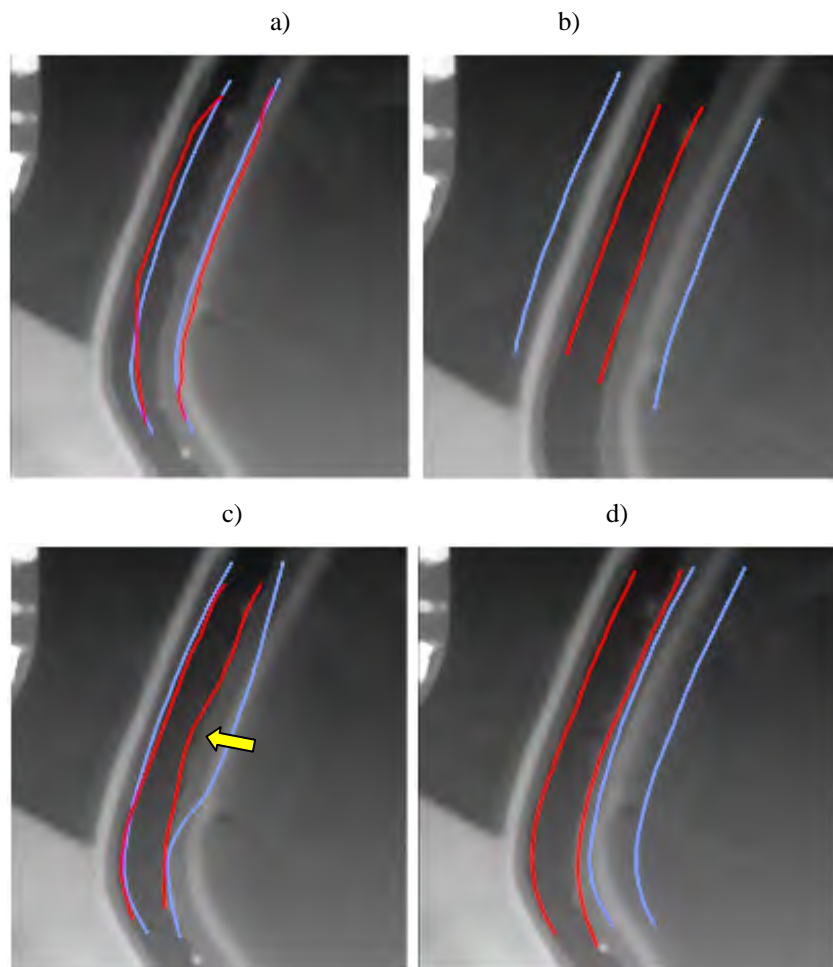


Figure 46. Initialisation scenarios for the different constraints (background: DSM; blue: initialisation; red: final solution): a) without constraints; b) high weights for twin snakes c) high weights for flow direction; d) high weights for gradient direction.

In Fig. 46b, the advantages of the twin energy are highlighted. The distance of the initial borderlines is too large, but the approximate river width is known. This information is exploited by the twin energy term. In this case the two snakes are attracted by this part of the energy functional until the range of influence of the image energy is reached. Using actual ATKIS data the assumption is made that the river width is nearly correct and can be used as the predefined distance between the two snakes. With the twin energy the two contours support each other on their way to a suitable result.

Fig. 46c shows the effect of the integration of the flow direction in the method. If some parts of the snake have already reached the river borderline, the other nodes in the vicinity are attracted by this force from the surrounding terrain to the lower river region. Due to the high weight for this energy in the experiment for Fig. 46c and the disturbances caused by shrubs, which hide the true river borderline in the DSM, the nodes in the middle of the right snake move to the centre of the river (yellow arrow). The vegetation hampers the fulfillment of the flow direction constraint.

Using the gradient direction information (Fig. 46d) helps to deal with poor initialization. The snakes are able to jump across several wrong edges in the image energy. This additional energy extends the range of the influence of the suitable edges similar to approaches modifying the image energy based on a distance transformation (gradient vector flow by Xu & Prince, 1997).

4.3.2.2 Evaluation of larger river segments

Fig. 47 depicts the adaptation of river borderlines with different initialisations to show the robustness of the method. Both examples belong to the Kellinghusen data set. The empirical weights for the different energy terms of these examples are shown in Table 27. The algorithm can adapt the 2D vector data, systematically shifted in x-direction by 10 m (Fig. 47a) and 15 m, to the ALS information. Even vegetation and the bridge in the middle of the image do not significantly influence the result. However, if the vector data are shifted by 20 m (Fig. 47b) some parts of the snakes do not reach the correct position any more. These problems (yellow arrows) occur at both ends of the snakes, in areas of strong curvature, and in the vicinity of vegetation and the bridge, where the lack of suitable image energy affects the outcome of the algorithm. For the areas with strong curvature the use of the rigid snake model could help. For evaluation purposes, the R.M.S. errors of the nodes with respect to the reference are calculated (Table 28). In case of a 10 m and 15 m shift the errors are smaller than 1.5 m for the left snake and 3 m for the right snake. The poorer result of the right snake is caused by the systematic shift of the initialisation. The entire right snake has to cross the river embankments with several edges in order to move to the correct position. The constraint energy terms are attenuated while approaching the desired edge and the snake is sometimes caught in a local minimum related to another edge from the river borderline. Therefore, it is assumed that the algorithm is able to solve random errors of the ATKIS data significantly better, which sometimes cross the correct position.

α	β	κ_i	κ_{Twin}	κ_{Flow}	$\kappa_{Gradient}$
0.16	1.2	3	0.2	10	0.05

Table 27. Weights for the energy terms used for Figs. 47 and 48.

		shift: 10 m		shift: 15 m		shift: 20 m	
		left	right	left	right	left	right
R.M.S.	init	8.90	8.95	13.34	13.42	17.77	17.88
error (m)	std.	1.15	2.48	1.23	2.67	3.40	3.31

Table 28: Evaluation of the results in Fig. 47 (left snake: 124 nodes; right snake: 120 nodes)

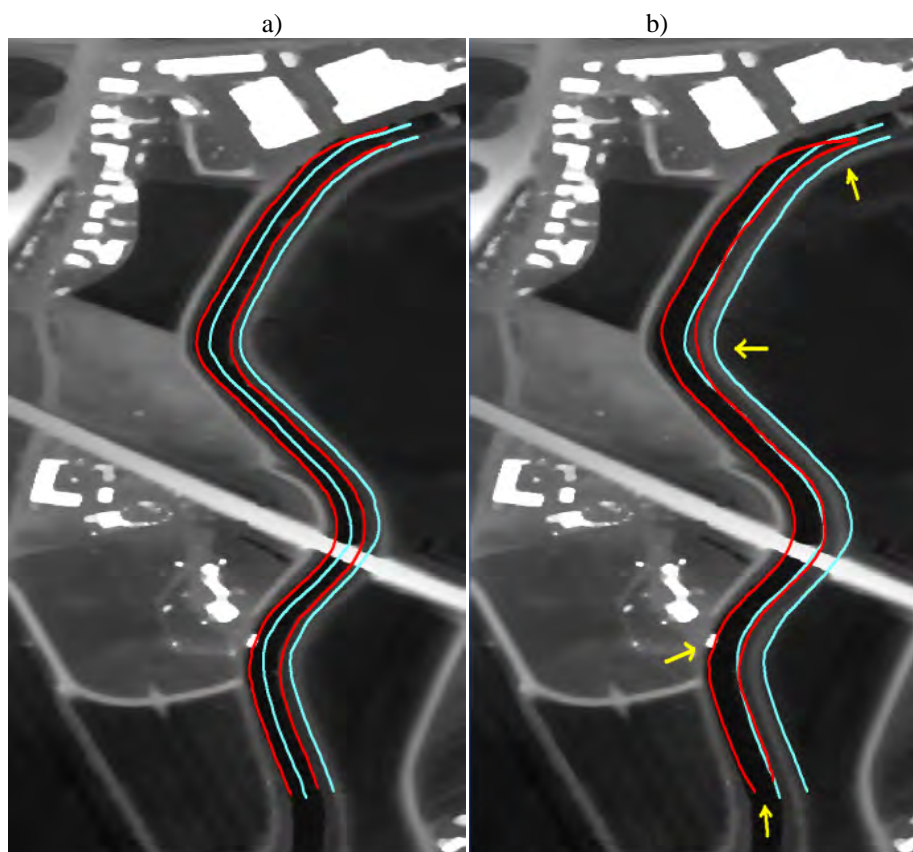


Figure 47. Adapted river with different initialisation (light blue: initialisation; red: final solution)

a) x -shift: 10 m b) x -shift: 20 m

The method was applied to a second example without changing the parameter settings (Fig. 48 and Table 29). The initialisation was shifted by 10 m in y -direction. The DSM is strongly influenced by vegetation (Fig. 48a). Tree branches hanging across the river generate strong edges in the image energy (yellow arrows). Without adapting the parameters of the snake the constraint energy terms are not able to release the upper snake from the related minima. By using the DTM the snakes move to a suitable solution comparable to the first example without changing the parameters (Fig. 48b). However, once more the systematic shift affects the snake in the shift direction (in this example the lower snake) more than the other. In summary, the accuracy achieved is not entirely satisfying yet for the snake that is initialised to be furthest away from the river.

		DSM		DTM	
		upper	lower	upper	lower
R.M.S.	init	8.16	8.13	8.16	8.13
error (m)	std.	3.01	2.53	1.04	2.42

Table 29: Evaluation of the results in Fig. 48 (upper snake: 101 nodes; lower snake: 104 nodes)

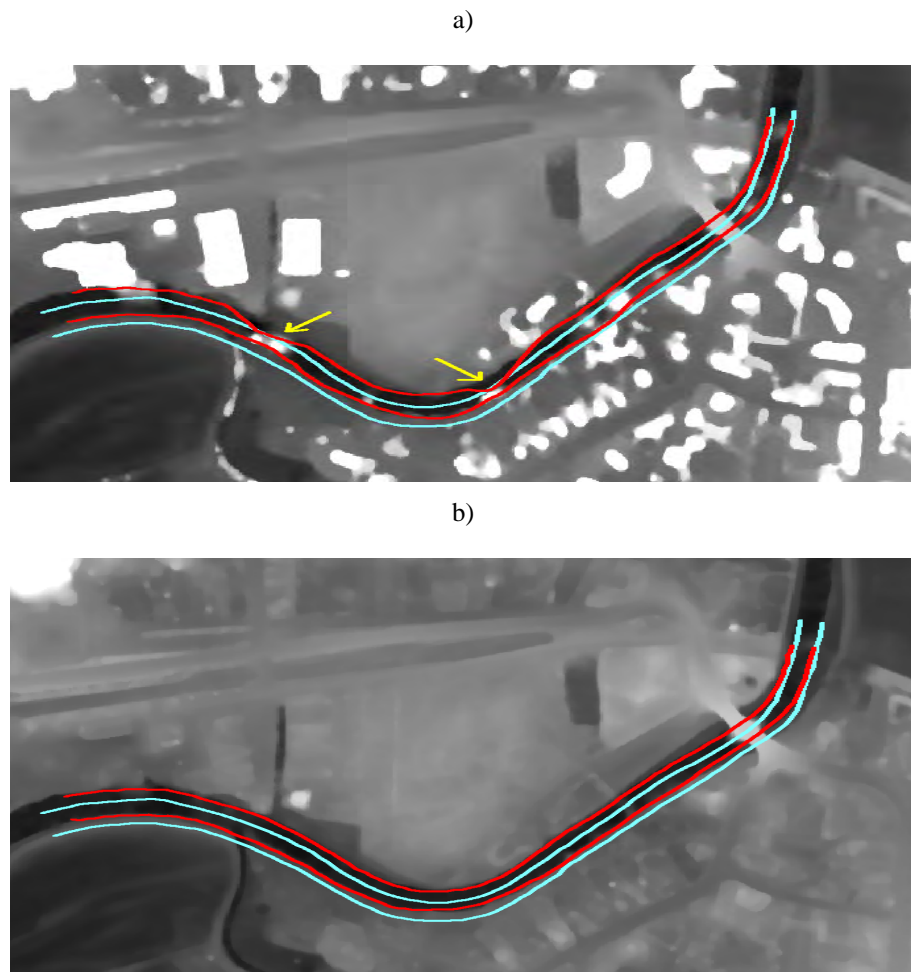


Figure 48. Adapted river with 10 m y-shift using unfiltered (a) and filtered (b) ALS data (light blue: initialisation; red: final solution)

5 Conclusion and outlook

This thesis presents a new approach for the adaptation of objects taken from a GIS databases to ALS features by means of active contours (snakes). Two different strategies are proposed. One is focused on networks of roads and small rivers, which are represented by their centre lines in the GIS data base. The other is designed for broader rivers having a region-based description. For both strategies the road and river objects can be extracted from the vector data of a GIS data base. They are then used to initialise the snakes, defining their topology and their internal energy, whereas ALS features exert external forces to the snake via the image energy. After the optimisation process the shapes and positions of the snakes should coincide with the ALS features.

The first strategy adapts the centre lines of linear GIS objects by applying the concept of network snakes. However, these centre lines are usually not well represented by the ALS features. Therefore, a new approach is proposed that allows to model networks having ribbon-like characteristics. This approach considers the topology as well as cross section information. Experiments illustrate that this concept increases the accuracy of the matched centre lines if the snake is already located between the object outlines. Further tests also highlight the generally faster convergence of the algorithm by using this extension.

An additional problem arises from the fact that the significance of the ALS features strongly varies for larger networks. For instance, these features are affected by the general slope of the terrain in the neighbourhood of the objects and by the reflection properties of different surface materials. Thus, a balanced weighting between the internal energy of the basic snake model and the image energy is hard to find even for small networks. Therefore, the new method combines the network snake approach with another concept, the rigid snake model, that redefines the internal energy and thus the geometrical model of the snake in order to prevent changes in shape or position not caused by significant features in the sensor data. For that purpose the initial shape is utilized creating template-like snakes with the ability of local adaptation. The proposed unified snake model benefits from the topology as well as from the initial shape of the GIS data. Examples using shifted and rotated initialisations demonstrate that this aspect improves the ability of the approach to deal with systematic errors. Furthermore, this combination significantly increases the robustness with respect to a change of the parameter setting. Experiments result in an accurate solution for a wide range of weights for the internal and the image energy. The rigid snake model also supports the transparency of the weights given the quality of the input data.

Due to the rigid geometry the position of contour nodes can be easily compared for the initialisation and the final solution providing suitable shift vectors. For instance, these vectors can be used in order to correct adjacent GIS objects by rubber sheeting algorithms.

The properties of the used ALS data sets including accuracies, point densities, and the availability of intensity information affect the generation of the proposed image energy as well as the adaptation results. However, even with a minimal configuration of the ALS data (DTM only), a considerable improvement of the registration accuracy can be achieved. The main reason for that is the applied object model that combines the advantages of several concepts with respect to active contours so that they support each other. Furthermore, the object model for linear networks is robust enough so that the method can be easily transferred from road to river objects by only slightly changing the definition of the image energy.

In addition to ALS features of the considered objects, context information, such as the outlines of bridges and buildings detected in the ALS data, is introduced as a new component of the image energy to support the optimisation process. This context information improves the ability of the method to deal with poor initialisation. However, if several segments of different roads in the network are initialised on the wrong side of the buildings, the snake will not be able to overcome the local energy maxima caused by the proposed building energy.

The main drawback of the modifications of the snake approach results from the increased dependency on the initialisation, i.e. on the quality of the GIS data. In general, active contour models strongly depend on an initialisation that is close to the corresponding image features. The proposed approach additionally relies on the initial shape of the vector data. However, the geometric quality of the GIS data is assumed to be sufficient for this kind of strategy. Experiments demonstrate that this statement is correct for the German ATKIS data base. Tests with OpenStreetMap roads show that the method sometimes suffers from a poor initial geometry. However, the proposed internal evaluation is able to detect several erroneous contour parts that are caused by the initial shape. It can also guide the operator while checking the optimisation result.

The second strategy adapts larger rivers based on a twin snake approach. This method is focused on the modelling of object knowledge by constraint energies. Whereas the network snake strategy primarily integrates the object knowledge via the internal energy, the constraint energy terms for larger rivers are able to establish similar snake properties. In this context, the twin constraint introduces a parameter for the object width similar to the ribbon approach. Furthermore, one twin partner, which is fixed during the optimisation of the other, acts as a supporting polygon stabilising the initial shape. However, experiments show that the initial shape will be lost step by step if the initialisation is very inaccurate and the algorithm thus takes many iterations for convergence. This aspect is caused by the original formulation of the internal energy, which slightly smoothes both twin partners despite the twin constraint. Therefore, the rigid shape model should also be integrated into this strategy and analysed in further research. Other semantic properties of rivers, such as the flow direction and the DTM gradients at the embankment, are also modelled by constraints. The latter represents one possibility in order to incorporate matching components into the snake algorithm if the extraction of suitable features from the DTM is feasible.

Besides a general improvement of the accuracy of topographic databases, the proposed method is able to assist other algorithms. For example, approaches for 3D road reconstruction, which use height and GIS data, can often cope with a slight misregistration, but fail in the presence of larger differences. Thus, our proposed method can be a suitable pre-processing step for these algorithms.

Due to cost efficiency reasons the NMAs more and more proceed to the generation of DSM and DTM from their periodically acquired optical image data. Therefore, the integration of these data in the adaptation process is the next logical extension of the algorithm. On the one hand the optical images provide much more spectral information than the ALS intensity values. On the other hand more sophisticated feature extraction or pre-processing steps for the generation of the image energy is necessary due to for instance shadow areas caused by the use of passive sensors.

In addition to buildings and bridges, trees also provide valuable context information for the adaptation process of roads and rivers, which have not yet been considered. In different experiments, trees and other vegetated areas disturb the design of the image energy. For example, trees are often extracted as buildings if ALS data is the only source (NDVI not

available). In this case the trees are treated as forbidden areas for roads and rivers by the algorithm. Considering tree branches hanging across roads and rivers, this assumption is not correct in every situation. Thus, the explicit modelling of trees in the image energy may further improve the quality of the results.

In this work the parameter setting is fixed during the optimisation process. However, different strategies are possibly able to improve the results. For instance, starting with a small viscosity parameter the algorithm can jump over wrong local minima and maxima in the image energy in case of a poor initialisation, whereas a high viscosity at the end of the process enables the method to exactly detect the minimum. Another possible strategy exploits a change of the weights for the rigid snake model. Systematic errors can be minimised by a very rigid geometry at the beginning, whereas a smaller internal energy allows a good adaptation to the ALS features at the end of the process. Furthermore, the shape can be reinitialised after a few iterations resulting in a slightly different object model.

The current internal evaluation analyses the internal energy as well as the entire image energy for each snake node in order to detect inaccurate contour parts after the optimisation process. A starting point for further research in that topic is the analysis of the individual components of the image energy, i.e. the individual data sets derived from the ALS information. In this sense the DTM slopes or confidence values of the extraction results of bridges and buildings can be exploited. Furthermore, the ribbon width contains valuable information similar to twin snake distances. Prior knowledge can be compared to the final values of this parameter after the optimisation for the detection of unsuitable local minima in the image data.

Another idea for the internal evaluation exploits the ability of the rigid shape model to cope with shifted initialisations. In this context the original GIS data can be shifted in two or more different directions by a few meters. Subsequently, these data sets are used as initialisations that can be separately optimised and the results are compared. Corresponding contour parts in different data sets that do not detect the same local minimum should be further analysed by the operator.

The proposed new method is an important contribution for a consistent modelling of 2D GIS data and the corresponding terrain heights. However, other objects classes with corresponding features in the DTM have to be considered in the adaptation process in order to provide a dense net of shift vectors.

References

- Abdelguerfi, M., Cooper, E., Wynne, C., Shaw, K. (1997). An Extended Vector Product Format (EVPF) suitable for the Representation of Three-dimensional Elevation in Terrain Databases. *International Journal of Geographical Information Science*, Vol. 11 (7), pp. 649-676.
- AdV (2011). ATKIS-Objektartenkatalog. <http://www.atkis.de> (2011/05/30).
- Ahokas, E., Kaartinen, H., Hyypä, J. (2003). A Quality Assessment of Airborne Laser Scanner Data. *International Archives of Photogrammetry, Remote Sensing and Spatial Information Sciences*, Vol. 34 (Part 3/W13), pp. 1-7.
- Alt, H., Godau, M., (1995). Computing the Fréchet Distance between two Polygonal Curves. *International Journal of Computational Geometry and Applications*, Vol. 5 (1/2), pp. 75–91.
- Alharthy, A., Bethel, J., (2003). Automated Road Extraction from Lidar Data. *Proceedings of the ASPRS Annual Conference*, Anchorage, Alaska, unpaginated CD-Rom.
- Axelsson, P. (1999). Processing of Laser Scanner Data - Algorithms and Applications. *ISPRS Journal of Photogrammetry and Remote Sensing*, Vol. 54 (2–3), pp. 138–147.
- Amini, A. A., Tehrani, S., Weymouth, T. E. (1988). Using Dynamic Programming for Minimizing the Energy of Active Contours in the Presence of Hard Constraints. *Proceedings of the 2nd International Conference on Computer Vision*, Dec. 5-8, IEEE Computer Society, Washington, DC., USA, pp. 95-99.
- Baltsavias, E. (1999). Airborne Laser Scanning: Basic Relations and Formulas. *ISPRS Journal of Photogrammetry and Remote Sensing*, Vol. 54 (2-3), pp. 199-214.
- Bartelme, N. (2005). *Geoinformatik*. Springer, Berlin, 4. Ed.
- Besl, P., McKay, N. (1992). A method for registration of 3-D shapes. *IEEE Transactions on Pattern Analysis and Machine Intelligence*, Vol. 14 (2), pp. 239-256.
- Blake, A., Isard, M. (1998). *Active Contours*. Springer, Berlin Heidelberg New York, 351 p.
- Borkowski, A. (2004). *Modellierung von Oberflächen mit Diskontinuitäten*. Habilitation, TU Dresden, Germany, 91p.
- Bremer, M., Liebig, W., Proessler, S. (1992). Einrichtung des ATKIS-DLM25/1 in Niedersachsen. *Nachrichten der Niedersächsischen Vermessungs- und Katasterverwaltung*, 42.Jahrg., Heft 3, pp. 134-157.
- Brenner, C. (2000). *Dreidimensionale Gebäuderekonstruktion aus digitalen Oberflächenmodellen und Grundrissen*. PhD-thesis, Deutsche Geodätische Kommission, Series C, Vol. 530.
- Briese, C. (2004). *Breakline Modelling from Airborne Laser Scanner Data*. PhD-thesis, TU Wien, Austria, 67p.
- Brockmann H., Mandlbürger G. (2001). Aufbau eines Digitalen Geländemodells vom Wasserlauf der Grenzoder. *Publikationen der Deutschen Gesellschaft für Photogrammetrie, Fernerkundung und Geoinformationen*, Vol. 10, pp. 199–208.

- Brovelli, M. A., Cannata, M., Longoni, U. M. (2002). Managing and Processing LIDAR Data within GRASS. Proc. GRASS Users Conference, Trento, Italy, 11–13 September, University of Trento, Italy, 29 pp.
- Brügelmann, R. (2000). Automatic Breakline Detection from Airborne Laser Range Data. *International Archives of Photogrammetry, Remote Sensing and Spatial Information Sciences*, Vol. 33 (Part B3), Amsterdam, Netherlands, pp. 109-115.
- Brzank, A. (2001). Automatische Ableitung von Bruchlinien aus Laserscannerdaten. Master thesis, TU Dresden, Germany, 86 p.
- Brzank, A., Lohmann, P. (2004). Steigerung der Genauigkeit von Digitalen Geländemodellen im Küstenbereich aus Laserscannermessungen. *Publikationen der Deutschen Gesellschaft für Photogrammetrie, Fernerkundung und Geoinformation*, Vol. 13, pp. 203-210.
- Brzank, A., Heipke, C., Göpfert, J., Soergel, U. (2008). Aspects of Generating Precise Digital Terrain Models in the Wadden Sea from Lidar – Water Classification and Structure Line Extraction. *ISPRS Journal of Photogrammetry and Remote Sensing*. Vol. 63 (5), pp. 510-528.
- Burghardt, D., Meier, S. (1997). Cartographic Displacement Using the Snake Concept. In: Förstner, Plümer (eds.), *Semantic Modeling for the Acquisition of Topographic Information from Images and Maps*, Basel, Birkhäuser Verlag, pp. 59-71.
- Butenuth, M. (2008). Network Snakes. PhD-thesis. Deutsche Geodätische Kommission, Series C, Vol. 620, 104p.
- Butenuth, M., Heipke, C. (2011). Network Snakes: Graph-Based Object Delineation with Active Contour Models. *Machine Vision and Applications*, DOI 10.1007/s00138-010-0294-8, in press.
- Canny, J. (1986). A Computational Approach to Edge Detection. *IEEE Transactions on Pattern Analysis and Machine Intelligence*, PAMI-8, Vol. 6, pp. 679-698.
- Caselles, V., Kimmel, R., Sapiro, G. (1997). Geodesic Active Contours. *International Journal of Computer Vision*, Vol. 22 (1), pp. 61-79.
- Clode, S., Rottensteiner, F., Kootsookos, P. (2005). Improving City Model Determination by Using Road Detection from LIDAR Data. *International Archives of Photogrammetry, Remote Sensing and Spatial Information Sciences*, Vol. 36 (Part 3/W24), pp. 159-164.
- Clode, S., Rottensteiner, F., Kootsookos, P., Zeiniker, E. (2007). Detection and Vectorization of Roads from Lidar Data. *Photogrammetric Engineering & Remote Sensing*, Vol. 73 (5), pp. 517-536.
- Cohen, L. D. and Cohen, I. (1993). Finite Element Methods for Active Contour Models and Balloons for 2-D and 3-D Images. *IEEE Transactions on Pattern Analysis and Machine Intelligence*, Vol. 15 (11), pp. 1131-1147.
- Cressie, N. A. (1990). The Origins of Kriging. *Mathematical Geology*, Vol. 22 (3), pp. 239-252.
- Deng, M., Chen, X., Li, Z. (2005). A Generalized Hausdorff Distance for Spatial Objects in GIS, *Proceedings of the 4th ISPRS Workshop on Dynamic and Multi-dimensional GIS*, pp. 10-15.

- Devogele, T., Parent, C. Spaccapietra S. (1998). On Spatial Database Integration, *International Journal of Geographical Information Science*, Vol. 12 (4), pp. 335–352.
- Duchon, J. (1976). Interpolation des Fonctions de Deux Variables Suivant le Principe de la Flexion des Plaques Minces. *RAIRO Analyse Numerique* Vol. 10 (12), pp. 5–12.
- Fritsch, D., Pfannenstein, A. (1992). Conceptual Models for Efficient DTM Integration into GIS. *Proceedings EGIS'92. Third European Conference and Exhibition on Geographical Information Systems*. Munich, Germany, pp. 701-710.
- Fua, P. (1995). Parametric Models are Versatile: The Case of Model Based Optimization. *International Archives of Photogrammetry and Remote Sensing*, Vol. 30 (Part III/2), pp. 828 - 833.
- Fua, P. (1996). Model-Based Optimization: Accurate and Consistent Site Modeling. *International Archives of Photogrammetry and Remote Sensing*, Vol. 31 (Part B3), pp. 222–223.
- Fua, P. (1998). Fast, Accurate and Consistent Modelling of Drainage and Surrounding Terrain. *International Journal of Computer Vision*, Vol. 26 (3), pp. 215-234.
- Fua, P, Brechbühler, C. (1996). Imposing Hard Constraints on Soft Snakes. In B. Buxton and R. Cipolla (eds.), *Proceedings 4th European Conference on Computer Vision*, Cambridge (England), Vol. 1065 of *Lecture Notes in Computer Science*, Springer-Verlag, pp. 495–506.
- Fua, P, Leclerc, Y. (1990). Model Driven Edge Detection. *Machine Vision and Applications*, Vol. 3, pp. 45–56.
- Fuchs, C., Förstner, W. (1995). Polymorphic Grouping for Image Segmentation. *Proceedings of the 5th International Conference on Computer Vision*. Cambridge, U.S.A, pp. 175-182.
- Gillman, D. W. (1985). Triangulations for Rubber-Sheeting. *Proceedings of AUTOCARTO 7*; Washington D.C., pp. 191-199.
- Gomes-Pereira, L., Wicherson, R. (1999). Suitability of Laser Data for Deriving Geographical Information – a Case Study in the Context of Management of Fluvial Zones. *ISPRS Journal of Photogrammetry and Remote Sensing*, Vol. 54 (2-3), pp. 105-114.
- Göpfert, J., Soergel, U., Brzank, A. (2008). Integration of Intensity Information and Echo Distribution in the Filtering Process of LIDAR Data in Vegetated Areas. *SilviLaser 2008*, Edinburgh, pp. 417-426.
- Göpfert, J., Rottensteiner, F. (2009). Adaptation of roads to ALS data by means of network snakes: *International Archives of Photogrammetry, Remote Sensing and Spatial Information Sciences*, Vol. 38 (Part 3/W8), pp. 24-29.
- Göpfert, J., Rottensteiner, F. (2010). Using building and bridge information for adapting roads to ALS data by means of network snakes. *International Archives of Photogrammetry, Remote Sensing and Spatial Information Sciences*, Vol. 38 (Part 3a), pp. 163-168.
- Göpfert, J., Alakese, Y., Rottensteiner, F., Heipke, C., Rosenhahn, B. (2010). Constraint energies for the adaptation of 2D river borderlines to airborne laserscanning data using snakes. *International Archives of Photogrammetry, Remote Sensing and Spatial Information Sciences*, Vol. 38 (Part 2), pp. 383-389.

- Gösseln, G. v., Sester, M. (2004). Integration of geoscientific data sets and the German digital map using a matching approach. *International Archives of Photogrammetry, Remote Sensing and Spatial Information Sciences*, Vol. 35 (Part B4), pp. 1249-1254.
- Grote, A., Heipke, C., Rottensteiner, F. (2011). Road network extraction in suburban areas. *Photogrammetric Record*, accepted May 2011, in press.
- Gruen, A., Li, H. (1997). Semi-Automatic Linear Feature Extraction by Dynamic Programming and LSB-Snakes. *Photogrammetric Engineering and Remote Sensing*, Vol. 63 (8), pp. 985-995.
- Haala, N., Brenner, C. (1999). Extraction of Buildings and Trees in Urban Environments. *ISPRS Journal of Photogrammetry and Remote Sensing*, Vol. 54 (2-3), pp. 130-137.
- Haala, N., Hastedt, H., Wolf, K., Ressel, C., Baltrusch, S. (2010). Digital Photogrammetric Camera Evaluation – Generation of Digital Elevation Models. *Photogrammetrie – Fernerkundung – Geoinformation*, Vol. 2, pp. 99-115.
- Hatger, C. (2005): On the use of airborne laser scanning data to verify and enrich road network features. *International Archives of Photogrammetry, Remote Sensing and Spatial Information Sciences*, Vol. 36 (Part3/W19), pp. 138-143.
- Hatger, C., Brenner, C., (2003). Extraction of road geometry parameters form laser scanning and existing databases. *International Archives of Photogrammetry, Remote Sensing and Spatial Information Sciences*, Vol. 34 (Part 3/W13), pp. 225-230.
- Haunert, J.-H. (2005). Link Based Conflation of Geographic Datasets. *Proceedings of 8th ICA WORKSHOP on Generalisation and Multiple Representation*, La Coruna, Spanien, published on CDROM.
- Hettwer, J. (2003). Numerische Methoden zur Homogenisierung großer Geodatenbestände. Publication of the Geodetic Institute of the Rheinisch-Westfälischen Technischen Hochschule Aachen. PhD-thesis, Aachen, Germany, 112p.
- Höfle, B., Pfeifer, N. (2007). Correction of Laser Scanning Intensity Data: Data and Model-Driven Approaches. *ISPRS Journal of Photogrammetry and Remote Sensing*, Vol. 62 (6), pp. 415-433.
- Horn, B. K. P. (1975). Obtaining Shape from Shading Information. Chapter 4 in Winston, P. H. (Ed.): *The Psychology of Computer Vision*, McGraw-Hill, New York, pp. 115-155.
- Horn, B.K.P., Bachman, B.L (1979). Using Synthetic Images to Register Real Images with Surface Models. *Communications of the A.C.M.*, Vol. 21 (11), pp. 914–924.
- Jasiobedzki, P. (1993). Adaptive Adjacency Graphs. B. C. Vemuri (eds.), *Geometric Methods in Computer Vision II.*, pp. 294-303.
- Jelalian, A. (1992). *Laser Radar Systems*. Artech House, Boston and London, 292p.
- Kager, H. (2004). Discrepancies between Overlapping Laser Scanning Strips - Simultaneous Fitting of Aerial Laser Scanner Strips. *International Archives of Photogrammetry, Remote Sensing and Spatial Information Sciences*, Vol. 35 (Part B/1), pp. 555-560.

- Kass M, Witkin A, Terzopoulos D. (1988). Snakes: Active Contour Models. *International Journal of Computer Vision*, Vol. 1 (4), pp. 321-331.
- Kerschner, M. (2001). Seam-Line Detection in Colour Orthoimage Mosaicking by Use of Twin Snakes. *ISPRS Journal of Photogrammetry and Remote Sensing*, Vol. 56 (1), pp. 53–64.
- Kerschner, M. (2003). Snakes für Aufgaben der digitalen Photogrammetrie und Topographie. PhD-thesis, IPF, Vienna University of Technology, 115p.
- Klötzer, F. (1997). Integration von triangulierten digitalen Geländemodellen und Landkarten. Diploma thesis of the Institute of Informatics, Rheinische Friedrich-Wilhelms-Universität Bonn, Germany, unpublished.
- Koch, A. (2006). Semantische Integration von zweidimensionalen GIS-Daten und Digitalen Geländemodellen. PhD-thesis, Deutsche Geodätische Kommission, Series C, Vol. 601, 97p.
- Koch, A., Heipke, C. (2006). Semantically correct 2.5D GIS data- the integration of a DTM and topographic vector data. *ISPRS Journal of Photogrammetry and Remote Sensing*, Vol. 61 (1), pp. 23-32.
- Kraus, K. (2000). Photogrammetrie – Topographische Informationssysteme, Vol. 3, Dümmler, Bonn, 437p.
- Kraus, K., Pfeifer, N. (1998). Determination of Terrain Models in Wooded Areas with Airborne Laser Scanner Data. *ISPRS Journal of Photogrammetry and Remote Sensing*, Vol. 53 (4), pp. 193-203.
- Laptev, I., Mayer, H., Lindeberg, T., Eckstein, W., Steger, C., Baumgartner, A. (2000). Automatic Extraction of Roads from Aerial Images Based on Scale Space and Snakes. *Machine Vision and Applications*, Vol. 12 (1), pp. 23-31.
- Lenk, U. (2001). 2.5D-GIS und Geobasisdaten - Integration von Höheninformation und Digitalen Situationsmodellen. PhD-thesis, Deutsche Geodätische Kommission, Series C, Vol. 546, 190p.
- Lenk, U., Heipke, C. (2006). The radial topology algorithm – a new approach for deriving 2.5D GIS data models. *Geoinformatica* 10 (4), pp. 447-468.
- Maas, H.-G. (2000). Least-Squares Matching with Airborne Laserscanning Data in a TIN Structure. *International Archives of Photogrammetry, Remote Sensing and Spatial Information Sciences*, Vol. 33 (Part 3A), pp. 548-555.
- Malladi, R., Sethian, J. A., and Vemuri, B. C. (1995). Shape Modeling with Front Propagation: A Level Set Approach. *IEEE Transactions on Pattern Analysis and Machine Intelligence*, Vol. 17 (2), pp. 158-175.
- Mallet, C., Bretar, F. (2009). Full-Waveform Topographic Lidar: State-of-the-Art. *ISPRS Journal of Photogrammetry and Remote Sensing*, Vol. 64 (1), pp. 1-16.
- Mallet, C., Bretar, F., Soergel, U. (2008). Analysis of Full-Waveform Lidar Data for Classification of Urban Areas. *Photogrammetrie – Fernerkundung – Geoinformation*, Vol. 2, pp. 337-349.
- Mandlbürger, G. (2006). Topographische Modelle für Anwendungen in Hydraulik und Hydrologie. PhD-thesis, Wien, Austria, 150p.
- Marr, D., Poggio, T. (1976). Cooperative Computation of Stereo Disparity. *Science*, Vol. 194, pp. 283-287.

- Mayer, H., Laptev, I., Baumgartner, A. (1998). Multi-Scale and Snakes for Automatic Road Extraction. Proc. Fifth European Conference on Computer Vision, Freiburg, Germany, Vol. 1406 of Lecture Notes in Computer Science, Springer Verlag, pp.720-733.
- McInerney, T. and Terzopoulos, D. (1995). Topologically Adaptable Snakes. Proceedings of the International Conference on Computer Vision, pp 840-845.
- Mustière S., Devogele T. (2008). Matching Networks with Different Levels of Detail, Geoinformatica, Springer (Publisher), Vol. 12 (4), pp. 435-453.
- Neuenschwander, W.M., Fua, P., Iverson, L., Szekely, G., Kubler, O. (1997). Ziplock Snakes. International Journal of Computer Vision, Vol. 25 (3), pp. 191-201.
- Niemeyer, J., Rottensteiner, F., Kühn, F., Soergel, U. (2010). Extraktion geologisch relevanter Strukturen auf Rügen in Laserscanner-Daten. 30th Annual scientific-technical meeting of the German Society of Photogrammetry and Remote Sensing (DGPF), Vol. 19 of the publications of the DGPF, pp. 298-307.
- Olteanu, A.-M. (2007). A multi-criteria fusion approach for geographical data matching. Proceedings of the 5th International Symposium on Spatial Data Quality (ISSDQ), Enschede, Netherlands, pp. 47-56.
- Oude Elberink, S., Vosselman, G. (2006). Adding the Third Dimension to a Topographic Database Using Airborne Laserscanning. International Archives of Photogrammetry, Remote Sensing and Spatial Information Sciences, Vol. 36 (Part 3), pp. 92-97.
- Papanikolaou K., Derenyi E. (1988). Structural Matching of Digital Images and Terrain Models. International Archives of Photogrammetry and Remote Sensing, Vol. 27 (Part B3), pp. 669 - 678
- Parent, C., Spaccapietra, S., Devogele, T. (1996). Conflicts in Spatial Database Integration. Proceedings of the 9th International Conference on Parallel and Distributed Computing Systems, PDCS '96, pp. 772-778.
- Pfeifer, N. (2007). Pleading for a European Airborne Laser Scanning - Digital Terrain Model. Main presentation EuroSDR, Brüssel.
- Pfeifer, N., Briese C. (2007). Laser Scanning - Principles and Applications. Geo-Sibir. 3rd International Scientific Conference, pp. 93 - 112.
- Polis, M. F., Gifford, S. J., Mckeown JR., D. M. (1995). Automating the Construction of Large-Scale Virtual Worlds. Computer Vol. 28 (7), pp. 57-65.
- Radeva, P., Serrat, J., Marti, E. (1995). A Snake for Model-Based Segmentation. Proceedings of the International Conference on Computer Vision (ICCV 95), Boston, MA, pp. 816-821.
- Ravanbakhsh, M. (2008). Road Junction Extraction from High Resolution Aerial Images Assisted by Topographic Database Information. PhD-thesis. Deutsche Geodätische Kommission, Series C, Vol. 621, 90p.
- Rieger, W. Kerschner, M., Reiter, T., Rottensteiner, F. (1999). Roads and Buildings from Laser Scanner Data within a Forest Enterprise. International Archives of Photogrammetry and Remote Sensing 32 (Part 3/W14), pp. 185-191.

- Roggero, M. (2001). Airborne Laser Scanning: Clustering in Raw Data. *International Archives of the Photogrammetry, Remote Sensing and Spatial Information Sciences* 34 (Part 3/W4), pp. 227-232.
- Rosen, B., Saalfeld, A. (1985). Match Criteria for Automatic Alignment. *Proceedings of the Digital Representations of Spatial Knowledge, Auto-Carto VII*, pp. 456-462.
- Rottensteiner, F., Briese, C. (2002). A New Method for Building Extraction in Urban Areas from High-Resolution Lidar Data. *International Archives of Photogrammetry, Remote Sensing and Spatial Information Sciences*, Vol. 34 (Part 3A), pp. 295-301.
- Rottensteiner, F., Trinder, J., Clode, S., Kubik, K. (2007). Building Detection by Fusion of Airborne Laserscanner Data and Multi-Spectral Images: Performance evaluation and sensitivity analysis. *ISPRS Journal for Photogrammetry and Remote Sensing*, Vol. 62 (2), pp. 135–149.
- Rousseaux, F., Bonin, O. (2003). Towards a Coherent Integration of 2D Linear Data into a DTM. *Proceedings of the 21st International Cartographic Conference (ICC)*, pp. 1936-1942.
- Russ, John C. (1995). *The Image Processing Handbook*. Boca Raton, CRC Press, 2nd Edition, 674 p.
- Saalfeld, A. (1988). Automated Map Compilation. *International Journal of Geographical Information Science*, Vol. 2 (3), pp. 217-228.
- Schenk, T. (2001). Modeling and Analyzing Systematic Errors in Airborne Laser Scanners. *Technical Notes in Photogrammetry* No. 19, Department of Civil and Environmental Engineering and Geodetic Science, The Ohio State University, Columbus, USA, 40p.
- Scholz, T. (1992). Zur Kartenhomogenisierung mit Hilfe strenger Ausgleichungsmethoden. PhD-thesis, Publication of the Geodetic Institute of the Rheinisch-Westfälischen Technischen Hochschule Aachen, Germany, Vol. 47, 137p.
- Sithole, G., Vosselman, G. (2003). Automatic Structure Detection in a Pointcloud of an Urban Landscape. *Proceedings 2nd Joint Workshop on Remote Sensing and Data Fusion over Urban Areas (Urban 2003)*, Berlin, Germany, pp. 67-71.
- Sithole, G., Vosselman, G. (2004). Experimental Comparison of Filter Algorithms for Bare-Earth Extraction from Airborne Laser Scanning Point Clouds. *ISPRS Journal of Photogrammetry and Remote Sensing*, Vol. 59 (1-2), pp. 85-101.
- Sithole, G. (2005). Segmentation and Classification of Airborne Laser Scanner Data. PhD-thesis, TU Delft, Netherlands, 146p.
- Sithole, G., Vosselman, G. (2006). Bridge Detection in Airborne Laser Scanner Data. *ISPRS Journal of Photogrammetry and Remote Sensing*, Vol. 61 (1), pp. 33-46.
- Steger, C. (1998). An Unbiased Extractor of Curvilinear Structures. *IEEE Transactions on Pattern Analysis and Machine Intelligence*, Vol. 20 (2), pp. 113-125
- Sui, L. (2002). Processing of Laser Scanner Data and Automatic Extraction of Structure Lines. *International Archives of Photogrammetry, Remote Sensing and Spatial Information Sciences*, Vol. 34 (Part 2), pp. 429-435.

- Tóvári, D., Vögtle, T. (2004). Object Classification in Laser-Scanning Data. *International Archives of Photogrammetry, Remote Sensing and Spatial Information Sciences*, Vol. 36 (Part 8/W2), pp. 45-49.
- Trinder, J. C., Maulik, U., Bandyopadhyay, S. (2000). Semiautomated Feature Extraction Using Simulated Annealing. *International Archives of the Photogrammetry, Remote Sensing and Spatial Information Sciences*, Vol. 33 (Part B3), pp. 905-911.
- Ulaby, F. T., Moore, R. K., Fung, A. K. (1982). *Microwave Remote Sensing: Active and Passive - Radar Remote Sensing and Surface Scattering and Emission Theory*, Vol. II, Artech House, Reading, Massachusetts, 609p.
- Vosselman, G. (1992): *Relational Matching*. Springer-Verlag Berlin Heidelberg, 190p.
- Vosselman, G. (2000). Slope Based Filtering of Laser Altimetry Data. *International Archives of Photogrammetry, Remote Sensing and Spatial Information Sciences*, Vol. 33 (Part B3), pp. 935-942.
- Vosselman, G. (2002). Strip Offset Estimation Using Linear Features. In *3rd International Workshop on Mapping Geo-Surfical Processes using Laser Altimetry*, Columbus, Ohio, USA.
- Wagner, W., Ullrich, A., Ducic, V., Melzer, T., Studnicka, N. (2006). Gaussian Decomposition and Calibration of a Novel Small-Footprint Full-Waveform Digitising Airborne Laser Scanner. *ISPRS Journal of Photogrammetry and Remote Sensing*, Vol. 60 (2), pp. 100-112.
- Walter, V., Fritsch, D. (1999). Matching Spatial Data Sets: a Statistical Approach. *International Journal of Geographical Information Science*, Vol. 13 (5), pp. 445-473.
- Weibel, R. (1993). On the Integration of Digital Terrain and Surface Modeling into Geographic Information Systems. *Proceedings 11th International Symposium on Computer Assisted Cartography (AUTOCARTO 11)*. Minneapolis, Minnesota, USA, pp. 257-266.
- Weidner, U., Förstner, W. (1995). Towards Automatic Building Reconstruction from High Resolution Digital Elevation Models. *ISPRS Journal of Photogrammetry and Remote Sensing*, Vol. 50 (4), pp. 38-49.
- Williams, D.J., Shah, M. (1992). A Fast Algorithm for Active Contours and Curvature Estimation. *CVGIP: Image Understanding*, Vol. 55 (1), pp. 14-26.
- Wolf, B. M., Heipke, C. (2007). Automatic Extraction and Delineation of Single Trees from Remote Sensing Data. *Machine Visions and Applications*, Vol. 18 (5), pp. 317-330.
- Xu, C, Prince, J.L., (1997). Gradient Vector Flow: A new External Force for Snakes. *Proceedings IEEE Conference on Computer Vision and Pattern Recognition*, pp. 66-71.
- Zhang, J., Goodchild, M. F. (2002). *Uncertainty in Geographical Information*. Taylor and Francis, New York.
- Zhu, P., Lu, Z., Chen, X., Honda, K., Eiumnoh, A. (2004). Extraction of City Roads through Shadow Path Reconstruction Using Laser Scanning. *Photogrammetric Engineering and Remote Sensing*, Vol. 70 (12), pp. 1433-1440.

Curriculum Vitae - Lebenslauf

Personalien:

Familienname	Göpfert
Vorname	Jens
Geburtsdatum	25.05.1977
Geburtsort	Lutherstadt Eisleben
Staatsangehörigkeit	deutsch
Familienstand	ledig

Beruflicher Werdegang:

seit 01/2005	Wissenschaftlicher Mitarbeiter am Institut für Photogrammetrie und GeoInformation, Leibniz Universität Hannover
--------------	--

Referendariat in der Vermessungsverwaltung:

10/2002 - 09/2004	Freistaat Sachsen
-------------------	-------------------

Studium:

10/1996 - 09/2002	Geodäsie an der Technischen Universität Dresden
10/2000 - 12/2000	Universität Linköping (Schweden) Mitarbeit am WITAS UAV research project

Zivildienst:

08/1995 – 08/1996	Alten- und Pflegeheim "Rudolf Breitscheid" Lutherstadt Eisleben
-------------------	---

Schulbildung:

08/1991 - 06/1995	Martin-Luther-Gymnasium Lutherstadt Eisleben
09/1983 - 07/1991	Oberschule "Geschwister Scholl" Lutherstadt Eisleben

Acknowledgement - Danksagung

In diesem Abschnitt möchte ich allen Menschen danken, die auf die eine oder andere Weise zum Gelingen der Arbeit beigetragen haben.

Ich danke insbesondere Prof. Dr.-Ing. Christian Heipke, der mir die Möglichkeit gab, einen Einblick in das wissenschaftliche Arbeiten an seinem Institut zu gewinnen, für viele fachliche Diskussionen sowie für die umfassende Unterstützung bei der Anfertigung dieses Werkes.

Mein besonderer Dank gilt auch Dr. techn. Franz Rottensteiner für die Übernahme des Referates, die fachlichen Diskussionen sowie das Korrigieren der ersten Entwürfe dieser Arbeit.

Prof. Dr.-Ing. Monika Sester möchte ich für die Übernahme des Referates danken sowie für die angenehme Zusammenarbeit während des gemeinsamen Projektes.

Prof. Dr.-Ing. George Vosselman danke ich für die Übernahme des Referates.

Mein Dank gilt auch dem Landesamt für Geoinformation und Landentwicklung Niedersachsen sowie dem Landesamt für Vermessung und Geoinformation Schleswig-Holstein für die finanzielle Unterstützung im Projekt und für die angenehme Zusammenarbeit.

Allen Mitarbeitern des IPI möchte ich für die schöne gemeinsame Zeit und für das angenehme Arbeitsklima danken. Besonderer Dank gebührt meinem langjährigen Zimmerkollegen am IPI und Wegbegleiter aus „Dresdner Tagen“ Dr.-Ing. Alexander Brzank.

Nicht zuletzt möchte ich mich bei meiner Familie und bei meinen Freunden bedanken, insbesondere bei meinen Eltern, die mich in jeder Lebenslage unterstützt und so die Anfertigung dieser Arbeit erst ermöglicht haben.